SECOND ORDER CONE PROGRAMMING (SOCP) BASED FAST AND EXACT CONVEX OPTIMAL POWER FLOW (OPF) MODELS FOR ELECTRIC GRID WITH RENEWABLES

by

Md Mahmud-Ul-Tarik Chowdhury

A dissertation submitted to the faculty of
The University of North Carolina at Charlotte
in partial fulfillment of the requirements
for the degree of Doctor of Philosophy in
Electrical Engineering

Charlotte

Approved by:

_____
Dr. Sukumar Kamalasadan

_____
Dr. Valentina Cecchi

_____
Dr. Abasifreke Ebong

_____
Dr. Joel Avrin

Abstract

MD MAHMUD-UL-TARIK CHOWDHURY. Second Order Cone Programming (SOCP) Based Fast and Exact Convex Optimal Power Flow (OPF) Models for Electric Grid with Renewables. (Under the direction of DR. SUKUMAR KAMALASADAN)

With the modernization of power grids, high penetration of distributed energy-based resources (DERs), and modern loads, optimal power flow (OPF) analysis is one of the essential tools for reliable power system planning and operation. This research proposes novel OPF models for power distribution and transmission networks using second-order cone programming (SOCP). The advantages of SOCP-based convex OPF models are the efficient computational ability for large network systems and the global optimality. To confirm solution accuracy, the necessary conditions for the tightness of the angle and conic relaxations of power flow models are addressed in this research work for the proposed OPF models. In this dissertation, an OPF architecture is proposed to retrieve the bus voltage angle difference for radial distribution networks and thus control the reactive power flow, leading to better voltage regulation in the network and promising a globally optimal solution. This research also presents a SOCP-based AC-OPF model for unbalanced three-phase radial power distribution networks. Mutual coupling effects are generally ignored in the existing multi-phase SOCP AC-OPF models. The proposed SOCP-OPF model introduces a coupling coefficient for the mutual coupling effects on the three-phase unbalanced lines to overcome this critical issue. The derivation of the coupling coefficients has been illustrated with the required proof that the relaxation is tight and the solution from the proposed OPF model is optimal for an unbalanced multi-phase distribution network. Besides the distribution networks, this work also presents a novel SOCP-based OPF formulation for transmission system power networks. Power transmission networks generally have meshed orientation. For meshed power networks, though the conic relaxation is exact due to the cyclic angle constraints, the angle relaxation may not be exact. An OPF model is proposed for the SOCP-OPF model for power transmission networks satisfying the cyclic angle constraints. For that, the model defines a convex envelope to represent the relative bus voltage angles that satisfy the cyclic constraint criteria for a mesh in the network. This dissertation also presents an OPF formulation for AC-DC hybrid power distribution networks. The model determines the optimal modulation index for the converters for minimum network loss. In addition, this dissertation also proposes a distributed OPF (D-OPF) model for distribution networks and a time-dependent (T-OPF) model for real-time OPF analysis. All the proposed models in this research are exact and produce globally optimal solutions for the reliable operation of the power grid.

DEDICATION

To my parents and my wife, Tashnia, for their love and support. Thank you Tashnia, for always being there.

ACKNOWLEDGEMENTS

First of all, I want to thank my adviser, Professor Sukumar Kamalasadan for giving me the opportunity for the research work in this dissertation. I would also like to thank the other members of my dissertation committee: Professors Abasifreke Ebong, Professor Valentina Cecchi, and Professor Joel Avrin, who have inspired my research. This work was supported by the U.S. National Science Foundation (NSF). I would also like to thank UNC, Charlotte, for the Graduate Assistant Support Plan (GASP) award. Many thanks to my fellow labmates and friends at UNC, Charlotte, who have directly or indirectly supported my work. Last but not least, I have been very fortunate to get support and encouragement from my wife, Sadeya Ulfat Tashnia, throughout my doctoral studies. I am very grateful to her.

Contents

List of Tables

List of Figures

CHAPTER 1: INTRODUCTION

1.1 Background

One of the most salient and fundamental tools of power system planning and economic and stable operation is Optimal Power Flow (OPF) analysis. Research on OPF analysis started in the mid-seventies due to computational congestion and for inspection of security-constrained [1, 2]. OPF analysis considers the power system's load flow and security constraints, which is a time-ahead operational planning tool for ensuring the system operation with the optimal control action across operational time frames of power systems. For the OPF operational planning, particular objectives (e.g., generation costs, network power losses, voltage and phase angle regulation) are considered by maintaining the bus voltages and branch flows within the network limits [3–5]. Initially, OPF analysis mainly focused on power transmission systems. But overgrowing use of renewable energy-based distributed energy resources (DERs) in modern power distribution networks is transforming to a complex structure from conventional distribution network structures [6]. A schematic of the modern power grid is shown in Fig.1.1. In addition to the modern DERs with different novel kinds of loads, the network operators (NOs) face challenges in operating the systems with steady-state network operation with issues like different congestion and voltage instability [7, 8]. So, besides the transmission network, the OPF analysis is also becoming increasingly important for distribution networks. Besides that, the advent of high penetration of DERs and controllable loads such as electric vehicles provide significant necessities to compensate for the randomness in the power system network, which requires the power system industry for novel OPF algorithms [9–11].

1.2 Motivation

Along with the operational network constraints, OPF is typically formulated using AC power flow equations, commonly referred to as AC-OPF [12]. Due to the nonlinearity of network characteristics, the nonlinearity of power flow equations, and other operational network constraints, the AC-OPF problem is originally NP-hard in nature [13,14]. Moreover, this nonlinearity in AC-OPF models leads to computational intractability for large power networks, and due to the non-convexity, a globally optimal solution is not guaranteed [15–18]. Besides that, the higher penetration of distributed renewable generation sources (DERs) into the power network adds additional complexity. This complex nature of the grid makes the AC-OPF analysis infeasible, and the chance of optimal solutions becomes uncertain [19].

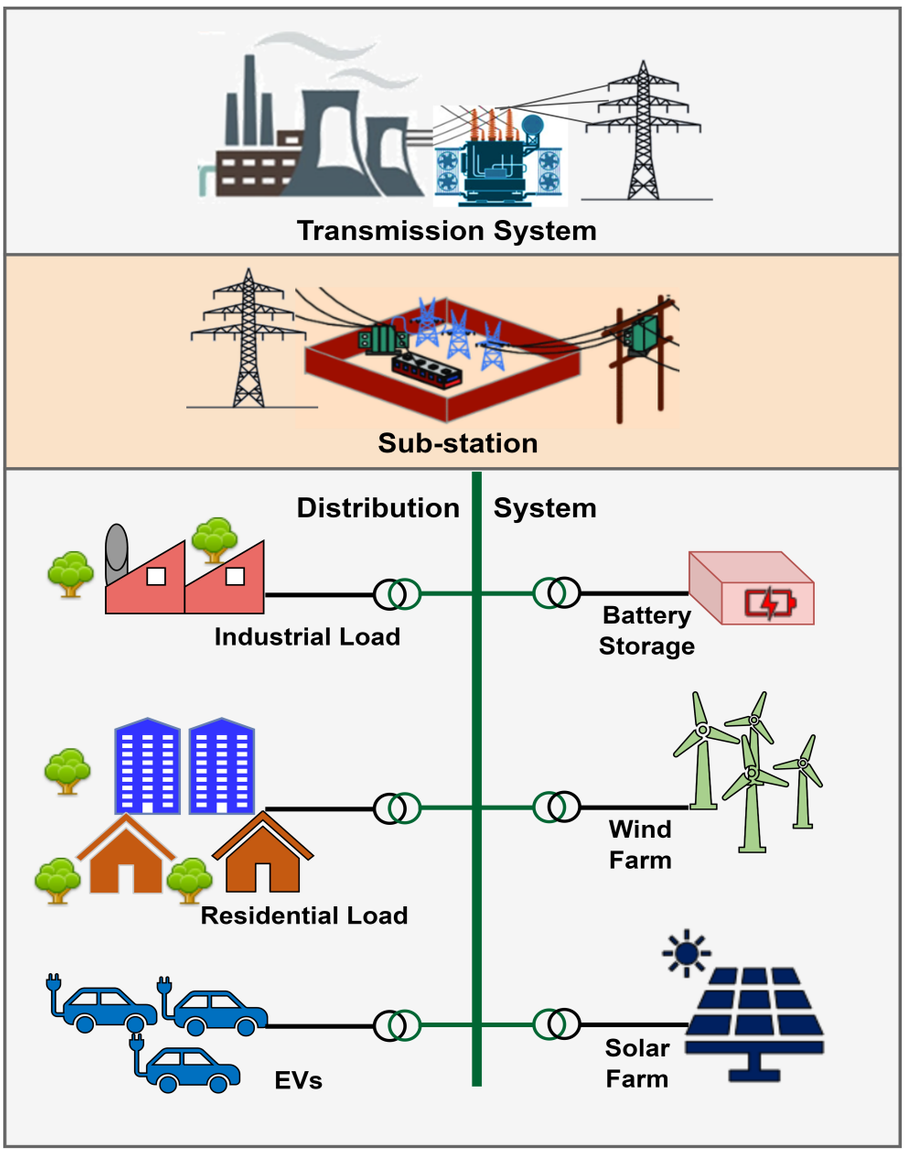

Figure 1.1: Schematic diagram of a modern power grid.

To overcome the complexity and to overcome the computational challenges of the nonlinear OPF analysis, conventionally, linear approximations of power flow equations are commonly used. However, these approximated linear formulations (i.e., DC-OPF [20, 21]) compromise the solution accuracy. Thus, the solutions obtained from such approximated formulations may not be AC-feasible or exact. However, not only the computational efficiency of the relaxed convex AC-OPF models are also conditionally exact (hence, AC-feasible) and [22]. Besides that, due to the ability to find global optima, the convex AC-OPF formulations have been extensively used for various operational applications from power system optimization and control [23, 24]. Besides that, most of the existing OPF models for power distribution systems are developed based on single-phase network analysis. But the distribution networks are multi-phase and unbalanced [25]. So, in certain cases, the single-phase OPF solution is inaccurate or insufficient for distribution networks [26]. So besides the single-phase OPF analysis, this dissertation also proposes a multi-phase convex OPF model.

Modern power converters with renewable-based DERs and widespread usage of DC loads (i.e., electric vehicles, modern home appliances) [27–30] are forming DC-DC grid sections

within the AC power grid. Case-wise, the benefits of the DC system over the AC system are shown in [31–34]. However, the total replacement of the AC system with the DC system is not viable at this point [31] since the prevailing distribution networks are predominantly AC. So, this dissertation also discusses SOCP-based convex OPF models for AC-DC hybrid networks. This dissertation presents a novel SOCP-OPF model for AC-DC radial configured distribution systems using McCormick relaxation and second-order cone programming (SOCP). The proposed AC-DC OPF model provides the optimal modulation index for the converters with the least computational challenge and the optimal power injection.

1.3 Main Contributions of the Dissertation

- In this dissertation, proposed a SOCP-based OPF model which provides an exact optimal solution with bus voltage phase angles for a radial network with high penetration of multiple DERs.

- The retrieved angle provides an efficient control feature for the reactive power flow and voltage regulation in radial power distribution networks with inverter-based DERs.

- Proposed a SOCP-OPF model, which provides an exact optimal global solution for a multi-phase unbalanced power distribution system with high DERs penetration and multi-phase mutual coupling impact on the network.

- Proposed an OPF model which provides a tight angle relaxation for an exact solution to the AC-OPF problem using SOCP by satisfying the cyclic constraints for the meshed transmission network.

- Proposed an OPF model for AC-DC hybrid distribution networks. The model considers the converters (i.e., AC-DC rectifiers and DC-AC inverters) and determines the optimal modulation index based on the objective functions and the network constraints.

- Proposed a distributed OPF model for radial type distribution hybrid power networks extendable to transmission-distribution network co-OPF analysis. Finally, the SOCP-OPF is analyzed with a real-time simulation platform for power distribution networks.

1.4 Dissertation outline

After Chapter 1, a comprehensive literature review on the state-of-the-art OPF models is discussed in Chapter 2. A brief comparison of different OPF models is also discussed. This chapter also sheds some light on the challenges and benefits of the convex OPF models.

Chapter 3 explores a novel SOCP-based OPF model for voltage regulation of power distribution systems with inverter-based DERs. This chapter also introduces an algorithm to retrieve the bus voltage phase angle with optimization analysis.

A SOCP-OPF model for three-phase unbalanced active distribution networks is proposed in Chapter 4. This model considers the mutual coupling impact on the network with a coupling coefficient. An algorithm for the determination of the coupling coefficient is discussed.

Chapter 5 discussed the inexactness of angle relaxation for the SOCP-OPF model due to the angle cyclic constraints for mesh power networks. Finally, Proposed a SOCP-OPF model in a meshed transmission system with cyclic constraints. This chapter also discussed a comparison of the proposed SOCP-OPF and the existing semi-definite programming (SDP) based OPF model for transmission networks.

In Chapter 6 SOCP-OPF model for AC-DC hybrid active distribution networks is discussed. The proposed model considers the modulation index of the converters as an optimization variable.

A SOCP-based distributed OPF model is proposed for the distribution network, which is extendable for transmission-distribution network co-simulation. Also, a SOCP-based model is discussed for real-time platform-based OPF analysis.

Finally, Chapter 8 concludes this dissertation with a light shade of future research scope.

CHAPTER 2: LITERATURE REVIEW

2.1 Introduction

Optimal scheduling of the power grid is a significant tool for the economic and optimal operation of the electric power grid [35]. Optimal power flow (OPF) evolved in 1962 [36] for finding a local optimum operating point for a power system. Since then, considerable research has been conducted to develop fast and efficient OPF models and propose algorithms for finding the global optimum solution. This section discusses a brief literature review on conventional OPF algorithms of OPF analysis. Researchers have been working on OPF problems since the mid-seventies. A literature survey of optimal power flow in the electricity market context is conducted in [37–40]. OPF based on reactive power planning is discussed in [41, 42]. A dynamic OPF for an active distribution network is proposed in [43]. A distributed OPF and controls survey for Electric Power Systems is conducted in [44]. Later, a survey of relaxations and approximations of the OPF is discussed in [45]. Below this section, a brief discussion of different OPF algorithms is conducted. The OPF formulations contain three types of variables and parameters (i.e., Control variables, state variables and parameters) for power system optimization.

2.2 Conventional OPF Methods in Power System

This section will light on a brief literature review of common OPF models for power systems planning and operation. In this dissertation, we will be focusing on the Gradient and non-random search-based OPF models. A few very common Optimization techniques are as follows:

- Common optimization techniques:
  - Random Search-based methods:
    - Evolutionary programming (EP)
    - Genetic algorithm (GA)
    - Particle swarm optimization (PSO)
    - Simulated annealing (SA)
  - Gradient and non-random search-based methods:
    - Linear programming (LP)
    - Non-linear programming (NLP)
      - Interior point method (IPM)

- Sequential quadratic programming method (SQP)
- Quasi-Newton method (QN)

* Convex optimization methods
  - Quadratic programming method (QP)
  - Second-order cone programming method (SOCP)
  - Semidefinite programming method (SDP)

In power system analysis, OPF models can be based on branch flow (BFM) or bus injection (BIM) based network power flow and power balance relations. The research in this dissertation is conducted mainly based on BFM-SOCP OPF analysis.

2.2.1 Linear Programming (LP)

One of the most commonly applied methods for OPF analysis in power systems is the linear programming (LP) based OPF models. The linear OPF methods consist of linear power balance equations, objective functions, and constraints. A conventional linear-integer programming-based algorithm for the optimum number of generation units is proposed in [46]. A linearized power flow and linearized OPF model for active distribution networks is proposed in [47]. LP method has the advantage of handling many variables, thus scalable for large power networks. However, approximate linear OPF formulations like DC-OPF [20, 21] compromise the solution accuracy. Thus, the solutions obtained from LP formulations are not always exact and may not be AC-feasible. LP-OPF is the most mature but least general OPF tool [45] used in power system optimization. LPs use a linear objective function $c_i(x_i)$ for the OPF. The canonical form of an LP is as follows:

$$min \sum_{i \in \mathcal{N}} c_i(x_i) \tag{2.1a}$$

where $\mathcal{N}$ is the set of all buses in the network.

$$s.t. \begin{cases} Ax_i = b_i \\ x_i \geq 0 \end{cases} \tag{2.1b}$$

2.2.2 Nonlinear Programming (NLP)

Typically, OPF power systems are formulated using AC power flow equations with additional constraints related to generation and voltage limits. So the OPF models are referred to as AC-OPF models. Due to the nonlinearity of power flow equations and network operational constraints, the AC-OPF problems are NP-hard in the original form [13,14]. Moreover, due to the non-convexity, the global optimal solution is not guaranteed always, and the non-

linearity in AC-OPF leads to computational intractability for large power networks [17, 18]. Multiple NLP OPF models are proposed in [48–51]. A few NLP techniques (i.e., Gradient Search Method, Newton Method, Quasi-Newton Method) are discussed here. Among these methods, the gradient search (GS) OPF method uses gradient function information moving in the opposite direction of the gradient function, which has the disadvantage of slow convergence with large power networks. On the other hand, Newton's optimization method has the advantage of fast convergence. A quadratic approximation is obtained from Taylor expansion for Newton's optimization method. However, the formation and inversion of the Hessian matrix impose a heavy computational burden for large network analysis and cannot solve the global optima. As an example, an OPF model based on Newton's method is proposed for HVDC systems in [52] incorporating voltage source converters (VSC). A hybrid OPF model with sequential quadratic programming (SQP) and differential evolution (DE) is proposed in [53]. Quasi-Newton method OPF has the advantage of a lower computational burden. The fundamental mathematical form of NLP-OPF is represented as follows (2.2a).

$$min \quad \sum_{i \in \mathcal{N}} c_i(x_i, y_i) \tag{2.2a}$$

where $\mathcal{N}$ is the set of all buses in the network.

$$s.t. \begin{cases} g(x_i, y_i) \leq b_i \\ h(x_i, y_i) = d_i \end{cases} \tag{2.2b}$$

2.2.3 Quadratic Programming (QP)

Quadratic programming-based OPF analysis (QP-OPF) is a specific optimization that differs from LP-OPF in the objective function [45]. Quadratic programming-based OPF models are helpful for loss minimization and conservative voltage regulation (CVR). As an example, a QP-based OPF model is used for PMU placement in [54]. A generalized linear programming (LP) OPF is a quadratic programming (QP) OPF with a quadratic objective function, which is represented as:

$$min \quad \sum_{i \in \mathcal{N}} {x_i}^T c_i(x_i) \tag{2.3a}$$

where $\mathcal{N}$ is the set of all buses in the network.

$$s.t. \begin{cases} Ax_i = b_i \\ x_i \geq 0 \end{cases} \tag{2.3b}$$

2.2.4 Convex OPF Models

It is already discussed that, due to the nonlinearity of power flow equations and network operational constraints, the power system OPF problems in their original form are NP-hard [13, 14]. The non-convexity and non-linearity in AC-OPF models face computational intractability for large power networks with high penetration of DERs. So, linear approximations of power flow equations are commonly used to overcome computational challenges. But the LP-OPF models compromise the solution accuracy [55]. On the contrary, the convex relaxation-based OPF models are conditionally exact and computationally efficient [22]. For computational efficiency, researchers have been interested in investigating the solution to the OPF analysis with convex-OPF models [3, 5, 22, 56–62]. Convex relaxation of OPF is generally classified into two types: bus injection (BIM) OPF model and branch flow (BFM) OPF model, but they are mathematically equivalent [63]. A few relaxation-based convex BIM and BFM-OPF models for power systems are discussed in this dissertation.

2.2.4.1 Relaxations of BFM-OPF models

Baran-Wu first introduced relaxation base branch flow OPF using second-order SOCP for optimal capacitor placement in distribution systems in [64, 65]. This model was non-convex due to quadratic equality constraints. Then, Jabr proposed a SOCP relaxation-based convex BFM-based OPF for the radial system in 2006 [22]. A BFM-based SDP-OPF is discussed in [66]. The first formulations of the convex continuous SOC AC-OPF with convex approximations to power flow in radial networks were proposed in [67]. The BFM OPF models relaxation method consists of two stages, angle relaxation and conic relaxation in power systems. The conic is exact for radial distribution and transmission networks, but the angle relaxation for transmission networks is not always. Due to the convexness, the solution to SOCP-OPF provides a globally optimal solution to the BFM-OPF problem. The exactness of convex SOCP BFM OPF models is discussed in [68, 69]. For acyclic systems, exact angle and conic relaxation conditions are also discussed in [70], which can be applied for special cases of mesh networks. Many relaxations-based OPF models are used in mesh networks using SDP and chordal relaxation [45, 56, 57]. A branch and bound method are applied to extend to OPF problem [71]. BFM-OPF includes line current and flow as OPF variables alongside the bus voltage, shown in (2.4b).

$$min \quad \sum_{i \in \mathcal{N}} c_i(x_i) \tag{2.4a}$$

where $\mathcal{N}$ is the set of all buses in the network.

$$s.t. \begin{cases} S_{ij} = V_i I_{ij}^* \\ V_i - V_j = Z_{ij} I_{ij} \\ S_j = \sum_{k:j\to k} S_{jk} - \sum_{i:i\to j}(S_{ij} - Z_{ij}|I_{ij}|^2) + y_j^*|V_j|^2 \end{cases} \tag{2.4b}$$

2.2.4.2 Relaxations of BIM-OPF models

Different relaxed OPF models (i.e., SDP, chordal relaxation, and SOCP) are proposed using BIM-based power flow models. A BIM-based SDP relaxation was first proposed in [10]. The analysis on SDP relaxation with the dual of OPF problem with sufficient conditions for zero duality gap is derived in [15]. SDP-based BIM OPF model for mesh networks and the exactness of the convexification is discussed in [3]. Chordal relaxation-based BIM OPF models are first proposed in [72, 73]. Chordal relaxation eliminates the rank-1 condition of SDP OPF models over the feasible area. The optimal OPF solution of the original AC-OPF problem is recovered from the solution of relaxed OPF problems, and [63] discussed the feasible region of the original OPF, which is an effective subset of the relaxed solution. BFM-OPF includes bus-injected power flow as OPF variables alongside the bus voltage, which is shown in (2.5b).

$$min \quad \sum_{i\in\mathcal{N}} c_i(x_i) \tag{2.5a}$$

$$s.t. \begin{cases} S_i = \sum_{(i,j)\in\mathcal{N}} \{V_i(V_i - V_j^*)y_{ij}^*\} \end{cases} \tag{2.5b}$$

2.2.4.3 Second Order Cone Programming (SOCP) based OPF model (Jabar's model)

SOCP based models have second-order cone constraints which can be represented as [45]:

$$min \quad \sum_{i\in\mathcal{N}} c_i(x_i) \tag{2.6a}$$

where $\mathcal{N}$ is the set of all buses in the network.

$$s.t. \begin{cases} ||E_i x + b_i|| \le g_i^T x + d_i \\ Ax = b \\ x \ge 0 \end{cases} \tag{2.6b}$$

For a power system network which can be represented as follows [22]. For a bus $i \in \mathcal{N}$, the voltage can be represented as: $V_i = |V_i|(\cos\theta_i + j\sin\theta_i)$ If; $V_i\cos\theta_i = m_i$ and $V_i\sin\theta_i = n_i$, So $V_i = m_i + jn_i$, thus $V_i^2 = m_i^2 + n_i^2$. For convexification new variables are defined as: $c_{ii} = m_i^2 + n_i^2$, $c_{ij} = m_i m_j + n_i n_j$ and $s_{ij} = m_i n_j - n_i m_j$. These new variables satisfies a new relation, $c_{ij}^2 + s_{ij}^2 = c_{ii}c_{jj}$. With the new variables, the SOCP-based BFM-OPF model is as:

$$min \quad \sum_{i\in\mathcal{N}} c(p_i) \tag{2.7a}$$

$$P_j^g - P_j^d = G_{ii}c_{ii} + \sum_{j\in\mathcal{N}}[G_{ij}c_{ij} - B_{ij}s_{ij}] \tag{2.7b}$$

where $\mathcal{N}$ is the set of all buses in the network.

$$Q_j^g - Q_j^d = -B_{ii}c_{ii} + \sum_{j\in\mathcal{N}}[-B_{ij}c_{ij} - G_{ij}s_{ij}] \tag{2.7c}$$

$$\underline{V}_i^2 \le m_i^2 + n_i^2 \le \overline{V}_i^2 \tag{2.7d}$$

$$c_{ij} = c_{ji} \tag{2.7e}$$

$$s_{ij} = -s_{ij} \tag{2.7f}$$

$$c_{ij}^2 + s_{ij}^2 = c_{ii}c_{jj} \tag{2.7g}$$

2.2.4.4 Second Order Cone Programming (SOCP) based BFM-OPF model

With the new set of variables defined as: $|I_{ij}|^2 = l_{ij}$, $|V_j|^2 = u_j$ and $|V_i|^2 = u_i$, the BFM-OPF model for a power system is as follows:

$$min \quad \sum_{i\in\mathcal{N}} c(p_i) \tag{2.8a}$$

where $\mathcal{N}$ is the set of all buses in the network.

$$P_j^g - P_j^d = \sum_{k:j\to k} P_{jk} - \sum_{i:i\to j}(P_{ij} - r_{ij}l_{ij}) + g_j u_j \tag{2.8b}$$

$$Q_j^g - Q_j^d = \sum_{k:j\to k} Q_{jk} - \sum_{i:i\to j} (Q_{ij} - x_{ij} l_{ij}) + b_j u_j \tag{2.8c}$$

$$u_j = u_i - 2(r_{ij} P_{ij} + x_{ij} Q_{ij}) + (r_{ij}^2 + x_{ij}^2) l_{ij} \tag{2.8d}$$

$$u_i + l_{ij} \geq \left\| \begin{array}{c} 2P_{ij} \\ 2Q_{ij} \\ u_i - l_{ij} \end{array} \right\|_2 \tag{2.8e}$$

With respect to the following network operational constraints:

$$\underline{P}_i^g \leq P_i^g \leq \overline{P}_i^g$$

$$\underline{Q}_i^g \leq Q_i^g \leq \overline{Q}_i^g$$

$$\underline{V}_i \leq V_i \leq \overline{V}_i$$

$$\underline{I}_{ij} \leq I_{ij} \leq \overline{I}_{ij}$$

where overline $\overline{(.)}$ and underline $\underline{(.)}$ represent the maximum and minimum limit of a variable or parameter for the OPF models

2.2.4.5 McCormick relaxation-based BFM-OPF model

McCormick envelopes can construct linear relaxations of the rectangular non-linear power flow equations. For the McCormick envelopes, the known bounds of each variable are used for standard optimization tools. The rectangular power flow model can be convexified with McCormick envelopes [74]. In McCormick, relaxation, a new variable is declared with envelopes for each bus $i \in \mathcal{N}$ as, $M_{ii} = m_i^2$ and $N_{ii} = n_i^2$. Beside this new variables are also declared for connecting edges $L_{ij} \in L$ like: $M_{ij} = m_i m_j$, $N_{ij} = n_i n_j$ and $O_{ij} = m_i n_j$. Then, the McCormick relaxation-based BFM-OPF model is represented as:

$$min \quad \sum_{i\in\mathcal{N}} c(p_i) \tag{2.9a}$$

$$P_j^g - P_j^d = G_{ii}(M_{ii} + N_{ii}) + \sum_{j\in\mathcal{N}} [G_{ij}(M_{ij} + N_{ij}) - B_{ij}(O_{ij} - O_{ji})] \tag{2.9b}$$

$$Q_j^g - Q_j^d = -B_{ii}(M_{ii} + N_{ii}) + \sum_{j\in\mathcal{N}} [-B_{ij}(M_{ij} + N_{ij}) - G_{ij}(O_{ij} - O_{ji})] \tag{2.9c}$$

$$\underline{V}_i^2 \leq M_{ii} + N_{ii} \leq \overline{V}_i^2 \tag{2.9d}$$

$$M_{ii}, N_{ii} \geq 0 \tag{2.9e}$$

The nonlinear variables like $M_{ij} = m_i m_j$ are convexified with McCormick envelopes as:

$$M_{ii} \geq \underline{m}_i m_j + m_i \underline{m}_j - \underline{m}_i \underline{m}_j \tag{2.10a}$$

$$M_{ii} \geq \overline{m}_i m_j + m_i \overline{m}_j - \overline{m}_i \overline{m}_j \tag{2.10b}$$

$$M_{ii} \leq \overline{m}_i m_j + m_i \underline{m}_j - \overline{m}_i \underline{m}_j \tag{2.10c}$$

$$M_{ii} \leq \underline{m}_i m_j + m_i \overline{m}_j - \underline{m}_i \overline{m}_j \tag{2.10d}$$

where $\underline{m}$ and $\overline{m}$ represent the minimum and maximum limits of the variables.

2.2.4.6 Semidefinite programming (SDP) based OPF model

Semidefinite programs generalize second-order cone programs with decision variables organized as a vector x; the decision variables in a semidefinite program take the form of a symmetric matrix X [45]. Let $X \geq 0$ indicate positive semidefinite matrix. So the SDP-based OPF models can be represented as:

$$min \quad \sum_{i \in \mathcal{N}} tr.C(X) \tag{2.11a}$$

$$s.t. \begin{cases} tr.(A_i X) = b_i X \geq 0 \end{cases} \tag{2.11b}$$

where $tr.()$ stands for the trace operator. A_i and C_i are square and symmetric matrices. b_i is a specified scalar vector. The following sections represent the BFM and BIM-OPF models based on SDP based relaxation method.

2.2.4.7 Semidefinite programming (SDP) based BFM-OPF model

If, S is denoted for the apparent power, $i_{ij}^2 = l_{ij}$ and $|v_i|^2 = u_i$, the SDP based BFM-OPF model is represented as follows:

$$min \quad \sum_{i \in \mathcal{N}} tr.C(s_i) \tag{2.12a}$$

$$\sum_{i:i\to j} diag(S_{ij} - z_{ij}l_{ij}) + s_{gj} - s_{dj} = \sum_{k:j\to k} diag(S_{jk}) \tag{2.12b}$$

$$u_j = u_i - (S_{ij}z_{ij}^* + z_{ij}S_{ij}^*) + z_{ij}l_{ij}z_{ij}^* \tag{2.12c}$$

$$\begin{bmatrix} u_i & S_{ij} \\ S_{ij}^* & l_{ij} \end{bmatrix} \geq 0 \tag{2.12d}$$

$$rank \begin{bmatrix} u_i & S_{ij} \\ S_{ij}^* & l_{ij} \end{bmatrix} = 1 \tag{2.12e}$$

Where, $(*) \in H$, Hermitian matrix. If, for a line $L_{ij} \in \mathcal{L}$ connecting the bus $(i,j) \in \mathcal{N}$, then the line constraints are imposed in a convex form as follows:

$$\begin{aligned} \underline{s}_i^g \leq s_i^g \leq \overline{s}_i^g \\ \underline{S}_{ij} \leq S_{ij} \leq \overline{S}_{ij} \\ \underline{u}_i \leq diag(u_i) \leq \overline{u}_i \end{aligned} \tag{2.12f}$$

2.2.4.8 Semidefinite programming (SDP) based BIM-OPF model

If power balance is considered at the bus $i \in \mathcal{N}$, the non-convex bus injection model (BIM) is:

$$P_i^g - P_i^d = \sum_{(i,j)\in\mathcal{N}} Re\{V_i(V_i - V_j^*)y_{ij}^*\} \tag{2.13a}$$

$$Q_i^g - Q_i^d = \sum_{(i,j)\in\mathcal{N}} Im\{V_i(V_i - V_j^*)y_{ij}^*\} \tag{2.13b}$$

$$\begin{aligned} \underline{P}_i^g \leq P_i^g \leq \overline{P}_i^g \\ \underline{Q}_i^g \leq Q_i^g \leq \overline{Q}_i^g \\ \underline{V}_i \leq |V_i| \leq \overline{V}_i \end{aligned} \tag{2.13c}$$

The capacity constraint for the line $L_{ij} \in L$ can be represented as:

$$|\theta_{ij}| = |\theta_i - \theta_j| \leq \overline{\theta}_{ij} \tag{2.14a}$$

$$|S_{ij}| = |\{V_i(V_i - V_j^*)y_{ij}^*\}| \leq \overline{S}_{ij} \tag{2.14b}$$

$$|P_{ij}| = |Real\{V_i(V_i - V_j^*)y_{ij}^*\}| \leq \overline{P}_{ij} \tag{2.14c}$$

$$|V_i - V_j| \leq (\Delta\overline{V}_{ij}) \tag{2.14d}$$

The bus injection model expressed in (2.15) and (2.14) is a non-convex formulation. For convexification of the model for SDP, new variables have been declared as $W_{ii} = V_i V_i^*$ and $W_{ij} = V_i V_j^*$. The SDP formulation can be expressed as:

$$min \quad \sum_{i \in \mathcal{N}} tr.C(s_i) \tag{2.15a}$$

$$P_i^g - P_i^d = \sum_{(i,j) \in \mathcal{N}} Re\{(W_{ii} - W_{ij})y_{ij}^*\} \tag{2.15b}$$

$$Q_i^g - Q_i^d = \sum_{(i,j) \in \mathcal{N}} Im\{(W_{ii} - W_{ij})y_{ij}^*\} \tag{2.15c}$$

$$\begin{aligned} \underline{P}_i^g \leq P_{g_i} \leq \overline{P}_i^g \\ \underline{Q}_i^g \leq Q_{g_i} \leq \overline{Q}_i^g \\ \underline{V}_i^2 \leq W_{ii} \leq \overline{V}_i^2 \end{aligned} \tag{2.15d}$$

If for a line $L_{ij} \in \mathcal{L}$ connecting the bus $(i,j) \in \mathcal{N}$, then the line constraints are imposed in a convex form:

$$Im\{W_{ij}\} \leq Re\{W_{ij}\} \tan(\overline{\theta}_{ij}) \tag{2.16a}$$

$$|S_{ij}| = |(W_{ii} - W_{ij})y_{ij}^*| \leq \overline{S}_{ij} \tag{2.16b}$$

$$|P_{ij}| = |Real[|(W_{ii} - W_{ij})y_{ij}^{*}|]| \leq \overline{P}_{ij} \tag{2.16c}$$

$$W_{ii} + W_{jj} - W_{ij} - W_{ji} \leq (\Delta\overline{V}_{ij}) \tag{2.16d}$$

$W \in \mathbb{H}^n$ is a semidefinite Hermitian matrix. For SDP formulation, OPF solution is tight and feasible if $W \geq 0$ and $rank\{W\} = 1$.

CHAPTER 3: A NEW SECOND-ORDER CONE PROGRAMMING MODEL FOR VOLTAGE CONTROL OF POWER DISTRIBUTION SYSTEM WITH INVERTER-BASED DISTRIBUTED GENERATION

3.1 Introduction and Contributions

Optimal power flow (OPF) has been a fundamental analysis of power system networks for optimal operation based on an objective function. The objective functions may include the minimization of generation cost and network power losses, voltage and phase angle regulation considering network transmission capacity and voltage fluctuations [4, 5]. Distributed generation systems (DGs) based on renewable energy have been overgrowing in modern power distribution networks, transforming the structure of conventional distribution to a complex one [6]. The engagement of the renewable energy-based DGs and novel types of critical loads influence the utility distribution industry for novel OPF algorithms [9–11, 75–78]. Power system analysis and operations greatly rely on the AC OPF for optimal operations [12]. However, the higher penetration of distributed renewable generation sources into the power network adds additional layers of complexity, leading the AC OPF to infeasible or uncertain solutions [19]. Distribution Network Operators (DNOs) face challenges to maintain steady-state network operation with issues like voltage rise and congestion when distribution networks are populated with renewable energy-based DGs [7, 8]. Besides, finding the optimum global point of operation for the non-deterministic polynomial and non-linear OPF model is hard [15, 16]. So, with the distributed DGs, the power system distribution networks demand a novel and computationally efficient OPF model.

One method for a computationally fast solution is to convert the AC OPF models to DC models but with the sacrifice of convergence and accuracy [79]. The DC OPF models become linear with the relaxation of the reactive power and assuming flat voltage magnitude of all buses throughout the network [80]. In linearized models, the network is simplified to guarantee computational efficiency and robustness [81]. Different types of optimal power flow models have been proposed in different research [45, 82–84]. Besides that, specially for radial distribution networks few more algorithms have been proposed in [85–87]. Due to the inexactness issue of DC OPF models and the non-convexity of AC OPF models, the complexity from the increasing penetration of DGs inspires the convex OPF models to ensure fast, feasible, and tight solutions. The convex second-order cone programming (SOCP) based OPF model was first proposed in [22], and the Semidefinite programming (SDP) model in [5]. The required conditions for the exact and feasible SDP solution in radial and mesh networks

are discussed in [3, 56, 57]. However, the SOCP models are computationally more friendly and efficient than the SDP relaxation models [58]. One challenge for an effective solution of the SOCP model is the need to relax and recover voltage angles. Possible and exact optimal global solution recovery within the quadratic and arctangent equalities from the SOCP convexification are discussed in [59, 60]. While there are no upper bounds or a wide boundary on the load flow in a radial distribution network, the OPF solution is tight and exact from a SOCP model [61, 62].

3.1.1 Major Contributions

In this chapter, we have proposed a branch flow-based SOCP OPF model, which is motivated by [3, 64, 68]. In [68] a SOCP-based optimization model and in [3, 64] an optimal placement of switched capacitors in distribution networks is discussed. The branch flow SOCP OPF model presented in this research is very suitable for distribution networks as it emphasizes the branch parameters. The main advantages of the modeling framework are as follows.

- The model can be used for both cost and loss minimization objective functions and is scalable for large networks due to its computational efficiency.
- The approach can model the high penetration of DGs in the power distribution network as it recovers the angle directly within the optimization process.
- The architecture provides an exact optimal solution with bus voltage phase angles for a radial network with high penetration of multiple DERs.
- The retrieved angle provides an efficient control feature to the reactive power flow and voltage profile.
- The approach can be used for voltage regulation in power distribution networks with high DGs penetration.

The chapter is organized into multiple sections. The theoretical analysis, OPF methodology, and relaxation framework are discussed in section 3.2. Section 3.3 discusses the model implementation methods and results for both the angle derivation and the reactive flow control methodology, and Section 3.4 concludes the chapter with a summary.

The variable and parameters used in this chapter are as follows:

N:	Set of all buses in the network
L:	Set of all branches in the network
V_i:	Voltage at the bus $i \in N$
u_i:	Square of the voltage magnitude at the bus $i \in N$
S_i^g:	Apparent power injection at the bus $i \in N$
S_i^d:	Apparent power demand at the bus $i \in N$
P_i^g:	Real power injection at the bus $i \in N$
P_i^d:	Real power demand at the bus $i \in N$
Q_i^g:	Reactive power injection at the bus $i \in N$
Q_i^d:	Reactive power demand at the bus $i \in N$
P_{ij}:	Real power flow through the line $L_{(i,j)} \in L$
Q_{ij}:	Reactive power flow through the line $L_{(i,j)} \in L$
I_{ij}:	Current flow through the line $L_{(i,j)} \in L$
l_{ij}:	Square of the magnitude of current flow through the line $L_{(i,j)} \in L$
θ_{ij}:	Bus voltage angle difference between the bus i and bus j, $(i,j) \in N$
Z_{ij}:	Impedance of the line $L_{(i,j)} \in L$
G_{ij}:	Conductance of the line $L_{(i,j)} \in L$
B_{ij}:	Susceptance of the line $L_{(i,j)} \in L$

3.2 Proposed Methodology

3.2.1 Branch Flow Model

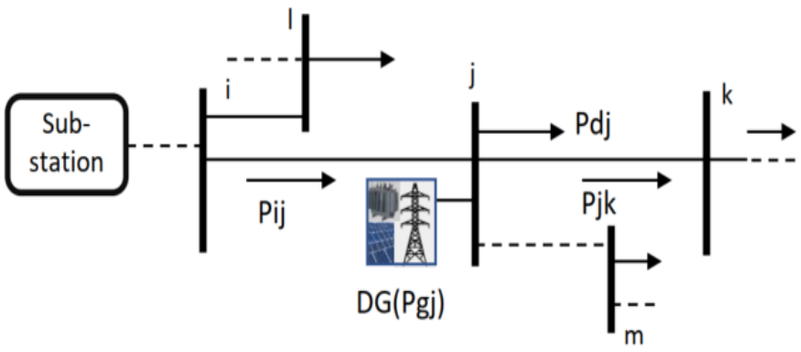

Figure 3.1: Branch flow model including DGs.

The proposed OPF methodology is based on a branch flow model, emphasizing the bus voltage, phase, and the branch flow parameters such as current, real, and reactive power flow through the branches. For a power distribution network, consisting with buses $[i, j, k] \in N$ as like Fig. 3.1, the fundamental power flow equations can be represented as:

$$S_{ij} = V_i I_{ij}^* \tag{3.1}$$

$$V_i - V_j = Z_{ij} I_{ij} \tag{3.2}$$

The power balance at the buses $[i, j, k] \in N$, in terms of the flows through the lines

$[L(i,j), L(j,k)] \in L$ is:

$$S_j^g - S_j^d = \sum_{k:j\to k} S_{jk} - \sum_{i:i\to j} (S_{ij} - Z_{ij}|I_{ij}|^2) + y_j^*|V_j|^2 \tag{3.3}$$

From (3.1) and (3.2),

$$|V_j|^2 = |V_i|^2 + |Z_{ij}|^2|I_{ij}|^2 - (Z_{ij}S_{ij}^* + Z_{ij}^*S_{ij}) \tag{3.4}$$

If a line $L_{ij} \in L$ connecting two buses $\{i,j\} \in N$, the real and reactive power flow across the line can be expressed as follows:

$$P_{ij} = G_{ij}V_i^2 - G_{ij}V_iV_j\cos(\theta_{ij}) - B_{ij}V_iV_j\sin(\theta_{ij}) \tag{3.5}$$

$$Q_{ij} = -B_{ij}V_i^2 + B_{ij}V_iV_j\cos(\theta_{ij}) - G_{ij}V_iV_j\sin(\theta_{ij}) \tag{3.6}$$

3.2.2 Convexification for the Proposed SOCP OPF

For an optimization problem, the mathematical form is:

$$\begin{aligned} &minimize/maximize && f(x) \\ &Subject\ \ to && \underline{b}_i \le f_i(x) \le \bar{b}_i \end{aligned}$$

The vector, $x = \{x_1, x_2, x_3.....x_n\}$ is the optimization variables for the objective function $f(x) \in \mathbb{R}$. Where, $f_i : \mathbb{R} \to \mathbb{R}^n$ are the constraints and b_i is the limit. The main focus of this work is on the convex optimization for a power system network, where the objective and constraints are convex, and satisfy the inequality:

$$f_i(A_1x + A_2y) \le f_i(A_1x) + f_i(A_2y), \forall x, y \in \mathbb{R}^n, A_1, A_2 \in \mathbb{R}$$

For a second order cone set C,

$$C = \{(x_1, x_2, ..., x_n) : x_n \ge \sqrt{x_1^2 + x_2^2 + ... + x_{n-1}^2}) \in \mathbb{C}$$

If the solution set of an optimization problem is $\mathbb{X} = \{x_1, x_2x_3.....\} \in \mathbb{C}$, for the second-order cone optimization, the cone $\mathbb{C}$ encloses the global space $\mathbb{S} \in \mathbb{C}$ which ensures the optimal global solution within the convex space.

The power flow equations from (3.1) to (3.4) are non-convex. So, the solution suffers from scalability and incapable of providing any feasible solution for the large power distribution

networks. However, if a convex space encloses the non-convex space for a global optimal feasible solution for $\mathbb{S}_x \in \mathbb{C}_x$, the power flow equations can be re-written as a convex set of equations. The solution from the convexed space is the optimal solution of the parent non-convex OPF problem [88]. With the help of a new set of variables, (3.1) to (3.4) are convexified as follows: $|I_{ij}|^2 = l_{ij}$; $|V_j|^2 = u_j$ and $|V_i|^2 = u_i$. Then from (3.3) and (3.4):

$$P_j^g - P_j^d = \sum_{k:j\to k} P_{jk} - \sum_{i:i\to j} (P_{ij} - r_{ij} l_{ij}) + g_j u_j \tag{3.7}$$

$$Q_j^g - Q_j^d = \sum_{k:j\to k} Q_{jk} - \sum_{i:i\to j} (Q_{ij} - x_{ij} l_{ij}) + b_j u_j \tag{3.8}$$

$$u_j = u_i - 2(r_{ij} P_{ij} + x_{ij} Q_{ij}) + (r_{ij}^2 + x_{ij}^2) l_{ij} \tag{3.9}$$

The equality in (3.1) can be represented in the form of a second order cone (SOC) as follows:

$$u_i + l_{ij} \geq \left\| \begin{matrix} 2P_{ij} \\ 2Q_{ij} \\ u_i - l_{ij} \end{matrix} \right\|_2 \tag{3.10}$$

The OPF model for a network is enclosed within a space, where a feasible solution satisfies an objective function based on some imposed constraints on a power network. For the objectives of the OPF, all of the physical laws of a power network are satisfied. This research investigates the generation cost and real power loss minimization objectives for a distribution network. Besides that, the voltage discrepancy can also be investigated. The objective functions are as follows:

- Line loss minimization,

$$min[\sum_{(i,j)\in L} r_{ij} l_{ij}] \tag{3.11}$$

- Generation cost minimization,

$$min[\sum_{i\in N_g} c_i P_{g_i}] \tag{3.12}$$

- Minimization in bus voltage difference,

$$min[\sum_{(i,j)\in N} \alpha_i (u_i - u_j)] \tag{3.13}$$

- Or, the combination of these three $f(x)$,

$$min[\sum_{(i,j)\in L} r_{ij}l_{ij} + \sum_{i\in N_g} c_i P_{g_i} + \sum_{i\in N_g} \alpha_i u_i] \tag{3.14}$$

where N_g is the set of DER connected buses. The following constraints are imposed with the model to observe the branch flow effect on a power network.

$$\begin{aligned} P_{g_i}^{min} &\leq P_{g_i} \leq P_{g_i}^{max} \\ Q_{g_i}^{min} &\leq Q_{g_i} \leq Q_{g_i}^{max} \\ P_{ij}^{min} &\leq P_{ij} \leq P_{ij}^{max} \\ Q_{ij}^{min} &\leq Q_{ij} \leq Q_{ij}^{max} \\ \theta_{ij}^{min} &\leq \theta_{ij} \leq \theta_{ij}^{max} \\ u_i^{min} &\leq u_i \leq u_i^{max} \end{aligned} \tag{3.15}$$

3.2.3 Angle Inclusion and Reactive Power Management

Real power flow change is mainly sensitive to the phase angle difference $\Delta\theta$, while the reactive power depends on the voltage magnitude where the X/R ratio is high, such as transmission networks [89]. However, for distribution network systems, the X/R ratio is low, so phase angles play a significant impact on the reactive power and thus on the voltage magnitude. A general method of relaxing this angle in convex optimization due to the non-convexity thus fails to deliver global optimal solutions. Contrary to the previous works, in the proposed model, the voltage phase angle is included in the convex space. The method is as follows. For the convexification of the bus voltage angle relationship, from (3.5) and (3.6) we get

$$-V_i V_j \sin(\Theta_{ij})(G_{ij}^2 + B_{ij}^2) = (B_{ij}P_{ij} + G_{ij}Q_{ij}) \tag{3.16}$$

However, (3.16) is still non-convex. As the bus $i \in N$ and bus $j \in N$ are two adjacent connected buses and if $[V_i^{max}, V_i^{min}, V_j^{max}, V_j^{min}] \approx 1$ in per unit then we can safely assume that $V_i V_j \approx 1$. For distribution networks, the angle difference for any two adjacent connected buses can thus be written as $\sin(\theta_{ij}) \approx \theta_{ij}$, where θ_{ij} is the bus voltage angle difference between the bus $i \in N$ and bus $j \in N$. Then from (3.16):

$$\Theta_{ij} = -\frac{B_{ij}P_{ij} + G_{ij}Q_{ij}}{B_{ij}^2 + G_{ij}^2} \tag{3.17}$$

Equation (3.17) is included with the SOCP model to retrieve the bus voltage angle difference between two connected buses $(i, j) \in N$ for the line $L(i, j) \in L$. If the substation bus is considered as the reference, the bus voltage phase angle for all the buses in the radial network is recovered from this bus voltage angle difference. Further, if a DG system integrated with battery and PV can feed constant real power support to the network, we can write

$$\theta_{ij} \propto Q_{ij} \tag{3.18}$$

Therefore, by controlling the bus angle difference, the reactive power flow, and finally, through this, the voltage magnitude can be controlled. Suppose a DG with reactive power support is available near the substation bus in a distribution network. In that case, the voltage profile can be controlled or keep stable for critical load changing without the need to have a load tap changer (LTC). This ensures an optimal point of operation for minimum generation cost or minimum loss and provides a point of control to the reactive power flow.

Based on this theoretical framework, an algorithm for controlling the reactive power flow and thus the voltage regulation in the network can be developed with the retrieved angle difference as shown in Algorithm 1.

3.3 Simulation and Evaluation

The proposed model is implemented as A: Angle recovery from the SOCP branch flow model, B: Reactive power flow control with the recovered bus voltage angle difference within the optimal solution space, and tested on several real-life IEEE standard network systems using Matlab/Simulink with MOSEK solver. The model's performance is verified with the Non-linear Programming (NLP) solution obtained from the OpenDSS and MatPower platforms.

3.3.1 Implementation of the Angle Recovery Model

For part A, the MOSEK solver in the Matlab platform has been used for the convex OPF model consisting of (3.7) to (3.10) and (3.17). The simulation results from the proposed model show that the results are tight and exact for different test cases and similar to the NLP solution.

3.3.1.1 Case 1 (IEEE 32-Bus Test System)

The model is tested on the modified IEEE 32-bus network system with and without DGs penetration. The placement of the DGs at the modified IEEE 32-bus distribution system is shown in Fig. 3.2. The IEEE 32-bus system is a modified version of the IEEE 33 bus radial distribution network. The substation bus (bus no. 0) is substituted with a generation system, and the system-rated voltage is 12.66 kV, with 31 lines connecting 32-

Algorithm 1 Reactive Power Control Algorithm

-Find the lines $L_{ij} \in L$ with the bus, $i \in N$ in the distribution network.
-Make reference to the optimized voltage profile at $'(t-1)'$ time period.
-At $'t'$ time period the PV source supplies or due to change in load the voltage profile fluctuates to $v_i(t)$.
-$\Delta v_i = v_{i,ref}\,(t-1) - v_i(t)$.
-Set the tolerance ξ

```
while |Δv_i| ≥ ξ do
    if Δv_i > 0 then
        Find the incoming and outgoing branch reactive flow with bus 'i'
        if If outgoing Q_ij == (+)ve then
            decrease the θ_ij : θ_ij ∈ [θ_ij^min, θ_ij^max]
        end
        else if If outgoing Q_ij == (−)ve then
            increase the θ_ij : θ_ij ∈ [θ_ij^min, θ_ij^max]
        end
        else if If incoming Q_ij == (+)ve then
            increase the θ_ij : θ_ij ∈ [θ_ij^min, θ_ij^max]
        end
        else if If incoming Q_ij == (−)ve then
            decrease the θ_ij : θ_ij ∈ [θ_ij^min, θ_ij^max]
        end
    end
    else if Δv_i < 0 then
        Find the incoming and outgoing branch reactive flow with bus 'i'
        if If outgoing Q_ij == (+)ve then
            increase the θ_ij : θ_ij ∈ [θ_ij^min, θ_ij^max]
        end
        else if If outgoing Q_ij == (−)ve then
            decrease the θ_ij : θ_ij ∈ [θ_ij^min, θ_ij^max]
        end
        else if If incoming Q_ij == (+)ve then
            decrease the θ_ij : θ_ij ∈ [θ_ij^min, θ_ij^max]
        end
        else if If incoming Q_ij == (−)ve then
            increase the θ_ij : θ_ij ∈ [θ_ij^min, θ_ij^max]
        end
    end
    Δv_i = v_{i,ref}(t−1) − v_i(t)_nth.
end
```

buses. The proposed SOCP model is designed in a way so that it can handle multiple DGs penetration in a network. The result comparison for the IEEE 32-bus network is shown in Table 3.1 and Table 3.2 for nonlinear power flow (MP-PF), NLP OPF (MP-OPF), and the proposed SOCP model (SOCP-OPF). For the minimum generation-cost objective function, the voltage profile from the proposed SOCP OPF model and NLP model is shown in Fig. 3.3. The retrieved bus voltage angle difference in the 32-bus network from the proposed SOCP OPF model and the NLP OPF model are compared in Fig. 3.4. It can be seen

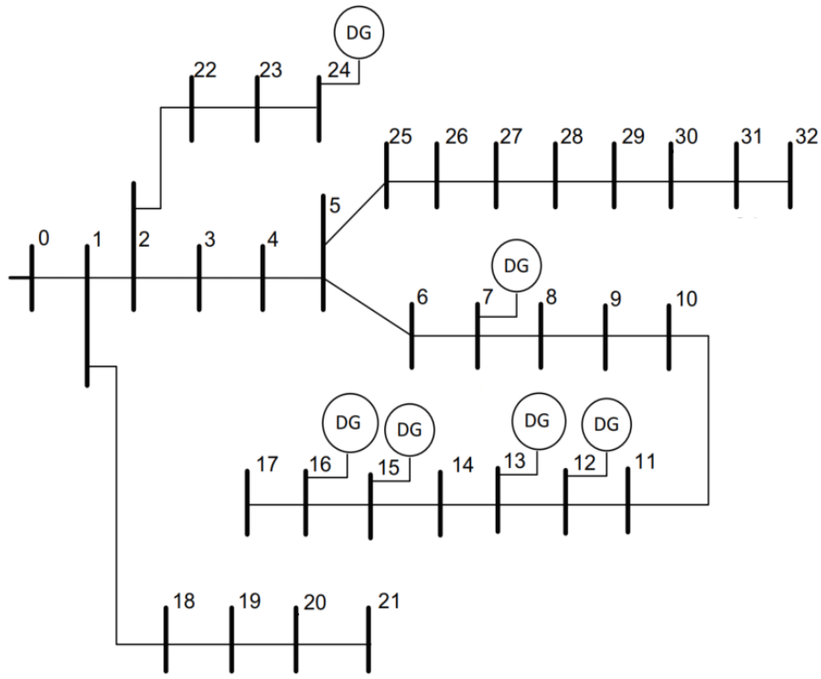

Figure 3.2: Modified IEEE 33-bus distribution network.

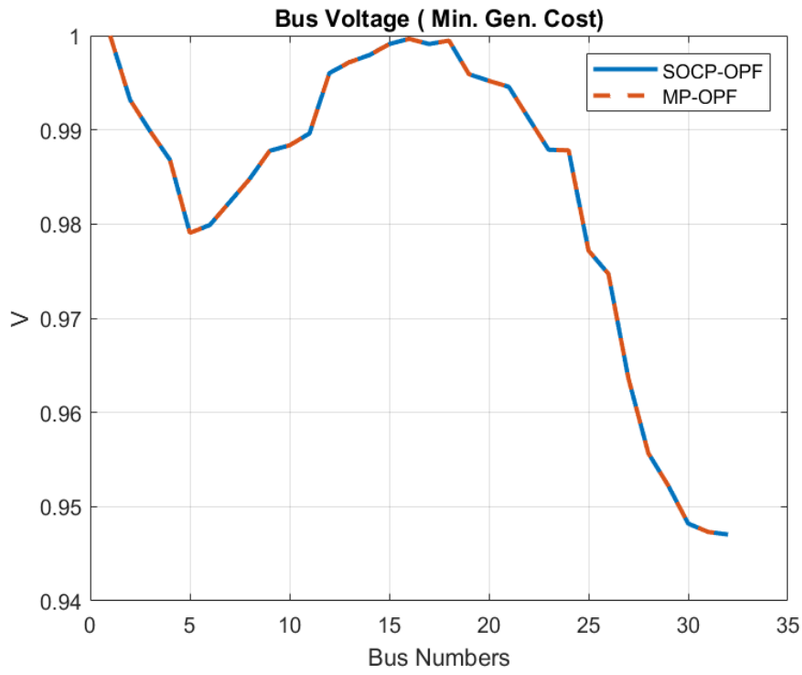

Figure 3.3: Voltage profile comparison between MatPower NLP and SOCP OPF.

that the bus angle difference from the proposed SOCP model matches the NLP results. The percent loss [(Total generation-Total load)*100/Total generation] in the network, the voltage mismatch for the different objective function with the convergence times, and the voltage mismatch between the proposed SOCP model and the NLP OPF is shown in Table 3.2. The convergence time is compared on a machine with an Intel(R) Core(TM) i7-10510U CPU @ 2.30 GHz processor and 16 GB RAM environment. For convex formulation, the proposed SOCP model is computationally more efficient than the NLP model. The % loss with the proposed method is less than the NLP PF and the NLP OPF. For the IEEE 32-bus network, the DG placement with the maximum and minimum generation capacity and the generator's

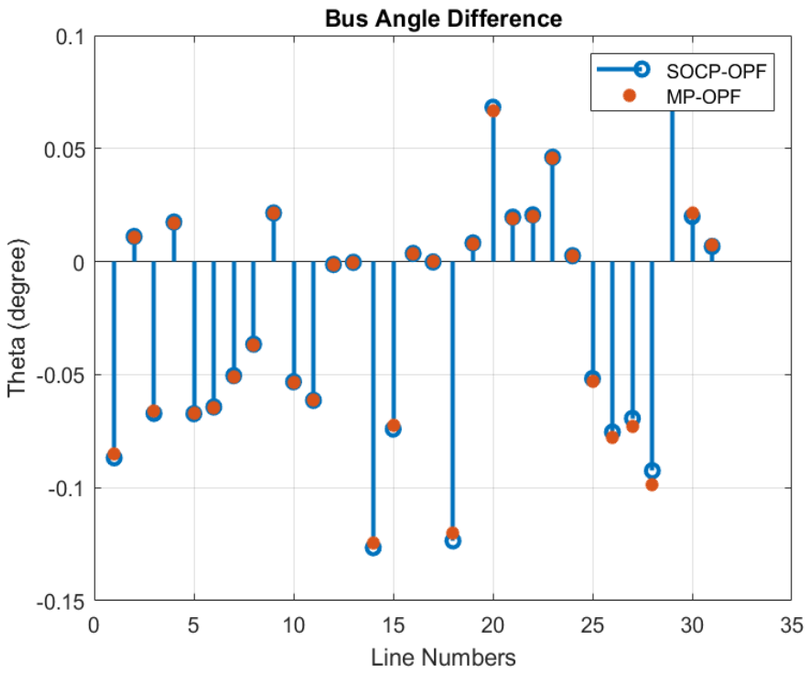

Figure 3.4: Bus voltage angle difference in IEEE 32-bus network for MatPower NLP and SOCP OPF.

Table 3.1: Modified 32-bus system power flow comparisons

						MP-PF		MP-OPF		SOCP-OPF	
No.	P_g^{max}	P_g^{min}	Q_g^{max}	Q_g^{min}	C	P_g	Q_g	P_g	Q_g	P_g	Q_g
1	10	-	10	-10	90	3.90	2.43	2.03	1.50	2.03	1.50
7	0.35	0.100	0.25	00	79	0.00	0.00	0.35	0.25	0.35	0.25
12	0.30	0.075	0.20	00	87	0.00	0.00	0.30	0.20	0.30	0.20
13	0.32	0.000	0.00	00	70	0.00	0.00	0.32	0.00	0.32	0.00
15	0.08	0.075	0.20	00	92	0.00	0.00	.075	0.20	0.075	0.20
16	0.30	0.300	0.00	00	70	0.00	0.00	0.30	0.00	0.30	0.00
24	0.41	0.100	0.20	00	81	0.00	0.00	0.41	0.20	0.41	0.20

cost coefficients are discussed in Table 3.1. With this network configuration, the power flow solution is similar to the benchmark OPF solution from the MatPower platform, verifying the tightness of the optimal global solution from the proposed model.

Table 3.2: Modified 32-bus network system analysis

	MP-PF	MP-OPF (min cost)	SOCP-OPF (min cost)	SOCP-OPF (min loss)
Time	.08 Sec	.92 Sec	.61 Sec	.53 Sec
% Loss	4.74%	1.85%	1.78%	1.77%
Gen. cost			319.72	320.21
	MP-OPF(mc) vs SOCP-OPF(mc)		SOCP-OPF(mc) vs SOCP-OPF(ml)	
Voltage mismatch	.0003%		.045%	
mc*=min cost			ml*=min loss	

Table 3.3: IEEE 123-bus system performance comparisons

123 Bus System	Total Load $P_d(MW)$	Total Gen SOCP $P_g(MW)$	% Loss SOCP (min)	% Loss SOCP (min)	% Loss (PF)	Cost SOCP (min)	Cost SOCP (min)
Base Case	1.1633	1.2017	3.20 %	3.20 %	3.20 %	110.55	110.55
10% DG	1.1633	1.1892	2.18 %	2.18 %	2.75 %	109.15	109.15
30% DG	1.1633	1.1836	1.71 %	1.71 %	2.71 %	108.44	108.44
50% DG	1.1633	1.1782	1.26 %	1.26 %	2.64 %	107.74	107.74

3.3.1.2 Case 1 (IEEE 123-Bus Test System)

Besides the IEEE 32-bus radial network system, the proposed model is analyzed on the IEEE 123-bus network system for the base case and DG penetration. For DG penetration, 10%, 30%, and 50% DGs of the total connected load in the network are considered. The comparative analysis has been shown in Table 3.3 for different percentages of DGs penetration in the network. The model is evaluated for both minimum generation cost and minimum loss objective functions. If the generation cost from the DG units is lower than the cost of the power available from the substation bus, then the % loss is found to be the same for both of the objective functions. From the results in Table 3.3, it can be observed that the % loss decreases with the higher penetration of DGs in the network. The OPF solution convergence time for the proposed SOCP compared to NLP OPF on other benchmark platforms is shown in Table 3.4 for the IEEE 123-bus network. The DG placement and the generation with each configuration are shown in Table 3.5. Due to the convexity of the proposed model, the proposed requires less time for convergence than the NLP OPF model. The 123-bus network base case's voltage profile and the DG penetration configuration are shown in Fig. 3.5 and 3.6, respectively. With the DG penetration, the OPF model voltage limit is kept between 0.9 pu to 1.1 pu for minimum and maximum voltage limits, respectively. From Fig. 3.6, it can be observed that the network voltage amplitude level rise with the increase of the DGs penetration. The bus voltage angle difference is retrieved from the proposed 123-bus network system model for comparison. The bus voltage angle difference from the proposed model for the base case is shown in Fig. 3.7. The result is verified with the angle recovered from the OpenDSS platform for the base case. Fig. 3.8 shows the angle retrieved from the proposed SOCP model while DGs are connected and verified with the result from the MatPower NLP. The results from the proposed SOCP model are similar to the OpenDSS and MatPower NLP solutions. The negligible discrepancy in the angle difference is due to the approximations for convexification of (3.17). Comparing the proposed model's solution with the OpenDSS and MatPower NLP solution validates the approximation of the model. It was also observed that the model is capable of an optimal global solution for other large distribution networks.

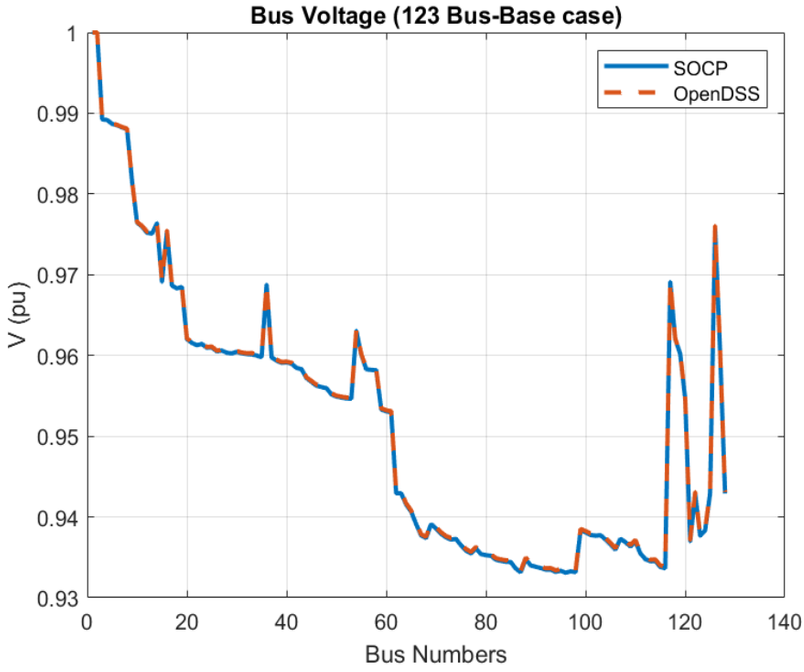

Figure 3.5: Voltage profile in IEEE 123-bus network base case.

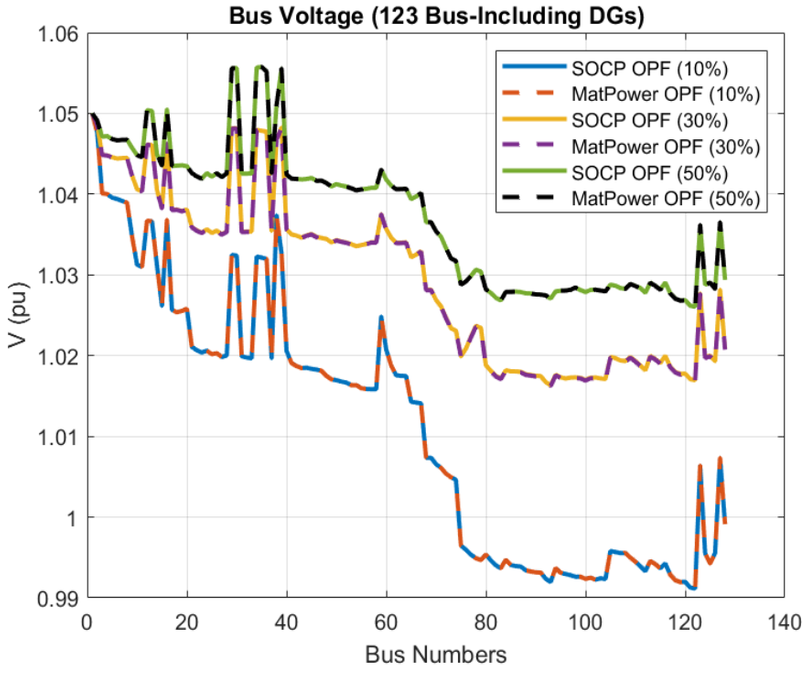

Figure 3.6: Voltage profile in IEEE 123-bus network with 10%, 30% and 50% DGs.

Table 3.4: IEEE 123-bus system time of convergence (ToC) comparisons

123 Bus System	SOCP ToC (min cost)	SOCP ToC (min loss)	Mat Power ToC (NLP)	Power Flow ToC (MP)
Base Case	0.28 sec	0.39 sec	0.45 sec	0.73 sec
10 % DGs	0.33 sec	0.39 sec	0.46 sec	0.80 sec
30 % DGs	0.36 sec	0.41 sec	0.48 sec	0.77 sec
50 % DGs	0.34 sec	0.39 sec	0.51 sec	0.81 sec

3.3.2 Reactive Power Flow Control

The reactive power flow control Algorithm 1 is proposed using the bus retrieved voltage angle difference as discussed in the previous section. The algorithm is capable of controlling

Table 3.5: Generation Profile for IEEE 123-bus system with DGs

Case	Bus No.	SOCP P_i^g mw	SOCP Q_i^g mvar	MP P_i^g mw	MP Q_i^g mvar	Case	Bus No.	SOCP P_i^g mw	SOCP Q_i^g mvar	MP P_i^g mw	MP Q_i^g mvar
Base	1	1.2034	.7153	1.2034	.7153		14	.0067	.0145	.0067	.0146
10% DGs	1	0.9270	.5103	0.9270	.5105		18	.0133	.0088	.0133	.0086
	11	0.0133	.0088	0.0133	.0088		19	.0067	.0087	.0067	.0088
	31	0.0133	.0088	0.0133	.0088		21	.0133	.0088	.0133	.0086
	54	0.0700	.0464	0.0700	.0464		24	.0133	.0087	.0133	.0083
	66	0.0067	.0044	0.0067	.0044		26	.0133	.0087	.0133	.0083
	73	0.0467	.0309	0.0467	.0309		30	.0133	.0082	.0133	.0078
	84	0.0817	.0541	0.0817	.0541		32	.0133	.0087	.0133	.0083
	95	0.0133	.0088	0.0133	.0088		34	.0067	.0041	.0067	.0047
	108	0.0133	.0088	0.0133	.0088		35	.0133	.0033	.0133	.0033
30% DGs	1	0.7236	.1253	0.7236	.1269		37	.0133	.0075	.0133	.0077
	8	0.0133	.0088	0.0133	.0087		40	.0067	.0212	.0067	.0224
	11	0.0133	.0088	0.0133	.0087		43	.0067	.0084	.0067	.0084
	18	0.0133	.0088	0.0133	.0087		45	.0133	.0057	.0133	.0057
	21	0.0133	.0088	0.0133	.0088		47	.0067	.0054	.0067	.0055
	30	0.0133	.0088	0.0133	.0088		50	.0700	.0464	.0700	.0458
	32	0.0133	.0088	0.0133	.0088		53	.0067	.0464	.0067	.0464
	37	0.0133	.0088	0.0133	.0088		55	.0133	.0088	.0133	.0088
	45	0.0133	.0087	0.0133	.0087		57	.0067	.0292	.0067	.0295
	50	0.0700	.0464	0.0700	.0463	50% DGs	60	.0067	.0464	.0067	.0464
	53	0.0067	.0464	0.0067	.0463		64	.0133	.0088	.0133	.0088
	57	0.0067	.0464	0.0067	.0463		67	.0467	.0044	.0467	.0044
	60	0.0067	.0464	0.0067	.0464		68	.0250	.0044	.0250	.0044
	64	0.0133	.0088	0.0133	.0088		71	.0133	.0088	.0133	.0088
	67	0.0467	.0044	0.0467	.0043		77	.0133	.0088	.0133	.0088
	77	0.0133	.0309	0.0133	.0308		78	.0817	.0044	.0817	.0044
	78	0.0817	.0461	0.0817	.0461		81	.0133	.0088	.0133	.0088
	86	0.0067	.0441	0.0067	.0440		84	.0133	.0088	.0133	.0088
	89	0.0133	.0087	0.0133	.0088		86	.0067	.0464	.0067	.0464
	98	0.0133	.0087	0.0133	.0088		89	.0133	.0088	.0133	.0088
	101	0.0133	.0087	0.0133	.0088		92	.0133	.0088	.0133	.0088
	102	0.0133	.0087	0.0133	.0088		96	.0133	.0088	.0133	.0088
	106	0.0133	.0087	0.0133	.0087		98	.0067	.0404	.0067	.0406
	109	0.0133	.0087	0.0133	.0087		101	.0133	.0088	.0133	.0088
	113	0.0067	.0464	0.0067	.0464		102	.0133	.0088	.0133	.0088
	116	0.0067	.0464	0.0067	.0463		106	.0133	.0088	.0133	.0088
50% DGs	1	0.5199	.0051	0.5199	.0051		109	.0133	.0088	.0133	.0088
	4	0.0067	.0139	0.0067	.0140		111	.0133	.0088	.0133	.0088
	8	0.0133	.0088	0.0133	.0088		113	.0067	.0464	.0067	.0463
	11	0.0133	.0088	0.0133	.0088		116	.0067	.0464	.0067	.0462

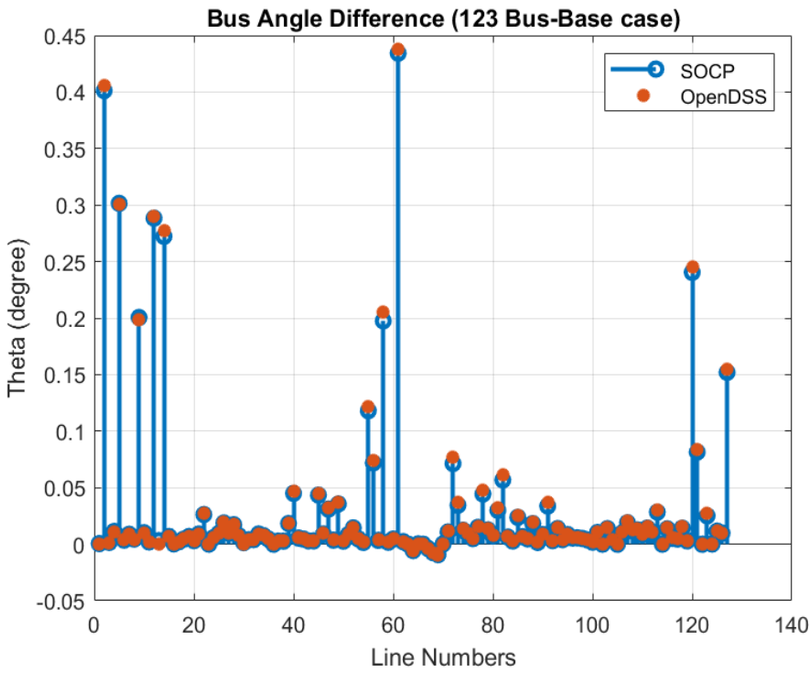

Figure 3.7: Bus voltage angle difference in IEEE 123-bus network base case.

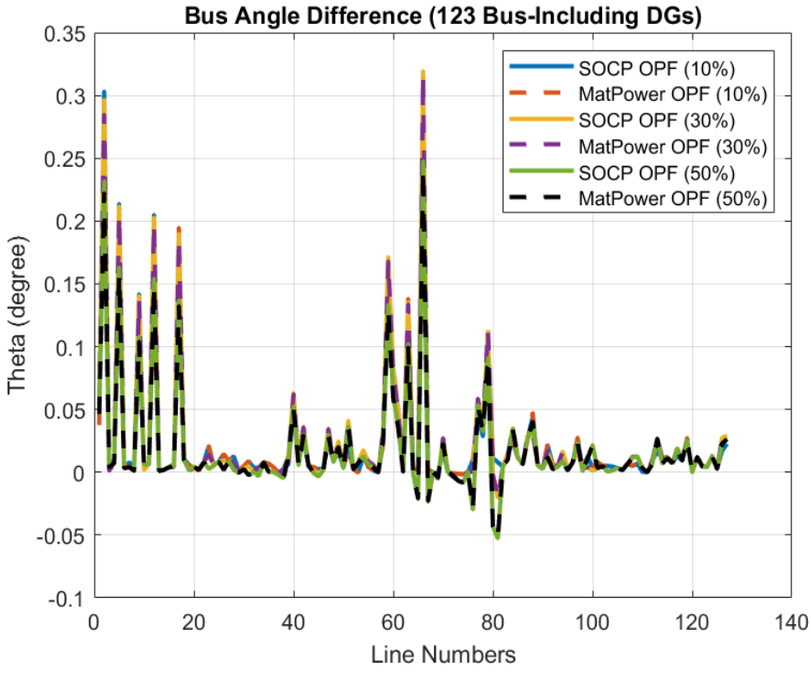

Figure 3.8: Bus voltage angle difference in IEEE 123-bus network with 10%, 30% and 50% DGs.

the voltage to any critical load bus with the control of DGs reactive power flow. Besides, it is shown that the proposed method can be more useful and economical than the load-tap changer (LTC) operations. The proposed control method's impact is shown in Fig. 3.9 (a)-(b) for IEEE 32-bus and for the IEEE 123-bus networks in 3.9 (c)-(d).

3.3.2.1 Case 1 (IEEE 32-Bus Test System)

In Fig. 3.9 (a), the change in voltage is shown at bus 12 of the IEEE 32-bus network. For a case, if a DG comes into production or if the voltage fluctuates due to the change of load, the proposed algorithm can maintain and regulate the voltage to its reference voltage level. In Fig. (3.9) (a), the 1st iteration voltage profile (red) is the fluctuation in the voltage due

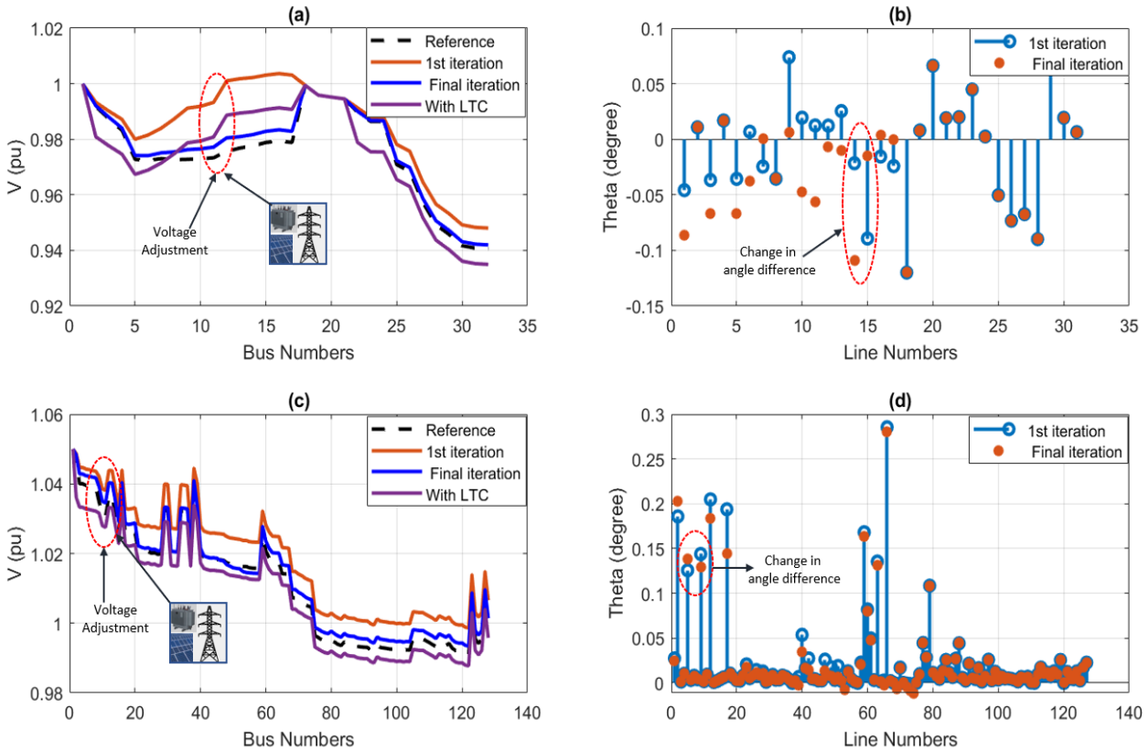

Figure 3.9: Voltage control with reactive power and angle difference management.

to the change of loading condition at the t_{th} period while the reference voltage profile (black) is the optimal point at the $(t-1)_{th}$ period. For voltage regulation, the reactive flow control algorithm is applied to the branches connected to bus 12. Line 14 and 15 are the connected lines to bus 12. It can be seen from the voltage profile (blue) after the final iteration that the voltage profile is near the reference voltage when introducing the proposed method. The voltage profile (purple) by controlling the LTC tap position at -2 is also shown in the same Fig. for comparison. This indicates that the proposed algorithm has better control over the voltage magnitude. Fig. 3.9(b) shows the change in the bus voltage angle difference across the lines connected to bus 12.

3.3.2.2 Case 1 (IEEE 123-Bus Test System)

The Algorithm 1 is also applied for the IEEE 123-bus network system for voltage regulation. Fig. 3.9 (c) shows the effectiveness of the proposed voltage and reactive flow control algorithm when there is a voltage fluctuation at bus 9 (original bus 7) in this research of the IEEE 123-bus network. The 1st iteration voltage profile (red) is the fluctuation in the voltage due to the change in loading condition at the t_{th} period, while the reference voltage profile (black) is the optimal point at the $(t-1)_{th}$ period. The voltage profile (blue) is the final iteration which is closer to the reference voltage (black). Also in Fig. 3.9 (c), the voltage profile (purple) for LTC tap position at -1 is shown. Fig. 3.9 (d) shows the change of the bus voltage angle difference at the lines 5 & 9, which are the connected branches to the bus 9. Angle difference in one branch is decreasing while increasing for the other branch, which controls the reactive flow, thus the voltage regulation. It can also be seen that the

tap position can be managed better especially if there is a DG source near the substation for a distribution network. Overall, it can be seen that the voltage can be controlled more precisely using the reactive flow control with the bus voltage angle difference adjustment from the algorithm proposed in this research.

3.4 Summary

This research has proposed and evaluated a branch flow-based SOCP OPF model capable of angle recovery and reactive power flow control and thus capable of voltage regulation. The proposed model concerns the branch current and branch power flows instead of only nodal injections. The recovered angle is in the form of bus angle difference for all interconnected lines throughout the network. Based on the retrieved angle, this research has also proposed a reactive flow control algorithm and voltage control. It is demonstrated that the proposed model is exact for the global OPF solution and tested in the modified IEEE 32-bus radial network and IEEE 123-bus network systems. Due to convexity, the model has better computational efficiency than the NLP OPF models. Finally, the proposed reactive flow and the voltage control algorithm provide a better and more economic control scheme in the power distribution networks.

CHAPTER 4: SECOND-ORDER CONE PROGRAMMING (SOCP) MODEL FOR THREE PHASE OPTIMAL POWER FLOW (OPF) IN ACTIVE DISTRIBUTION NETWORKS

4.1 Introduction and Contributions

With the high penetration of distributed renewable energy-based generations, power distribution system OPF modeling has become more complex. For instance, the conventional approach of iterative power flow methods becomes computationally complex and inaccurate, affecting the operation reliability of the power grid. Typically, OPF is formulated using AC power flow equations with additional constraints referred to as AC-OPF. However, the AC-OPF problem is challenging and hard to solve due to the quadratic and non-linear characteristics of the power flow equations [5, 15]. Due to the non-convexity of power flow equations and constraints, the original AC-OPF problem is NP-hard [13].

To overcome this issue, linear approximations of power flow equations such as DC-OPF [20] are commonly used, compromising the solution's accuracy. Also, the DC-OPF doesn't account for the optimal point of the reactive power and thus becomes unsuitable for an unbalanced distribution network [44]. Conversely, the convex relaxations of AC-OPF problems are generally shown to be exact under certain conditions and computationally efficient [90] [57] [70]. Due to the computational superiority and ability to find the optimal solutions, the convex AC-OPF formulations have been extensively used in power system optimization applications [91] [92] [93]. Typically, power distribution systems are unbalanced due to the unequal three-phase loads, untransposed lines, and conductor bundling [94]. Even though distribution networks are multi-phase and unbalanced, most OPF models for power distribution systems are developed based on single-phase network analysis [25]. In recent years, the high penetration of DERs has contributed heavily to further imbalance, which is challenging to forecast with single-phase OPF analysis due to the random generations [26]. So, this article proposes a three-phase SOCP-OPF model.

4.1.1 Existing Research Works:

Researchers have been exploring efficient OPF models for multi-phase power networks. A three-phase non-linear OPF model was proposed in [95], which includes the mutual impedance for minimizing network loss. The power flow formulation considers the inverse matrix of the primitive impedance matrix of size $(3n_l \times 3n_l)$, where 'n_l' is the number of branches in the network. This confines the scalability of the NLP-OPF model. Multiple ap-

proximated linear three-phase power flow models were proposed to overcome the scalability issue for active distribution networks considering different types of loads [14,18,96]. However, those linear models are approximated and thus will not provide exact solutions always. Besides these linear models, Chordal relaxation-based convex AC-OPF models for multi-phase unbalanced distribution systems have also been proposed in [17, 97]. Convex approaches, based on branch flow models (BFM) using semidefinite programming (SDP) and a linear model for OPF in multi-phase radial networks, were proposed in [66]. For the linear model, the line loss in the network is ignored. Another variant that extends the convex modeling to incorporate delta connections is proposed in [98] and the exactness of the convex relaxation is evaluated in [99]. For scalability, an SDP-OPF formulation for unbalanced microgrids was illustrated in [100], which is solvable in polynomial time. If the solution is infeasible for a system, sufficient conditions are developed to provide a feasible solution in [101, 102].

A convex SOCP load flow model for radial distribution networks was first proposed in [22]. For SOCP relaxation, the angle and conic relaxation steps are always exact for radial networks, provided there are no upper bounds on loads [68, 69]. In [90], a SOCP-based OPF framework decomposes the three-phase networks into three independent single-phase networks. One of the significant drawbacks of these state-of-the-art SOCP models is that these models ignore the mutual coupling in the multi-phase networks. Compared to the SOCP-OPF model, the SDP-OPF formulation is theoretically stronger [103]. However, in SDP-OPF models, the matrix size grows as the number of buses' squares, making it computationally challenging to solve OPF for a large network [104]. Moreover, SDP formulation finds a physically meaningful solution if the line-flow capacity is considerably high [101]. However, SOCP-based AC-OPF models are scalable, computationally feasible [105], and more efficient [90] compared to SDP-OPF models.

4.1.2 Major Contributions

This article proposes a BFM-based SOCP-OPF model that considers multi-phase mutual coupling effects. The proposed SOCP-OPF model aims to develop a computationally efficient and scalable three-phase OPF algorithm to find globally optimal solutions for unbalanced power distribution systems. The proposed OPF model is inspired by the research works in [68, 69, 106]. Numerical simulations have been conducted on different IEEE test networks to validate the proposed model's computational efficiency and scalability. The performance of the proposed SOCP-OPF model is compared with the BFM-SDP OPF [66], linear OPF [66], and NLP-OPF models. The salient contributions of the proposed work are:

- The proposed SOCP-OPF model provides an optimal global solution in multi-phase unbalanced distribution systems, including mutual coupling effects.

- The derivation of a convex representation of the ZIP loads for the proposed OPF model is included in the model.

- The approach is computationally feasible and scalable with high penetration of DERs'.

The chapter is organized as follows. Section 4.2 discusses the proposed three-phase OPF methodology and relaxation framework. Section 4.3 discusses the model's exactness and optimality. Section 4.4 evaluates the simulation results. Finally, Section 4.5 concludes the chapter with a summary.

The variable and parameters used in this chapter are as follows:

ξ^{ϕ}:	Coupling coefficient
$\mathcal{N}^{\phi}$:	Set of all buses in the network
$\mathcal{N}_g^{\phi}$:	Set of all buses with DERs in the network
$\mathcal{L}^{\phi}$:	Set of all branches in the network
V_i^{ϕ}:	Voltage at bus $N_i \in \mathcal{N}^{\phi}$
$\overline{V}_i^{\phi}$:	Max. voltage limit at bus $N_i \in \mathcal{N}^{\phi}$
$\underline{V}_i^{\phi}$:	Min. voltage limit at bus $N_i \in \mathcal{N}^{\phi}$
u_i^{ϕ}:	Square of the voltage magnitude at bus $N_i \in \mathcal{N}^{\phi}$
$[s_g^{\phi}]_i$:	Apparent power injection at bus $N_i \in \mathcal{N}_g^{\phi}$
$[s_d^{\phi}]_i$:	Apparent power demand at bus $N_i \in \mathcal{N}^{\phi}$
$[p_g^{\phi}]_i$:	Real power injection at bus $N_i \in \mathcal{N}_g^{\phi}$
$[p_d^{\phi}]_i$:	Real power demand at bus $N_i \in \mathcal{N}^{\phi}$
$[q_g^{\phi}]_i$:	Reactive power injection at bus $N_i \in \mathcal{N}_g^{\phi}$
$[q_d^{\phi}]_i$:	Reactive power demand at bus $N_i \in \mathcal{N}^{\phi}$
P_{ij}^{ϕ}:	Real power flow through line, $L_{ij}^{\phi} \in \mathcal{L}^{\phi}$
Q_{ij}^{ϕ}:	Reactive power flow through line, $L_{ij}^{\phi} \in \mathcal{L}^{\phi}$
I_{ij}^{ϕ}:	Current flow through line, $L_{ij}^{\phi} \in \mathcal{L}^{\phi}$
l_{ij}^{ϕ}:	Current magnitude square through line, $L_{ij}^{\phi} \in \mathcal{L}^{\phi}$
z_{ij}^{ϕ}:	Impedance of the branch, $L_{ij}^{\phi} \in \mathcal{L}^{\phi}$
r_{ij}^{ϕ}:	Resistance of the branch, $L_{ij}^{\phi} \in \mathcal{L}^{\phi}$
x_{ij}^{ϕ}:	Reactance of the branch, $L_{ij}^{\phi} \in \mathcal{L}^{\phi}$
$\overline{u}_i^{\phi}$:	Max. voltage magnitude square at bus $N_i \in \mathcal{N}^{\phi}$
$\underline{u}_i^{\phi}$:	Min. voltage magnitude square at bus $N_i \in \mathcal{N}^{\phi}$
$[\overline{p}_g^{\phi}]_i$:	Max. generator real power limit at bus $N_i \in \mathcal{N}_g^{\phi}$
$[\underline{p}_g^{\phi}]_i$:	Min. generator real power limit at bus $N_i \in \mathcal{N}_g^{\phi}$
$[\overline{q}_g^{\phi}]_i$:	Max. generator reactive power limit at bus $N_i \in \mathcal{N}_g^{\phi}$
$[\underline{q}_g^{\phi}]_i$:	Min. generator reactive power limit at bus $N_i \in \mathcal{N}_g^{\phi}$
$\overline{I}_{ij}^{\phi}$:	Max. current flow through the line, $L_{ij}^{\phi} \in \mathcal{L}^{\phi}$
$\underline{I}_{ij}^{\phi}$:	Min. current flow through the line, $L_{ij}^{\phi} \in \mathcal{L}^{\phi}$
$\overline{S}_{ij}^{\phi}$:	Max. apparent power flow through line, $L_{ij}^{\phi} \in \mathcal{L}^{\phi}$
$\underline{S}_{ij}^{\phi}$:	Min. apparent power flow through line, $L_{ij}^{\phi} \in \mathcal{L}^{\phi}$

4.2 Proposed Methodology

For the proposed OPF model, multi-phase radial distribution networks are considered where $\mathcal{L}^{\phi}$ represents the set of connected multi-phase branches, and $\mathcal{N}^{\phi}$ is the set of multi-phase buses in the network. N_i^{ϕ} and N_j^{ϕ} denote the bus indexes, which can be three, two, or single phases. For the branch $L_{ij}^{\phi} \in \mathcal{L}^{\phi}$, the multi-phase real power flow and reactive power flow are represented as P_{ij}^{ϕ} and Q_{ij}^{ϕ} respectively from bus $N_i^{\phi} \in \mathcal{N}^{\phi}$ to bus $N_j^{\phi} \in \mathcal{N}^{\phi}$. S_{ij}^{ϕ} is

the apparent power flow. $[p_g^\phi]_j$ and $[q_g^\phi]_j$ are the injected power while, $[p_d^\phi]_j$ and $[q_d^\phi]_j$ are the real and reactive power demand at the bus $N_j^\phi \in \mathcal{N}^\phi$.

4.2.1 Three-Phase Branch Flow Model

The power flow and the voltage drop of the multi-phase line segment $L_{ij}^\phi \in \mathcal{L}^\phi$ connecting two buses $N_i^\phi \in \mathcal{N}^\phi$ and $N_j^\phi \in \mathcal{N}^\phi$ of a network can be represented as follows:

$$S_{ij}^\phi = V_i^\phi I_{ij}^{\phi *} \tag{4.1}$$

$$V_i^\phi - V_j^\phi = z_{ij}^\phi I_{ij}^\phi \tag{4.2}$$

where I_{ij}^ϕ is the current flow from the bus $N_i^\phi \in \mathcal{N}^\phi$ to bus $N_j^\phi \in \mathcal{N}^\phi$ through the branch $L_{ij}^\phi \in \mathcal{L}^\phi$ with an impedance of z_{ij}^ϕ. The power balance at the bus $N_j^\phi \in \mathcal{N}^\phi$ is as follows:

$$\begin{aligned}\begin{bmatrix}[s_g^a]_j\\ [s_g^b]_j\\ [s_g^c]_j\end{bmatrix} - \begin{bmatrix}[s_d^a]_j\\ [s_d^b]_j\\ [s_d^c]_j\end{bmatrix} &= \sum_{k:j\to k} \begin{bmatrix}S_{jk}^a\\ S_{jk}^b\\ S_{jk}^c\end{bmatrix} - \sum_{i:i\to j} \begin{bmatrix}S_{ij}^a\\ S_{ij}^b\\ S_{ij}^c\end{bmatrix} \\ + \sum_{i:i\to j} \begin{bmatrix}z_{ij}^{aa} & z_{ij}^{ab} & z_{ij}^{ac}\\ z_{ij}^{ba} & z_{ij}^{bb} & z_{ij}^{bc}\\ z_{ij}^{ca} & z_{ij}^{cb} & z_{ij}^{cc}\end{bmatrix} &\begin{bmatrix}(I_{ij}^a)^2\\ (I_{ij}^b)^2\\ (I_{ij}^c)^2\end{bmatrix} + \begin{bmatrix}y^{aa*} & 0 & 0\\ 0 & y^{bb*} & 0\\ 0 & 0 & y^{cc*}\end{bmatrix} \begin{bmatrix}(V_j^a)^2\\ (V_j^b)^2\\ (V_j^c)^2\end{bmatrix}\end{aligned} \tag{4.3}$$

where $\{N_i^\phi, N_j^\phi, N_k^\phi\} \in \mathcal{N}^\phi$, and $\{L_{ij}^\phi, L_{jk}^\phi\} \in \mathcal{L}^\phi$. From (4.1) and (4.2) it can be derived as follows:

$$V_j^\phi = V_i^\phi - \frac{z_{ij}^\phi S_{ij}^{\phi *}}{V_i^{\phi *}} \tag{4.4}$$

Considering the square in (4.4), the voltage relationship between bus $N_i^\phi \in \mathcal{N}^\phi$ & bus $N_j^\phi \in \mathcal{N}^\phi$ is as follows:

$$\begin{aligned}\begin{bmatrix}(V_j^a)^2\\ (V_j^b)^2\\ (V_j^c)^2\end{bmatrix} = \begin{bmatrix}(V_i^a)^2\\ (V_i^b)^2\\ (V_i^c)^2\end{bmatrix} + \begin{bmatrix}(z_{ij}^{aa})^2 + (x_{ij}^{aa})^2 & (r_{ij}^{ab})^2 + (x_{ij}^{ab})^2 & (r_{ij}^{ac})^2 + (x_{ij}^{ac})^2\\ (r_{ij}^{ba})^2 + (x_{ij}^{ba})^2 & (r_{ij}^{bb})^2 + (x_{ij}^{bb})^2 & (r_{ij}^{bc})^2 + (x_{ij}^{bc})^2\\ (r_{ij}^{ca})2 + (x_{ij}^{ca})^2 & (r_{ij}^{cb})^2 + (x_{ij}^{cb})^2 & (r_{ij}^{cc})^2 + (x_{ij}^{cc})^2\end{bmatrix} \begin{bmatrix}(I_{ij}^a)^2\\ (I_{ij}^b)^2\\ (I_{ij}^c)^2\end{bmatrix} \\ - \begin{bmatrix}z_{ij}^{aa} & z_{ij}^{ab} & z_{ij}^{ac}\\ z_{ij}^{ba} & z_{ij}^{bb} & z_{ij}^{bc}\\ z_{ij}^{ca} & z_{ij}^{cb} & z_{ij}^{cc}\end{bmatrix} \begin{bmatrix}S_{ij}^{a\,*}\\ S_{ij}^{b\,*}\\ S_{ij}^{c\,*}\end{bmatrix} - \begin{bmatrix}z_{ij}^{aa*} & z_{ij}^{ab*} & z_{ij}^{ac*}\\ z_{ij}^{ba*} & z_{ij}^{bb*} & z_{ij}^{bc*}\\ z_{ij}^{ca*} & z_{ij}^{cb*} & z_{ij}^{cc*}\end{bmatrix} \begin{bmatrix}S_{ij}^a\\ S_{ij}^b\\ S_{ij}^c\end{bmatrix}\end{aligned} \tag{4.5}$$

where $z_{ij} = r_{ij} + jx_{ij}$. Relaxing the phase angle and considering, $|I_{ij}^{\phi}|^2 = l_{ij}^{\phi}$; $|V_j^{\phi}|^2 = u_j^{\phi}$ and $|V_i^{\phi}|^2 = u_i^{\phi}$; (4.5) can be represented as follows:

$$\begin{bmatrix} u_j^a \\ u_j^b \\ u_j^c \end{bmatrix} = \begin{bmatrix} u_i^a \\ u_i^b \\ u_i^c \end{bmatrix} + \begin{bmatrix} (z_{ij}^{aa})^2 + (x_{ij}^{aa})^2 & (r_{ij}^{ab})^2 + (x_{ij}^{ab})^2 & (r_{ij}^{ac})^2 + (x_{ij}^{ac})^2 \\ (r_{ij}^{ba})^2 + (x_{ij}^{ba})^2 & (r_{ij}^{bb})^2 + (x_{ij}^{bb})^2 & (r_{ij}^{bc})^2 + (x_{ij}^{bc})^2 \\ (r_{ij}^{ca)}2 + (x_{ij}^{ca})^2 & (r_{ij}^{cb})^2 + (x_{ij}^{cb})^2 & (r_{ij}^{cc})^2 + (x_{ij}^{cc})^2 \end{bmatrix} \begin{bmatrix} l_{ij}^a \\ l_{ij}^b \\ l_{ij}^c \end{bmatrix} - \begin{bmatrix} z_{ij}^{aa} & z_{ij}^{ab} & z_{ij}^{ac} \\ z_{ij}^{ba} & z_{ij}^{bb} & z_{ij}^{bc} \\ z_{ij}^{ca} & z_{ij}^{cb} & z_{ij}^{cc} \end{bmatrix} \begin{bmatrix} S_{ij}^{a\,*} \\ S_{ij}^{b\,*} \\ S_{ij}^{c\,*} \end{bmatrix} - \begin{bmatrix} z_{ij}^{aa*} & z_{ij}^{ab*} & z_{ij}^{ac*} \\ z_{ij}^{ba*} & z_{ij}^{bb*} & z_{ij}^{bc*} \\ z_{ij}^{ca*} & z_{ij}^{cb*} & z_{ij}^{cc*} \end{bmatrix} \begin{bmatrix} S_{ij}^a \\ S_{ij}^b \\ S_{ij}^c \end{bmatrix} \tag{4.6}$$

When the current $I_{ij}^{\phi} = |I_{ij}^{\phi}| \angle \theta_{ij}^{\phi}$ is not relaxed, the polarity of the current changes based on the phase angle. As the phase angle of the current is relaxed and $l_{ij}^{\phi} \geq 0$, (4.5) and (4.6) do not address the mutual coupling impact correctly. So a co-efficient ξ^{ϕ} is introduced with (4.6) to address the coupling effect for multi-phase networks properly. The angle relaxation is discussed in more detail in Section 4.2.2.1, and the derivation of the co-efficient ξ^{ϕ} for the proposed OPF model is discussed in section 4.2.3 of this article.

4.2.2 Convexification for the Proposed OPF Model

4.2.2.1 Angle Relaxation

The power flow equations from (4.1) to (4.5) are non-convex, and the mutual coupling effect on the multiple phases of the network depends on the phase angles. But, in the proposed convex model, the phase angle of the voltage and the current are relaxed as $I_{ij}^{\phi} \Rightarrow |I_{ij}^{\phi}|$ and $V_j^{\phi} \Rightarrow |V_j^{\phi}|$. So, to introduce the mutual coupling for multi-phase branches, a coupling coefficient ξ^{ϕ} is considered for the proposed OPF model. For the convexification of (4.1) to (4.5), new variables have been introduced with the model. Considering, $|I_{ij}^{\phi}|^2 = l_{ij}^{\phi}$; $|V_j^{\phi}|^2 = u_j^{\phi}$ and $|V_i^{\phi}|^2 = u_i^{\phi}$ and the coupling coefficient ξ^{ϕ}, the convex form of the power balance equation (4.3) can be written as:

$$\begin{bmatrix} [s_g^a]_j \\ [s_g^b]_j \\ [s_g^c]_j \end{bmatrix} - \begin{bmatrix} [s_d^a]_j \\ [s_d^b]_j \\ [s_d^c]_j \end{bmatrix} = \sum_{k:j\to k} \begin{bmatrix} S_{jk}^a \\ S_{jk}^b \\ S_{jk}^c \end{bmatrix} - \sum_{i:i\to j} \begin{bmatrix} S_{ij}^a \\ S_{ij}^b \\ S_{ij}^c \end{bmatrix} + \sum_{i:i\to j} \begin{bmatrix} z_{ij}^{aa} & \xi^b z_{ij}^{ab} & \xi^c z_{ij}^{ac} \\ \xi^a z_{ij}^{ba} & z_{ij}^{bb} & \xi^c z_{ij}^{bc} \\ \xi^a z_{ij}^{ca} & \xi^b z_{ij}^{cb} & z_{ij}^{cc} \end{bmatrix} \begin{bmatrix} l_{ij}^a \\ l_{ij}^b \\ l_{ij}^c \end{bmatrix} + \begin{bmatrix} y^{aa} & 0 & 0 \\ 0 & y^{bb} & 0 \\ 0 & 0 & y^{cc} \end{bmatrix} \begin{bmatrix} u_j^a \\ u_j^b \\ u_j^c \end{bmatrix} \tag{4.7}$$

where $\{\xi^a, \xi^b, \xi^c\} \in \xi^\phi$ refers to the coupling coefficients. Splitting the (4.7) in terms of real and reactive power after angle relaxation, the power balance at bus $N_j^\phi \in \mathcal{N}^\phi$ are as follows:

$$\begin{bmatrix} [p_g^a]_j \\ [p_g^b]_j \\ [p_g^c]_j \end{bmatrix} - \begin{bmatrix} [p_d^a]_j \\ [p_d^b]_j \\ [p_d^c]_j \end{bmatrix} = \sum_{k:j\to k} \begin{bmatrix} P_{jk}^a \\ P_{jk}^b \\ P_{jk}^c \end{bmatrix} - \sum_{i:i\to j} \begin{bmatrix} P_{ij}^a \\ P_{ij}^b \\ P_{ij}^c \end{bmatrix} + \sum_{i:i\to j} \begin{bmatrix} r_{ij}^{aa} & \xi^b r_{ij}^{ab} & \xi^c r_{ij}^{ac} \\ \xi^a r_{ij}^{ba} & r_{ij}^{bb} & \xi^c r_{ij}^{bc} \\ \xi^a r_{ij}^{ca} & \xi^b r_{ij}^{cb} & r_{ij}^{cc} \end{bmatrix} \begin{bmatrix} l_{ij}^a \\ l_{ij}^b \\ l_{ij}^c \end{bmatrix} + \begin{bmatrix} g^{aa} & 0 & 0 \\ 0 & g^{bb} & 0 \\ 0 & 0 & g^{cc} \end{bmatrix} \begin{bmatrix} u_j^a \\ u_j^b \\ u_j^c \end{bmatrix} \tag{4.8}$$

$$\begin{bmatrix} [q_g^a]_j \\ [q_g^b]_j \\ [q_g^c]_j \end{bmatrix} - \begin{bmatrix} [q_d^a]_j \\ [q_d^b]_j \\ [q_d^c]_j \end{bmatrix} = \sum_{k:j\to k} \begin{bmatrix} Q_{jk}^a \\ Q_{jk}^b \\ Q_{jk}^c \end{bmatrix} - \sum_{i:i\to j} \begin{bmatrix} Q_{ij}^a \\ Q_{ij}^b \\ Q_{ij}^c \end{bmatrix} + \sum_{i:i\to j} \begin{bmatrix} x_{ij}^{aa} & \xi^b x_{ij}^{ab} & \xi^c x_{ij}^{ac} \\ \xi^a x_{ij}^{ba} & x_{ij}^{bb} & \xi^c x_{ij}^{bc} \\ \xi^a x_{ij}^{ca} & \xi^b x_{ij}^{cb} & x_{ij}^{cc} \end{bmatrix} \begin{bmatrix} l_{ij}^a \\ l_{ij}^b \\ l_{ij}^c \end{bmatrix} + \begin{bmatrix} b^{aa} & 0 & 0 \\ 0 & b^{bb} & 0 \\ 0 & 0 & b^{cc} \end{bmatrix} \begin{bmatrix} u_j^a \\ u_j^b \\ u_j^c \end{bmatrix} \tag{4.9}$$

where $z_{ij}^\phi = r_{ij}^\phi + jx_{ij}^\phi$, $S_{ij}^\phi = P_{ij}^\phi + jQ_{ij}^\phi$, $y_j^\phi = g_j^\phi + jb_j^\phi$, $[s_g^\phi]_j = [p_g^\phi]_j + j[q_g^\phi]_j$, and $[s_d^\phi]_j = [p_d^\phi]_j + j[q_d^\phi]_j$.

As (4.6) does not address the mutual coupling impact; accordingly the coupling coefficient ξ^ϕ is introduced in (4.8) and (4.9). To address the voltage drop between the bus $N_i^\phi \in \mathcal{N}^\phi$ & bus $N_j^\phi \in \mathcal{N}^\phi$ the convex relationship can be written as:

$$\begin{bmatrix} u_j^a \\ u_j^b \\ u_j^c \end{bmatrix} = \begin{bmatrix} u_i^a \\ u_i^b \\ u_i^c \end{bmatrix} + \begin{bmatrix} [(r_{ij}^{aa})^2 + (x_{ij}^{aa})^2] & |\xi^b|[(r_{ij}^{ab})^2 + (x_{ij}^{ab})^2)] & |\xi^c|[(r_{ij}^{ac})^2 + (x_{ij}^{ac})^2)] \\ |\xi^a|[(r_{ij}^{ab})^2 + (x_{ij}^{ab2})] & [(r_{ij}^{bb})^2 + (x_{ij}^{bb})^2] & |\xi^c|[(r_{ij}^{bc})^2 + (x_{ij}^{bc})^2)] \\ |\xi^a|[(r_{ij}^{ca})^2 + (x_{ij}^{ca})^2)] & |\xi^b|[(r_{ij}^{cb})^2 + (x_{ij}^{cb2})] & [(r_{ij}^{cc})^2 + (x_{ij}^{cc})^2] \end{bmatrix} \begin{bmatrix} l_{ij}^a \\ l_{ij}^b \\ l_{ij}^c \end{bmatrix} - 2 \begin{bmatrix} r_{ij}^{aa} & \xi^b r_{ij}^{ab} & \xi^c r_{ij}^{ac} \\ \xi^a r_{ij}^{ba} & r_{ij}^{bb} & \xi^c r_{ij}^{bc} \\ \xi^a r_{ij}^{ca} & \xi^b r_{ij}^{cb} & r_{ij}^{cc} \end{bmatrix} \begin{bmatrix} P_{ij}^a \\ P_{ij}^b \\ P_{ij}^c \end{bmatrix} - 2 \begin{bmatrix} x_{ij}^{aa} & \xi^b x_{ij}^{ab} & \xi^c x_{ij}^{ac} \\ \xi^a x_{ij}^{ba} & x_{ij}^{bb} & \xi^c x_{ij}^{bc} \\ \xi^a x_{ij}^{ca} & \xi^b x_{ij}^{cb} & x_{ij}^{cc} \end{bmatrix} \begin{bmatrix} Q_{ij}^a \\ Q_{ij}^b \\ Q_{ij}^c \end{bmatrix} \tag{4.10}$$

where $[-]^T$ indicates the transpose of a matrix. For each of the branches in the network, the feasible set is still non-convex due to the quadratic equality as follows:

$$l_{ij}^\phi = \frac{(S_{ij}^\phi)^2}{u_i^\phi} \Rightarrow l_{ij}^\phi = \frac{(P_{ij}^\phi)^2 + (Q_{ij}^\phi)^2}{u_i^\phi} \tag{4.11}$$

4.2.2.2 Conic Relaxation

With the conic-relaxation, the non-convex optimal solution space is enclosed within a feasible convex space [107]. After the angle relaxation, the OPF model is still no-convex due to (4.11), which is convexified by the following conic relaxation with a conic inequality in (4.12). For the proposed OPF model, all branches (all phases independently) satisfy this conic constraint in (4.12).

$$u_i^{\phi} + l_{ij}^{\phi} \geq \left\| \begin{array}{c} 2P_{ij}^{\phi} \\ 2Q_{ij}^{\phi} \\ u_i^{\phi} - l_{ij}^{\phi} \end{array} \right\|_2 \tag{4.12}$$

4.2.2.3 OPF Architecture

For a power distribution network, the OPF solution is the point of operation to supply the demand in the whole network so that all physical laws of power flow are satisfied considering the imposed constraints. Suppose a power flow solution set is $\psi^{\phi} = \{s_i^{\phi}, S_{ij}^{\phi}, I_{ij}^{\phi}, V_i^{\phi}\}$ satisfies the objective considering the imposed constraints on the network, then ψ^{ϕ} will be the optimal point of operation for the network. As the proposed model in this chapter is convex, we have considered convex objective functions. We have considered the minimum real power loss, $r_{ij}^{\phi}|I_{ij}^{\phi}|^2$ and power generation cost, $c_i[P_g^{\phi}]_i$ as objectives in this article. So, the objective function $f(x_i^{\phi})$ is increasing with proportional to the current flow I_{ij}^{ϕ}. The objectives considered with the proposed branch flow SOCP-OPF model are as follows:

a) Network real power loss minimization:

$$min\{\sum_{L_{ij} \in \mathcal{L}^{\phi}} \left[r_{ij}^{\phi}\right] \left[l_{ij}^{\phi}\right]\} \tag{4.13}$$

b) Real power generation cost minimization:

$$min\{\sum_{N_i^{\phi} \in \mathcal{N}_g^{\phi}} c_i[p_g^{\phi}]_i\} \tag{4.14}$$

where c_i is the generation cost coefficient for the DER at the bus $N_i^{\phi} \in \mathcal{N}_g^{\phi}$. The decision variables are the power generation $[p_g^{\phi}]_i$ and $[q_g^{\phi}]_i$ in this chapter. Finally, the proposed SOCP-OPF model with a convex objective function is as follows:

$$min \sum_{N_i^{\phi} \in \mathcal{N}^{\phi}} f(x_i^{\phi}) \tag{4.15}$$

subject to: (4.8)-(4.10) and (4.12); with the following imposed constraints on the control

variables:

$$\begin{cases} [\underline{p}_g^{\phi}]_i \leq [p_g^{\phi}]_i \leq [\overline{p}_g^{\phi}]_i \\ [\underline{q}_g^{\phi}]_i \leq [q_g^{\phi}]_i \leq [\overline{q}_g^{\phi}]_i \\ \underline{u}_i^{\phi} \leq u_i^{\phi} \leq \overline{u}_i^{\phi} \\ l_{ij}^{\phi} \leq \overline{l}_{ij}^{\phi} \end{cases} \tag{4.16}$$

where $[p_g^{\phi}]_i$ and $[q_g^{\phi}]_i$ are the real and reactive power generation of the DER at the bus $N_i^{\phi} \in \mathcal{N}_g^{\phi}$. Voltage limits are defined as, $\underline{u}_i^{\phi} = |\underline{V}_i^{\phi}|^2$ and $\overline{u}_i^{\phi} = |\overline{V}_i^{\phi}|^2$ for the bus $N_i^{\phi} \in \mathcal{N}^{\phi}$. Current flow limit is defined as $\overline{l}_{ij}^{\phi} = |\overline{I}_{ij}^{\phi}|^2$. $\overline{I}_{ij}^{\phi}$ is the rated current flow limit for the branch $L_{ij}^{\phi} \in \mathcal{L}^{\phi}$.

4.2.3 Derivation of the Coupling Coefficient ξ^{ϕ}

For a three-phase system, the mutual coupling impact depends on the voltage and current phase angles. However, in the proposed SOCP-OPF model, the phase angles are relaxed, and new variables are introduced for convexification. Further, a new coupling coefficient ξ^{ϕ} is introduced to address the effect of the mutual coupling impedance effect. In this section, the derivation of ξ^{ϕ} is discussed. A three-phase line with a mutual coupling impedance effect is illustrated using Fig. 4.1. The voltage drop between the two ends of the line model in

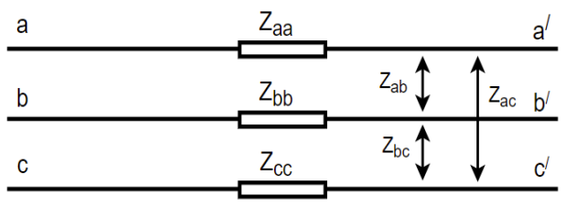

Figure 4.1: Three phase network line model.

Fig. 4.1 can be represented as follows:

$$V_a - V_{a/} = Z_{aa}I_a + Z_{ab}I_b + Z_{ac}I_c \tag{4.17}$$

If the square of the currents is considered for an unbalanced network, then $I_a^2 + I_b^2 + I_c^2 = |I_a|^2\angle 0 + |I_a|^2\angle(-240 + \alpha_1) + |I_a|^2\angle(240 + \alpha_2)$. For a three-phase network, this can be re-written as:

$$l_a + l_a(-.5 - .86j + \lambda^b) + l_a(-.5 + .86j + \lambda^c) \approx 0 \tag{4.18}$$

In (4.18), λ^b and λ^c are for the angle α_1 and α_2 which are due to the unbalanced nature of a power distribution networks and the imaginary parts of the 2^{nd} and 3^{rd} terms of (4.18) cancel out each other. As mentioned before, the phase angle is relaxed and convexified using

the amplitude of the current $|I_{ij}^{\phi}|^2 = l_{ij}^{\phi}$ and as $l_{ij}^{\phi} \geq 0$, the mutual coupling is adjusted with the help of the coupling coefficient ξ^{ϕ} so that, for a-phase $l_a + \xi^b l_a + \xi^c l_a \approx 0$. Therefore, comparing with the coefficients of (4.18):

$$[\xi^a, \xi^b, \xi^c] = -0.5 \pm \lambda^{\phi}$$

λ^{ϕ} stands as λ^a for the phase-a, λ^b for the phase-b and λ^c for the phase-c of a branch in the network. The value of λ^{ϕ} changes depending on the unbalanced nature of the network. The asymmetrical impedance of the low-voltage distribution networks, asymmetrical load, and single-phase loads result in unbalanced distribution networks. However, in practical systems, the network characteristics remain as close to a balanced network as possible [108, 109], so the value of λ^{ϕ} is small (i.e., for the IEEE 123-bus network λ^{ϕ}=[-0.1,0.1]).

4.2.4 Modeling of the ZIP Load

The proposed model is applicable to a network with ZIP loads as well. A ZIP load is formulated as follows [110]:

$$\begin{bmatrix} [p_d^a]_i \\ [p_d^b]_i \\ [p_d^c]_i \end{bmatrix} = \begin{bmatrix} [a_1^a]_i & 0 & 0 \\ 0 & [a_1^b]_i & 0 \\ 0 & 0 & [a_1^c]_i \end{bmatrix} \begin{bmatrix} u_i^a \\ u_i^b \\ u_i^c \end{bmatrix} + \begin{bmatrix} [a_2^a]_i & 0 & 0 \\ 0 & [a_2^b]_i & 0 \\ 0 & 0 & [a_2^c]_i \end{bmatrix} \begin{bmatrix} (u_i^a)^{1/2} \\ (u_i^b)^{1/2} \\ (u_i^c)^{1/2} \end{bmatrix} + \begin{bmatrix} [a_3^a]_i \\ [a_3^b]_i \\ [a_3^c]_i \end{bmatrix} \tag{4.19}$$

$$\begin{bmatrix} [q_d^a]_i \\ [q_d^b]_i \\ [q_d^c]_i \end{bmatrix} = \begin{bmatrix} [b_1^a]_i & 0 & 0 \\ 0 & [b_1^b]_i & 0 \\ 0 & 0 & [b_1^c]_i \end{bmatrix} \begin{bmatrix} u_i^a \\ u_i^b \\ u_i^c \end{bmatrix} + \begin{bmatrix} [b_2^a]_i & 0 & 0 \\ 0 & [b_2^b]_i & 0 \\ 0 & 0 & [b_2^c]_i \end{bmatrix} \begin{bmatrix} (u_i^a)^{1/2} \\ (u_i^b)^{1/2} \\ (u_i^c)^{1/2} \end{bmatrix} + \begin{bmatrix} [b_3^a]_i \\ [b_3^b]_i \\ [b_3^c]_i \end{bmatrix} \tag{4.20}$$

where $[a_1^{\phi}]_i$, $[a_2^{\phi}]_i$, $[a_3^{\phi}]_i$ and $[b_1^{\phi}]_i$, $[b_2^{\phi}]_i$, $[b_3^{\phi}]_i$ are scalar parameters for the active and reactive loads at the bus $N_i^{\phi} \in \mathcal{N}^{\phi}$. $[a_1^{\phi}]_i$ and $[b_1^{\phi}]_i$, $[a_2^{\phi}]_i$ and $[b_2^{\phi}]_i$, $[a_3^{\phi}]_i$ and $[b_3^{\phi}]_i$, are specified for the constant impedance (Z), constant current (I) and constant power (P) respectively. The constant current term in the ZIP load model is non-convex due to the variable $u_i^{1/2} = V_i$. However, a second-order variable can be convexified for a boundary near unity as follows [107]:

$$x^2 \approx (\underline{x} + \overline{x})x - \underline{x}\overline{x} \tag{4.21}$$

If the voltage constraints for the AC-OPF are $[\underline{V}_i, \overline{V}_i]$,

$$u_i \approx (\underline{V}_i + \overline{V}_i)V_i - \underline{V}_i\overline{V}_i; \quad i \in \mathcal{N} \tag{4.22}$$

In (4.19) and (4.20), the non-convex terms can be represented as the following for the convexification with the proposed model.

$$\begin{bmatrix}(u_i^a)^{1/2}\\(u_i^b)^{1/2}\\(u_i^c)^{1/2}\end{bmatrix} = \begin{bmatrix}V_i^a\\V_i^b\\V_i^c\end{bmatrix} \approx \begin{bmatrix}\frac{u_i^a+\overline{V}_i^a\underline{V}_i^a}{\overline{V}_i^a+\underline{V}_i^a}\\\frac{u_i^b+\overline{V}_i^b\underline{V}_i^b}{\overline{V}_i^b+\underline{V}_i^b}\\\frac{u_i^c+\overline{V}_i^c\underline{V}_i^c}{\overline{V}_i^c+\underline{V}_i^c}\end{bmatrix} \tag{4.23}$$

The reason for this conversion is that; it makes the model capable of analyzing the effect of voltage-dependent loads on the power distribution network.

4.2.5 Modeling of the Regulators

Regulators are essentially considered as tap-changing transformers in the model. The regulators/transformers in the network are generally used to keep the system voltages within the allowable range. Usually, distribution regulators have 16 taps up and 16 taps down of the rated voltage (33 tap positions, including the zero tap position). Each tap adjusts the voltage by 0.625% [111]. In the proposed model, the square of bus voltage magnitude ($|V^\phi|^2 = u^\phi$) is used, so the regulators and the transformers are modeled as described in this section. For the transformers/regulators, $ratio = [a_a, a_b, a_c]$, where $[V_s^a, V_s^b, V_s^c]^T = [a_a V_p^a, a_b V_p^b, a_c V_p^c]^T$ and $[Z_{ij_s}^a, Z_{ij_s}^b, Z_{ij_s}^c]^T = [a_a^2 Z_{ij_p}^a, a_b^2 Z_{ij_p}^b, a_c^2 Z_{ij_p}^c]^T$ then the ratio can be represented as follows:

$$\begin{bmatrix}a_a\\a_b\\a_c\end{bmatrix} = \begin{bmatrix}1 & 0.00625\\1 & 0.00625\\1 & 0.00625\end{bmatrix}\begin{bmatrix}1 & 1 & 1\\n^a & n^b & n^c\end{bmatrix} \tag{4.24}$$

where n^ϕ is the tap number of the regulator. This article does not consider the mixed integer OPF, and n^ϕ is not a variable. For a branch where regulators and transformers are placed, the voltage can be represented as follows:

$$\begin{aligned}\begin{bmatrix}u_j^a\\u_j^b\\u_j^c\end{bmatrix} = \begin{bmatrix}u_i^a a_a^2\\u_i^b a_b^2\\u_i^c a_c^2\end{bmatrix} + \begin{bmatrix}[(r_{ij}^{aa})^2+(x_{ij}^{aa})^2] & |\xi^b|[(r_{ij}^{ab})^2+(x_{ij}^{ab})^2] & |\xi^c|[(r_{ij}^{ac2}+(x_{ij}^{ac})^2]\\|\xi^a|[(r_{ij}^{ab})^2+(x_{ij}^{ab})^2)] & [r_{ij}^{bb2}+(x_{ij}^{bb})^2] & |\xi^c|[(r_{ij}^{bc2}+(x_{ij}^{bc})^2]\\|\xi^a|[(r_{ij}^{ca})^2+(x_{ij}^{ca})^2] & |\xi^b|[(r_{ij}^{cb})^2+(x_{ij}^{cb})^2] & [(r_{ij}^{cc})^2+(x_{ij}^{cc})^2]\end{bmatrix}\begin{bmatrix}l_{ij}^a\\l_{ij}^b\\l_{ij}^c\end{bmatrix}\\ -2\left\{\begin{bmatrix}r_{ij}^{aa} & \xi^b r_{ij}^{ab} & \xi^c r_{ij}^{ac}\\\xi^a r_{ij}^{ba} & r_{ij}^{bb} & \xi^c r_{ij}^{bc}\\\xi^a r_{ij}^{ca} & \xi^b r_{ij}^{cb} & r_{ij}^{cc}\end{bmatrix}\begin{bmatrix}P_{ij}^a\\P_{ij}^b\\P_{ij}^c\end{bmatrix}\right\}.\times\begin{bmatrix}a_a\\a_b\\a_c\end{bmatrix} - 2\left\{\begin{bmatrix}x_{ij}^{aa} & \xi^b x_{ij}^{ab} & \xi^c x_{ij}^{ac}\\\xi^a x_{ij}^{ba} & x_{ij}^{bb} & \xi^c x_{ij}^{bc}\\\xi^a x_{ij}^{ca} & \xi^b x_{ij}^{cb} & x_{ij}^{cc}\end{bmatrix}\begin{bmatrix}Q_{ij}^a\\Q_{ij}^b\\Q_{ij}^c\end{bmatrix}\right\}.\times\begin{bmatrix}a_a\\a_b\\a_c\end{bmatrix}\end{aligned} \tag{4.25}$$

where $[-].\times[-]$ represents the element-wise multiplication.

4.3 Exactness and Optimality of the OPF Model

This section discusses the exactness and optimality of the proposed SOCP-OPF model for multi-phase radial networks.

4.3.1 Exactness

The exactness of SOCP relaxation for single-phase OPF is guaranteed under certain conditions, which are illustrated in [90] [57, 70]. For single-phase radial power networks, the power flow relations are as follows:

$$S_{jk} = s_j + \sum_{i:i\to j}(S_{ij} - z_{ij}l_{ij})u_j - u_k = 2Re(z_{jk}^* S_{jk}) - |z_{jk}|^2 l_{jk} u_j l_{jk} \geq |S_{jk}|^2 \tag{4.26a}$$

For linear approximation, $[l_{ij}, l_{jk}] = 0$ is considered in (4.26). In radial networks, for a solution set s from the linear model, the line flow and the voltage amplitude square are defined as S_{jk}^{lin} and u_j^{lin}, respectively. For a power flow direction from bus N_j to bus 0 (substation bus) through a unique path $\mathcal{P}_i$ of the network, it is proved in [90], that $S_{jk} \leq S_{jk}^{lin}$ and $u_j \leq u_j^{lin}$. Physically, S_{jk}^{lin} denotes the power injections through branch $L_{jk} \in \mathcal{P}_i$ towards the bus 0. For checking the tightness, a matrix function is defined as:

$$\underline{A}_{jk} = I_2 - \frac{2}{\underline{u}_j}[z_{jk}]\Big([S_{jk}^{lin}(\bar{s})]^+\Big) \tag{4.27}$$

where $\bar{s}$ is the maximum capacity of power injection and I_2 is an identity matrix of size (2×2). Further, $[z_{ij}] = [r_{ij} \;\; x_{ij}]^T$ and $[S_{jk}^{lin}(\bar{s})]^+ = [[P_{jk}^{lin}(\bar{s})]^+ \;\; [Q_{jk}^{lin}(\bar{s})]^+]$ with the definition as, $[a_j]^+ = max\{0, a_j\}$. For convenience, $\underline{A}_{jk}$ and z_{jk} are labeled as $\underline{A}_j$ and z_i for further discussion. If $\mathcal{S}_{volt}$ is a power injection region where voltage upper bounds do not bind and the objective function $f(x)$ is strictly increasing, then SOCP is exact if the following conditions hold [90]:

1. If, in the network, for each unique path $\mathcal{P}_i$ from bus N_j to bus 0 have k links as $((i_k, i_{k-1}), ..., (i_1, i_0))$. Then $\underline{A}_{i_s}\underline{A}_{i_{s+1}}...\underline{A}_{i_{t-1}} z_{i_t} > 0$ for all $1 \leq s \leq t \leq k$.

2. The power injections (s) satisfies $u_j^{lin}(s) \leq \overline{u}_j$.

The condition (1) depends on the network parameters (r_{ij}, x_{ij}, $\overline{p}_i$, $\overline{q}_i$, $\underline{u}_i$), which can be checked ex-ante the OPF analysis. For the proposed SOCP-OPF model in this article, the line impedance is addressed in (4.7)-(4.10) considering the mutual impedance with the means of a coupling coefficient ξ^ϕ. For all the branches in each phase, the conic constraint (4.12) is satisfied independently. For multi-phase networks, even with the mutual coupling, the conditions $S_{jk}^\phi \leq S_{jk}^{\phi,lin}$ and $u_j^\phi \leq u_j^{\phi,lin}$ are valid for each phase independently which is proved in the following sub-section in 4.3.1.1. When $u_j^{\phi,lin}(s) \leq \overline{u}_i^\phi$, SOCP relaxation is exact

for the proposed model if the following condition satisfies.

- For each phase of the network independently, with each unique path $\mathcal{P}_i$ from bus N_j to bus 0; $\underline{A}^{\phi}_{i_s}\underline{A}^{\phi}_{i_{s+1}}...\underline{A}^{\phi}_{i_{t-1}}z^{\phi}_{i_t} > 0$ for all $1 \leq s \leq t \leq k$.

This can be checked ex-ante of the SOCP-OPF analysis. The SOCP-OPF is exact if all branches have a minimum solution gap. The solution gap, defined as $\sigma = |u_i l^{\phi}_{ij} - (S^{\phi}_{ij})^2|$ is measured after the OPF analysis. It was observed that the solution gap (σ) is very small from the proposed model (considered as $\sigma \leq 10^{-7}$).

4.3.1.1 Proof of Exactness

For each unique path ($\mathcal{P}_i$) in the radial network for a power flow from bus N_j to bus 0 in phase-a:

$$S^a_{jk} = s_j + \sum_{i:i\to j}(S^a_{ij} - z^{aa}_{ij}l^a_{ij} - \xi^b z^{ab}_{ij}l^b_{ij} - \xi^c z^{ac}_{ij}l^c_{ij})$$

For linear approximation, $[l^a_{ij}, l^b_{ij}, l^c_{ij}] = 0$; so for a power injection for the phase-a at bus N^a_j:

$$S^{a,lin}_{jk} = s_j + \sum_{i:i\to j} S^{a,lin}_{ij}(s)$$

When in practical power networks, self-impedance is higher than mutual impedance $S^a_{jk} \leq S^{a,lin}_{jk}(s)$. In the same way, it can also be shown for the other phases. So in general form, it is proved as, $S^{\phi}_{jk} \leq S^{\phi,lin}_{jk}(s)$. From the proposed OPF model, the voltage drop relationship between bus N^a_j and N^a_k for the phase-a is as follows:

$$u^a_j - u^a_k = 2Re(z^{a*}_{jk}S^{\phi}_{jk}) - |z^{aa}_{jk}|^2 l^a_{jk} - |\xi^b||z^{ab}_{jk}|^2 l^b_{jk} - |\xi^c||z^{ac}_{jk}|^2 l^c_{jk}$$

where $z^a_{jk} = [z^{aa}_{jk} \;\; \xi^b z^{ab}_{jk} \;\; \xi^c z^{ac}_{jk}]$; $S^{\phi}_{jk} = [S^a_{jk} \;\; S^b_{jk} \;\; S^c_{jk}]^T$. If the voltage amplitude square at the bus 0 is u^{ϕ}_0, then for power flow from bus N^a_j to bus 0 through each unique path $\mathcal{P}_i$, the voltage relation for phase-a is as follows:

$$\begin{aligned}
&u^a_j - u^a_0 = 2\sum_{(j,k)\in\mathcal{P}_i} Re(z^{a*}_{jk}S^{\phi}_{jk}) \\
&- \sum_{(j,k)\in\mathcal{P}_i}(|z^{aa}_{jk}|^2 l^a_{jk} + |\xi^b||z^{ab}_{jk}|^2 l^b_{jk} + |\xi^c||z^{ac}_{jk}|^2 l^c_{jk}) \\
&\Rightarrow u^a_j - u^a_0 \leq 2\sum_{(j,k)\in\mathcal{P}_i} Re(z^{a*}_{jk}S^{\phi}_{jk}) \\
&\Rightarrow u^a_j - u^a_0 \leq 2\sum_{(j,k)\in\mathcal{P}_i} Re(z^{a*}_{jk}S^{\phi,lin}_{jk}(s)) \\
&\Rightarrow u^a_j - u^a_0 \leq u^{a,lin}_j - u^a_0 \\
&\Rightarrow u^a_j \leq u^{a,lin}_j
\end{aligned}$$

In the same way, it can also be shown for the other phases. So in general form it is proved as; $u_j^{\phi} \leq u_j^{\phi,lin}$.

4.3.2 Optimality

The objective function $f(x_i^{\phi})$ for the proposed OPF model is convex and increasing with the current flow 'I_{ij}^{ϕ}'. Let us consider an optimal solution set from the proposed SOCP-OPF model as, $\tilde{\psi} = (\tilde{S}_{ij}^{\phi}, \tilde{l}_{ij}^{\phi}, \tilde{u}^{\phi}, \tilde{s}_g^{\phi})$; where a branch $L_{ij}^{\phi} \in \mathcal{L}^{\phi}$ has strict inequality such that $\tilde{u}_i^{\phi}\tilde{l}_{ij}^{\phi} > (\tilde{P}_{ij}^{\phi})^2 + (\tilde{Q}_{ij}^{\phi})^2$. Further, let us assume there exists another feasible solution set as $\hat{\psi} = (\hat{S}_{ij}^{\phi}, \hat{l}_{ij}^{\phi}, \hat{u}^{\phi}, \hat{s}_g^{\phi})$, where $\hat{l}_{ij}^{\phi} = \tilde{l}_{ij}^{\phi} - \epsilon^{\phi}$, $\hat{S}_{ij}^{\phi} = \tilde{S}_{ij}^{\phi} - \epsilon^{\phi}\xi^{\phi}z_{ij}^{\phi}$, $\hat{u}_i^{\phi} = \tilde{u}_i^{\phi}$, $[\hat{s}_g^{\phi}]_i = [\tilde{s}_g^{\phi}]_i$, $[\hat{s}_d^{\phi}]_i = [\tilde{s}_d^{\phi}]_i + \epsilon^{\phi}\xi^{\phi}z_{ij}^{\phi}$ and $[\hat{s}_d^{\phi}]_j = [\tilde{s}_d^{\phi}]_j$ for a $\epsilon^{\phi} \geq 0$. As $\hat{l}_{ij}^{\phi} = \tilde{l}_{ij}^{\phi} - \epsilon^{\phi}$ has a strict smaller value, then the OPF objective value $f(\hat{\psi})$ is smaller than the objective value as $f(\tilde{\psi})$. This contradicts the optimality of the solution set $\tilde{\psi}$. Thus to prove that the solution $\tilde{\psi}$ is a globally optimal solution, it is sufficient to show $\epsilon^{\phi} = 0$. The following remarks illustrate the optimality of the proposed SOCP-OPF model.

Remark. *An optimal point of solution will be within the convex space if the solution satisfies (4.8)-(4.10), (4.12) and (4.16).*

Proof. As, $\tilde{\psi}$ is an optimal solution from the proposed SOCP-OPF model, so it satisfies (4.8)-(4.10), (4.12) and (4.16). For analyzing (4.8)-(4.9) together, the power flow equation with the apparent power generation s_g^{ϕ} and apparent power flow S_{ij}^{ϕ} are considered here for the bus $N_i^{\phi} \in \mathcal{N}^{\phi}$ and $N_j^{\phi} \in \mathcal{N}^{\phi}$. If, $\hat{\psi}$ is a solution within the solution space, $\hat{\psi}$ also satisfies (4.8)-(4.10), (4.12) and (4.16). For the solution set $\hat{\psi}$ at the bus $N_i^{\phi} \in \mathcal{N}^{\phi}$:

$$
\begin{aligned}
\hat{s}_i^{\phi} &= [\hat{s}_g^{\phi}]_i - [\hat{s}_d^{\phi}]_i = [\tilde{s}_g^{\phi}]_i - [\tilde{s}_d^{\phi}]_i - \epsilon^{\phi}\xi^{\phi}z_{ij}^{\phi} \\
&= \sum_{j:i\to j} \tilde{S}_{ij}^{\phi} - \sum_{k:k\to i} (\tilde{S}_{ki}^{\phi} - \xi^{\phi}z_{ki}^{\phi}\tilde{l}_{ki}^{\phi}) + {y_i}^{\phi}\tilde{u}_i^{\phi} - \epsilon^{\phi}\xi^{\phi}z_{ij}^{\phi} \\
&= \sum_{j':i\to j', j\neq j'} \hat{S}_{ij'}^{\phi} + (\hat{S}_{ij}^{\phi} + \epsilon^{\phi}\xi^{\phi}z_{ij}^{\phi}) - \sum_{k:k\to i} (\hat{S}_{ki}^{\phi} - \xi^{\phi}z_{ki}^{\phi}\hat{l}_{ki}^{\phi}) + {y_i}^{\phi}\hat{u}_i^{\phi} - \epsilon^{\phi}\xi^{\phi}z_{ij}^{\phi} \\
&= \sum_{j:i\to j} \hat{S}_{ij}^{\phi} - \sum_{k:k\to i} (\hat{S}_{ki}^{\phi} - \xi^{\phi}z_{ki}^{\phi}\hat{l}_{ki}^{\phi}) + {y_i}^{\phi}\hat{u}_i^{\phi}
\end{aligned}
$$

At the bus $N_j^{\phi} \in \mathcal{N}^{\phi}$,

$$
\begin{aligned}
\hat{s}_j^{\phi} &= [\hat{s}_g^{\phi}]_j - [\hat{s}_d^{\phi}]_j = [\tilde{s}_g^{\phi}]_j - [\tilde{s}_d^{\phi}]_j \\
&= \sum_{k:j\to k} \tilde{S}_{jk}^{\phi} - \sum_{i:i\to j} (\tilde{S}_{ij}^{\phi} - \xi^{\phi}z_{ij}^{\phi}\tilde{l}_{ij}^{\phi}) + y_j\tilde{u}_j^{\phi} \\
&= \sum_{k:j\to k} \hat{S}_{jk}^{\phi} - \sum_{i':i'\to j, i'\neq i} (\hat{S}_{i'j}^{\phi} - \xi^{\phi}z_{i'j}^{\phi}\hat{l}_{i'j}^{\phi}) + y_j\hat{u}_j^{\phi} - [(\hat{S}_{ij}^{\phi} + \epsilon^{\phi}\xi^{\phi}z_{ij}^{\phi}) - \xi^{\phi}z_{ij}^{\phi}(\hat{l}_{ij}^{\phi} + \epsilon^{\phi})] \\
&= \sum_{k:j\to k} \hat{S}_{jk}^{\phi} - \sum_{i:i\to j} (\hat{S}_{ij}^{\phi} - \xi^{\phi}z_{ij}^{\phi}\hat{l}_{ij}^{\phi}) + y_j\hat{u}_j^{\phi}
\end{aligned}
$$

So, for both nodes $N_i^\phi \in \mathcal{N}^\phi$ & $N_j^\phi \in \mathcal{N}^\phi$, $\hat{\psi}$ satisfies (4.8)-(4.9). For $\hat{\psi}$, (4.10) is checked for the branch $L_{ij} \in \mathcal{L}^\phi$ as follows:

$$\begin{aligned}
&\tilde{u_j}^\phi = \tilde{u_i}^\phi - 2\xi^\phi(r_{ij}^\phi \tilde{P}_{ij}^\phi + x_{ij}^\phi \tilde{Q}_{ij}^\phi) + [(r_{ij}^\phi)^2 + (x_{ij}^\phi)^2]|\xi^\phi|\tilde{l}_{ij}^\phi \\
&\Rightarrow \hat{u_j}^\phi = \hat{u_i}^\phi - 2\xi^\phi[r_{ij}^\phi(\hat{P}_{ij}^\phi + \epsilon^\phi \xi^\phi r_{ij}^\phi) + x_{ij}^\phi(\hat{Q}_{ij}^\phi + \epsilon^\phi \xi^\phi x_{ij}^\phi)] + [(r_{ij}^\phi)^2 + (x_{ij}^\phi)^2]|\xi^\phi|(\hat{l}_{ij}^\phi + \epsilon^\phi) \\
&\Rightarrow \hat{u_j}^\phi = \hat{u_i}^\phi - 2\xi^\phi(r_{ij}^\phi \hat{P}_{ij}^\phi + x_{ij}^\phi \hat{Q}_{ij}^\phi) + [(r_{ij}^\phi)^2 + (x_{ij}^\phi)^2]|\xi^\phi|\hat{l}_{ij}^\phi \\
&\qquad\qquad - 2{\xi^\phi}^2\epsilon^\phi[(r_{ij}^\phi)^2 + (x_{ij}^\phi)^2] + |\xi^\phi|\epsilon^\phi[(r_{ij}^\phi)^2 + (x_{ij}^\phi)^2]
\end{aligned}$$

In the proposed model, it is derived that $\xi^\phi = -0.5 \pm |\lambda|$. Hence, $-2{\xi^\phi}^2\epsilon^\phi[(r_{ij}^\phi)^2 + (x_{ij}^\phi)^2] + |\xi^\phi|\epsilon^\phi[(r_{ij}^\phi)^2 + (x_{ij}^\phi)^2] \approx 0$. So, $\hat{\psi}$ satisfies (4.10) for the link $L_{ij} \in \mathcal{L}^\phi$, as follows:

$$\hat{u}_j^\phi = \hat{u}_i^\phi - 2\xi^\phi(r_{ij}^\phi \hat{P}_{ij}^\phi + x_{ij}^\phi \hat{Q}_{ij}^\phi) + [(r_{ij}^\phi)^2 + (x_{ij}^\phi)^2]|\xi^\phi|\hat{l}_{ij}^\phi$$

As, $\tilde{\psi}$ is within the conic convex space then from (4.12):

$$\begin{aligned}
&\tilde{u}_i^\phi \tilde{l}_{ij}^\phi - (\tilde{S}_{ij}^\phi)^2 > 0 \\
&\Rightarrow \hat{u_i}^\phi(\hat{l}_{ij}^\phi + \epsilon^\phi) - (\hat{S}_{ij}^\phi + \xi^\phi z_{ij}^\phi \epsilon^\phi)^2 > 0 \\
&\Rightarrow \hat{u_i}^\phi \hat{l}_{ij}^\phi - (\hat{S}_{ij}^\phi)^2 + \epsilon^\phi[\hat{u}_i^\phi - (\xi^\phi)^2(z_{ij}^\phi)^2\epsilon^\phi - 2\hat{S}_{ij}^\phi \xi^\phi z_{ij}^\phi] > 0
\end{aligned}$$

$\epsilon^\phi[\hat{u}_i^\phi - (\xi^\phi)^2(z_{ij}^\phi)^2\epsilon^\phi - 2\hat{S}_{ij}^\phi \xi^\phi z_{ij}^\phi]$ is negligible when the relaxation is exact for a power network.

□

Remark. *If $\epsilon = 0$, then $\tilde{\psi} = \hat{\psi}$, so no other solution set exists within the solution space for which the objective function value is smaller than $f(\tilde{\psi})$. The solution $\tilde{\psi}$ from the proposed OPF model is globally optimal.*

Proof. In this article, the objective function $f(x_i^\phi)$ is convex for the proposed SOCP-OPF model. For the two minima at $\tilde{\psi}$ and $\hat{\psi}$, $f(\hat{\psi}) \leq f(\tilde{\psi})$. From the definition of convexity:

$$f(h\hat{\psi} + (1-h)\tilde{\psi}) \leq hf(\hat{\psi}) + (1-h)f(\tilde{\psi}) \tag{4.28}$$

where $h \in [0, 1]$. As $hf(\hat{\psi}) \leq hf(\tilde{\psi})$; then,

$$hf(\hat{\psi}) + (1-h)f(\tilde{\psi}) \leq hf(\tilde{\psi}) + (1-h)f(\tilde{\psi}) \Rightarrow hf(\hat{\psi}) + (1-h)f(\tilde{\psi}) \leq f(\tilde{\psi})$$

Using (4.29) to the definition of the convexity in (4.28):

$$f(h\hat{\psi} + (1-h)\tilde{\psi}) \leq f(\tilde{\psi}) \tag{4.29}$$

Since $f(\tilde{\psi})$ is the optimal point from the proposed OPF model, so for any other solution

within the space is $f(\psi) > f(\tilde{\psi})$. Which contradicts with (4.29). To satisfy both conditions it must be $\tilde{\psi} = \hat{\psi}$, thus $\epsilon^{\phi} = 0$. So, the solution from the proposed model is a globally optimal solution for convex objectives. □

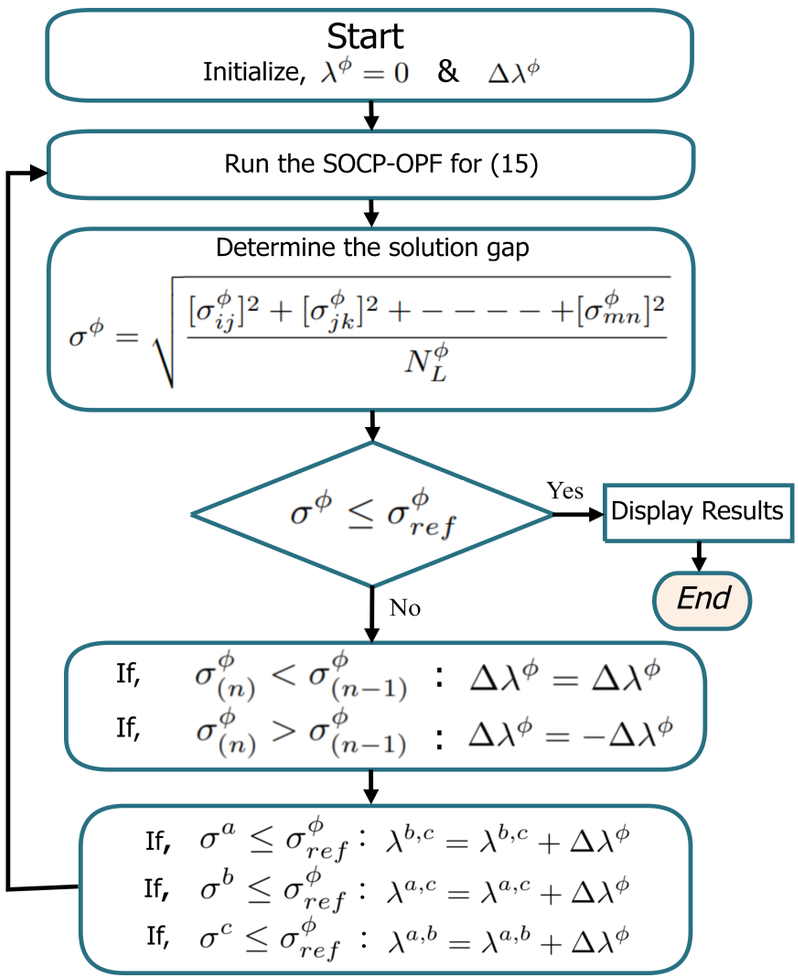

Figure 4.2: Flow chart of the proposed SOCP-OPF algorithm. The 'n' indicates the iteration number.

Table 4.1: λ^{ϕ} swipe and % of network loss in the IEEE 123-bus (with 20% DERs) network

No.	λ^{a}	Optimal λ^{b}	Optimal λ^{c}	% of Network Loss
Point of Operation-1	-0.1	0.05	0.05	2.6830
Point of Operation-2	0.0	0	0	2.6171
Point of Operation-3	0.1	0.045	0.055	2.5808

4.3.3 Inclusion of λ^{ϕ} in the Proposed OPF Model

The proposed SOCP-OPF model solves unbalanced distribution networks for an optimal point of operation with conic relaxation. Inclusion of λ^{ϕ} and the minimization of solution gap $\sigma = |u_i l_{ij}^{\phi} - (S_{ij}^{\phi})^2|$ is illustrated in Fig. 4.2. The determination of the λ^{ϕ} depends on the σ^{ϕ} and requires multiple iterations based on the unbalanced nature of the network. σ_{ref}^{ϕ} and the increment step size of $\Delta\lambda^{\phi}$ are defined at the optimization's beginning. After solving the optimization for (4.14), the average of solution gap σ^{ϕ} is determined and checked with the σ_{ref}^{ϕ} for determining the optimal value of λ^{ϕ} (i.e., λ^{a},λ^{b} & λ^{c}) for the network. Among the iteration steps (n) few points of operation (i.e.,$\lambda^{a} = -0.1$, $\lambda^{a} = 0.0$, $\lambda^{a} = 0.1$) are shown

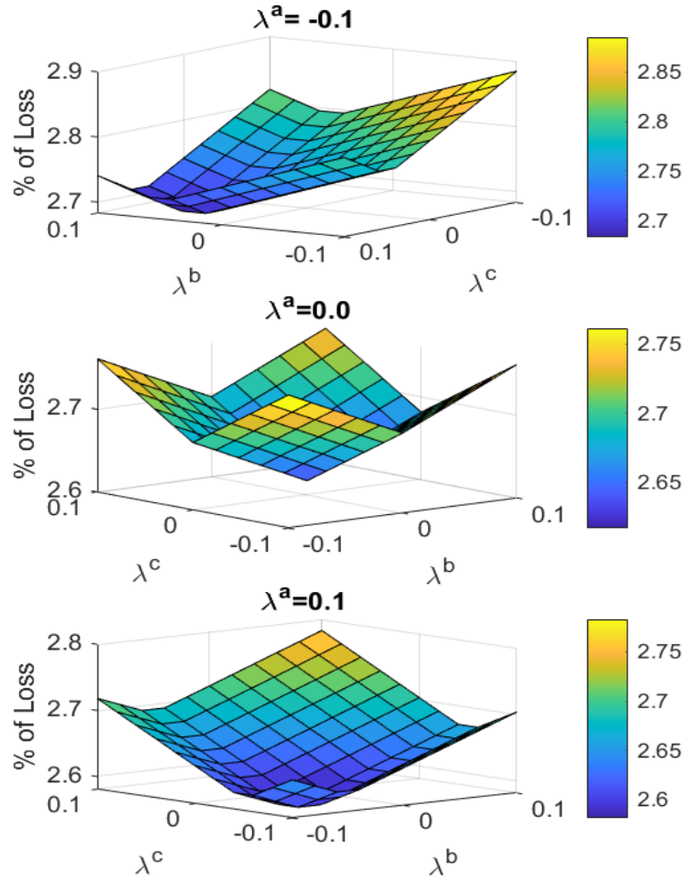

Figure 4.3: Illustration of the λ^{ϕ} swipe for the IEEE 123-bus network (with 20% DERs).

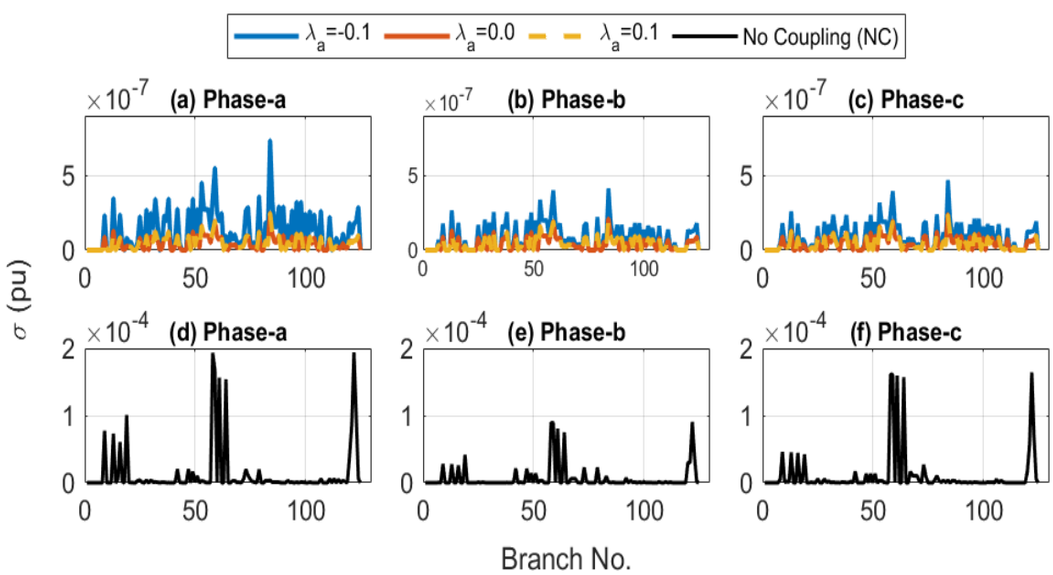

Figure 4.4: Illustration of the solution gap (σ) with the λ^{ϕ} sweep for the IEEE 123-bus network (with 20% DERs). (a), (b) & (c) considering coupling coefficient (ξ^{ϕ}) and (d), (e) & (f) with no coupling impact.

in Fig. 4.3 for the IEEE 123-bus network (with DERs), how the point of OPF varies with the value of λ^{ϕ}. Fig. 4.4 shows the impact of λ^{b}, λ^{c} and λ^{a} on the solution gap (σ). If the coupling impact is not considered, the solution gap is higher. The desired values of the λ^{ϕ} are determined when the value of the objective function is minimum. With the change of λ^{ϕ}, three operation points are represented in Table 4.1 as an example, and the desired values

are $\lambda^a = 0.1, \lambda^b = 0.045$, and $\lambda^c = 0.055$. The proposed model is implemented on different practical IEEE networks for analysis, and the results are discussed in the next section.

4.4 Simulation and Evaluation

The proposed SOCP-OPF model is simulated in Matlab with the MOSEK solver with a machine configuring an Intel(R) Core(TM) i7-10510U CPU @ 2.30 GHz processor, 16 GB RAM. It is observed that the model can handle high penetration of DERs and solve large distribution network systems for the optimal point of operation. When the OPF model is implemented for base case networks, it only considers the mutual coupling effect between lines. The model also considers unbalanced DERs (shown in Table 4.2 for the IEEE 123-bus network). So, when the DERs supply an unbalanced current to the lines, the mutual coupling effect is considered for determining the coupling coefficient due to this unbalanced current. The chapter also showcases the effectiveness of the proposed model under such conditions. In short, the model can address the multi-phase network's coupling effect with and without considering DERs. The analysis and the observations are discussed in the following subsections.

4.4.1 Case 1 (IEEE 123-Bus Network Test System)

First, the model is tested on the IEEE 123-bus distribution network. The bus renumbering of the 123-bus network in this article is illustrated in Fig. 4.5. The physical transformers between the nodes $(76-77)$ and the regulators between the nodes $(1-2), (23-24), (109-114)$ and $(123-124)$ are modeled as described in section II(E) of this article. The behavior of closed switches is regularized using a short-line model with negligible impedance ($\approx .0001 + j.0001pu$). The voltage limits $[\underline{V}, \overline{V}]$ are $[0.9, 1.1]$ for the OPF simulations. The proposed model is relaxed with a second-order cone inequality (4.12), the solution gap, defined earlier as $\sigma = |u_i l_{ij}^{\phi} - (S_{ij}^{\phi})^2|$ for each branch and used the 2nd order norm as shown in the flowchart in Fig. 4.2 for the simulation.

The results from the proposed SOCP-OPF model are verified with the solution from a Non-Linear Programming (NLP) based on a fixed point iteration method. Besides that, the performance of the proposed SOCP-OPF model is compared with a) convex SDP-OPF b) linear OPF (considering (4.8)-(4.10) excluding the terms associated with l_{ij}) and, c) a SOCP-OPF model without considering the coupling impact. For the base case of the IEEE 123-bus network, the results are optimal and very close to the solution compared to the NLP-OPF and SDP-OPF models. Also, as the proposed model considers the mutual coupling for multi-phase lines, the solution gap is very negligible comparing the loading condition (constant power and ZIP loads) of the 123-bus network.

Besides the base case, the proposed SOCP-OPF model also considers the high penetration

Table 4.2: Position and capacity of the DERs (20%) on the IEEE 123-bus network system

Bus No.	p_g^a (kw)	p_g^b (kw)	p_g^c (kw)	q_g^a $(kvar)$	q_g^b $(kvar)$	q_g^c $(kvar)$
14	0∼40	-	-	-20∼20	-	-
19	-	0∼40	-	-	-10∼10	-
20	-	0∼40	-	-	-10∼10	-
25	0∼20	-	-	-10∼10	-	-
30	-	-	0∼40	-	-	-20∼20
33	105	70	70	-70∼70	-40∼40	-40∼40
34	-	-	0∼40	-	-	-20∼20
61	-	-	0∼40	-	-	-20∼20
64	0∼40	-	-	-20∼20	-	-
72	-	-	0∼40	-	-	-20∼20
97	0∼35	0∼35	0∼35	-20∼20	-20∼20	-20∼20
110	0∼40	-	-	-20∼20	-	-
117	-	-	0∼20	-	-	-10∼10
119	-	-	0∼40	-	-	-20∼20

of DERs in a distribution network. The model has also been tested on the IEEE 123-bus network with penetration of DERs (20% of the total connected loads). The DERs can supply the real power and supply or absorb reactive power in the network upon requirements based on the objective function. The DERs' placement in the network and the capacity of the DERs are illustrated in Table 4.2. The negative limit expresses the reactive power absorption

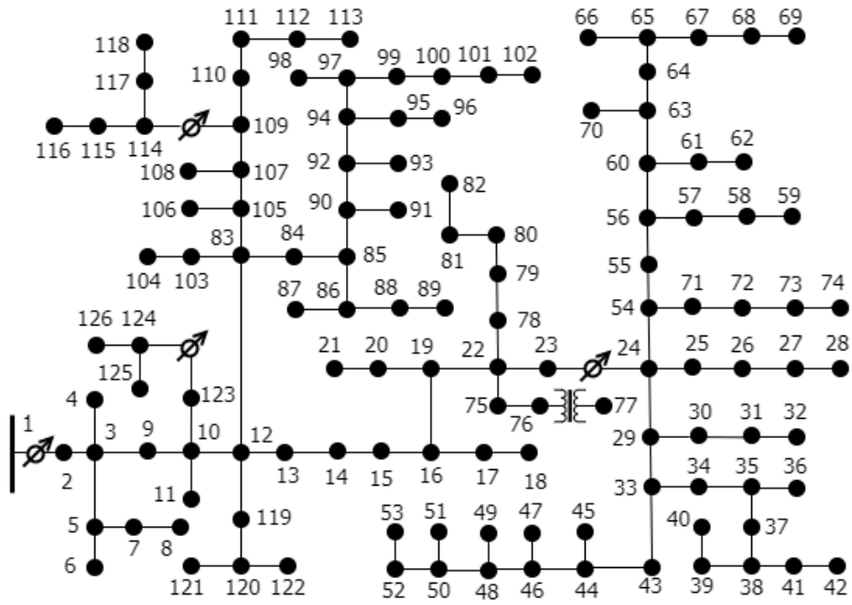

Figure 4.5: Adapted IEEE 123-bus network with the renumbered buses.

capacity of the DERs. Fig. 4.6 compares the three-phase voltage profile from the proposed SOCP model (when, $\lambda^a = 0.1, \lambda^b = 0.045$, and $\lambda^c = 0.055$) with the NLP-OPF solution as well as with a convex SDP-OPF, linear OPF, and existing SOCP-OPF models, while DERs are connected in the network. The comparison of the generation of the proposed OPF model with other models is illustrated in Table. 4.3.

As the linear OPF model ignores the network loss, the generation results are not considered in this table. When the coupling coefficient is considered, the solution results are more

analogous to the benchmark models (i.e., NLP, SDP). The objective value is measured at the points (i.e., $\lambda_a = -0.1$, $\lambda_a = 0.0$, $\lambda_a = 0.1$) of operation concerning λ^{ϕ} and is demonstrated in Fig. 4.3. The solution gap for three points of λ^{ϕ} is shown in Fig. 4.4. The solution gap is minimum at the operational point for $\lambda^a = 0.1, \lambda^b = 0.045$, and $\lambda^c = 0.055$. The primal and dual error convergence for the 123-bus network system from the proposed OPF model is illustrated in Fig. 4.9. From the analysis, for the 123-bus network, the SOCP-OPF is tight, and the solution from the model is globally optimal. Also, it proves the model's capacity to handle the unbalanced behavior of a network with high penetration of DERs.

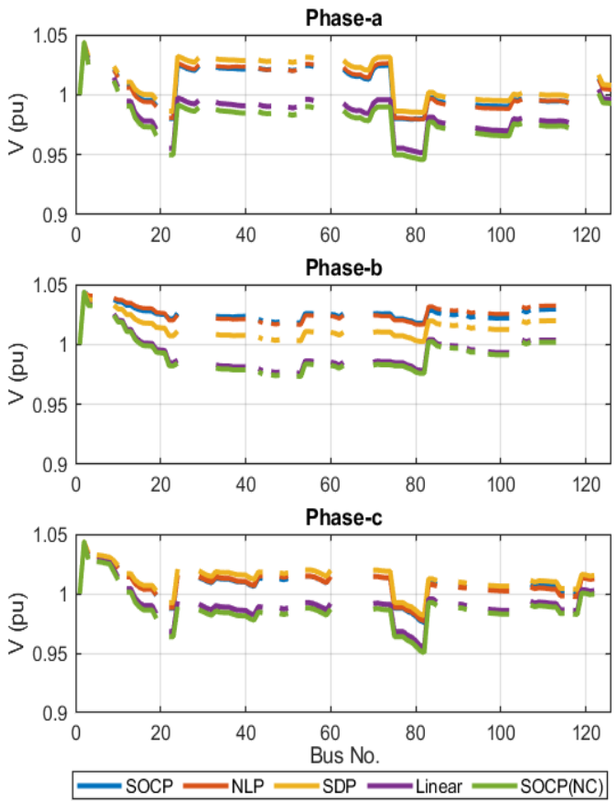

Figure 4.6: Three-phase voltage profile for the IEEE 123-bus network with 20% DERs and considering ZIP loads. Legend 'SOCP' is for the proposed OPF model and 'SOCP(NC)' for the SOCP-OPF with no coupling coefficient.

4.4.2 Case 2 (650-Bus & 2500-Bus Network Test Systems)

The proposed SOCP-OPF model is tested with more extensive networks to check the scalability. The 650-bus and 2500-bus network systems are derived from the IEEE 8500-bus network. The 2500-bus network is the medium voltage (MV) version of the 8500-bus network system. All the low voltage lines and nodes are aggregated to the respective MV nodes. The 650-bus system is the 3-phase version of the 8500-bus network system. All the single-phase MV nodes from the 2500-bus system are aggregated to the closest 3-phase nodes. The proposed SOCP-OPF is compared with NLP-OPF, SDP-OPF, linear OPF, and existing SOCP-OPF solutions. For the OPF analysis, the limit for the $[\underline{V}, \overline{V}]$ is $[0.9, 1.1]$. However, it is observed that within these limits, the SOCP-OPF without the coupling is infeasible for the 650-bus network. Similarly, the linear and SOCP models without considering the

Table 4.3: Comparison of different OPF models with the proposed SOCP-OPF model

Network	Phase	Connected Load		NLP		SDP		SOCP (Proposed)		SOCP (No Coupling)	
		$p_d(kw)$	$q_d(kvar)$	$P_g(kw)$	$q_g(kvar)$	$p_g(kw)$	$q_g(kvar)$	$p_g(kw)$	$q_g(kvar)$	$p_g(kw)$	$q_g(kvar)$
123-bus (base case)	a	1420	775	1467.91	871.00	1468.73	879.88	1471.30	875.65	1469.20	929.34
	b	915	515	935.24	551.57	940.65	560.66	942.00	545.80	946.30	589.26
	c	1155	630	1195.10	685.15	1190.98	701.23	1189.50	694.50	1195.60	732.30
123-bus (20% DGs)	a	1420	775	1454.80	850.86	1454.68	848.82	1454.50	861.44	1456.8	881.55
	b	915	515	951.16	540.26	950.85	542.89	945.50	537.18	937.54	558.53
	c	1155	630	1187.16	676.80	1202.81	684.95	1186.10	684.42	1188.90	705.80

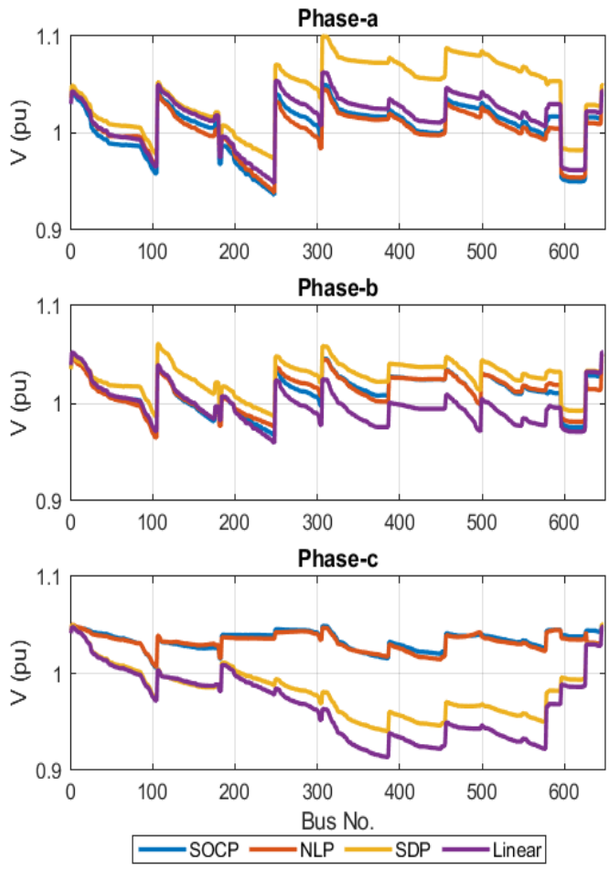

Figure 4.7: Three phase voltage profile for the 650-bus network.

coupling (these are state-of-the-art), are infeasible for the 2500-bus network. The three-phase voltage profile for the 650-bus and IEEE 2500-bus networks are shown in Fig. 4.7 and Fig. 4.8, respectively. Fig. 4.9 illustrates the primal and dual error convergence for different distribution network systems from the proposed SOCP-OPF model.

Finally, the SOCP-OPF solution convergence time is compared with the existing OPF models. The convergence time comparison among different OPF models and the voltage mismatch between the solution from the proposed SOCP-OPF model and the NLP-OPF solution for different power distribution network systems are illustrated in Table 4.4. The solution convergence speed of the proposed SOCP-OPF model is considerably high, and the voltage mismatch in different radial-type distribution networks is minimal and within the standard operation limit.

Table 4.4: Convergence time and voltage mismatch comparison

Network	Convergence Time (Sec)				SOCP vs NLP Voltage Mismatch (%)		
	SOCP	NLP	SDP	Linear	Phase a	Phase b	Phase c
13-bus	0.38	1.29	0.47	0.19	.0480	.0486	.0727
123-bus	0.41	1.59	0.55	0.28	.0271	.0198	.0050
650-bus	0.59	6.17	2.47	0.32	.0302	.0116	.0261
2500-bus	1.49	48.2	-	-	.0240	.0020	.0001

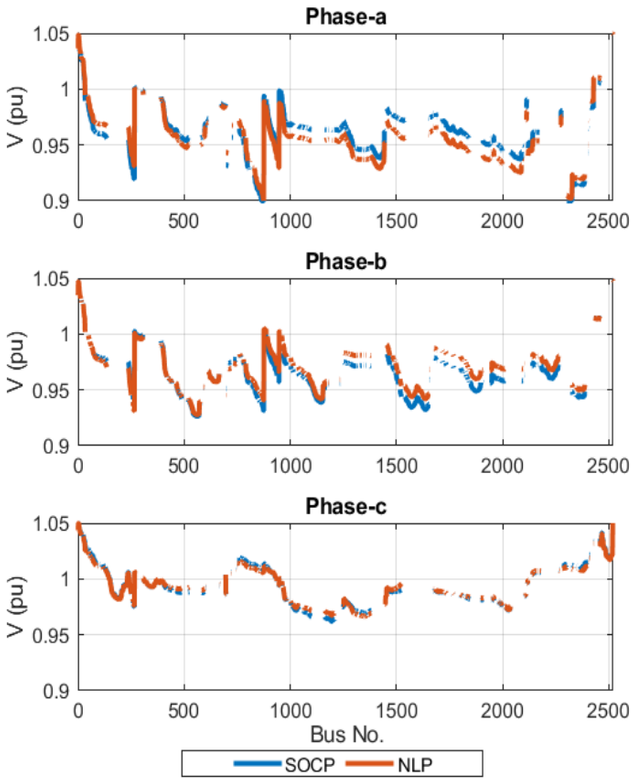

Figure 4.8: Three phase voltage profile for the IEEE 2500-bus network.

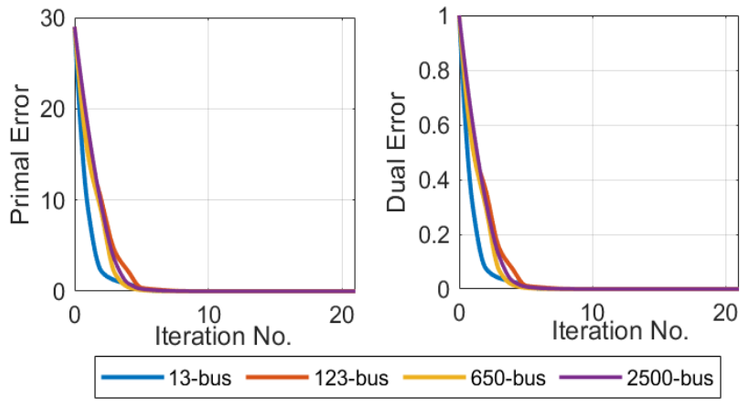

Figure 4.9: Primal and Dual error vs iteration number for different networks.

4.5 Summary

This chapter proposes a SOCP-OPF model for unbalanced multi-phase power distribution networks. The model relaxes the voltage and current phase angles and introduces a coupling coefficient. The mutual coupling coefficients address the mutual coupling impedance impact on a multi-phase network due to the phase angles. The improvement in the proposed model's tightness with the mutual coupling coefficient is evaluated. The model is simulated for different loading conditions and high DERs penetration for multiple unbalanced multi-phase networks. It has been proven that the OPF model is exact, and the solution is globally optimal. Also, the proposed model is feasible for large networks and computationally fast. For future research, the tightness of the multi-phase SOCP-OPF model will be analyzed more extensively. Further, the OPF model can be extended to mixed-integer (MI) and receding horizon control (RHC) SOCP-OPF analysis for multi-phase power distribution networks.

CHAPTER 5: A SECOND-ORDER CONE PROGRAMMING (SOCP) BASED OPTIMAL POWER FLOW (OPF) MODEL WITH CYCLIC CONSTRAINTS FOR POWER TRANSMISSION SYSTEMS

5.1 Introduction and Contribution

Optimal Power Flow (OPF) analysis is one of the salient tools in power system planning and operation for particular objectives (e.g., generation costs, power losses) by maintaining the bus voltages and branch flows within the operational limits [112–115]. OPF analysis is typically formulated using AC power flow equations considering multiple operational constraints, referred to as AC-OPF. Due to the non-convexity of power flow equations and network constraints, the AC-OPF problem originally is non-deterministic polynomial (NP)-hard [13, 14]. Moreover, the non-convexity in AC-OPF formulation leads to computational intractability, particularly for large power networks; thus, a globally optimal solution may not be guaranteed [18, 114]. Conventionally, linear approximations of power flow equations are commonly used to overcome the computational challenges of the non-convex AC-OPF formulations. However, approximation of linear formulations like DC-OPF [20, 21] compromise the solution accuracy. Thus, the solutions from such formulations may not be optimal.

On the contrary, the convex relaxations of AC-OPF problems are conditionally exact (hence, AC-feasible) and computationally efficient [22]. Due to the ability to find global optima, the convex AC-OPF formulations have been extensively used in various power system optimization applications [23,24,116]. Additionally, the convex envelopes have been a promising approach for the non-linear terms in OPF analysis [117]. However, it was noted that the accuracy of the convex relaxations depends on the tightness of these convex envelopes [118]. A robust convex restriction to solve robust OPF problems is introduced in [119]. To this end, sufficient conditions for the exactness of the relaxations are illustrated in [56,57]. Among the variants of convex OPF formulations, the second-order cone programming (SOCP) [22], and semi-definite programming (SDP) [5] based models are used commonly for OPF problems. SOCP-based load flow formulation was first proposed for radial distribution networks in [22], and a conic quadratic model was proposed in [120] for meshed networks. For the SOCP-OPF model, the angle and conic relaxations are exact in radial networks with no upper bounds on loads.

In the mesh networks, angle relaxation of AC-OPF can be inexact as the cyclic constraints are not satisfied (i.e., the sum of voltage angle difference around any loop should be zero) [74]. The conditions for the angle recovery for the SOCP-OPF model are discussed in [68, 69].

Three methods are proposed in [74] for enhancing the original SOCP-OPF model for mesh networks that ensure the cyclic constraints for the mesh networks. However, the model suffers computational challenges for large meshed networks. In [121], instead of considering the cyclic constraints directly for the meshed networks, an alternative SOCP-OPF model using difference-of-convex programming (DCP) is used, which requires convex-concave procedure (CCP) based iterations. A SOCP-OPF model is proposed with relaxation by generating new cutting planes using SDP relaxation in [122]. Though the SDP cuts effectively exclude infeasible solutions and enhance the SOCP relaxation of OPF, they add computational burden on the solution process. Reference [123] proposes relaxation of the cyclic constraints, where a higher-order moment relaxation matrix for each maximal clique is formed to satisfy the cyclic constraints. In conclusion, the existing SOCP-OPF models face challenges with the cyclic constraints for tight and scalable OPF methods for the meshed networks.

On the other hand, SDP formulation retains the angle information and can find an exact solution of OPF analysis for meshed networks with certain conditions and limitations [3,124]. So, SDP relaxations are theoretically more robust [122] compared to SOCP relaxations for meshed transmission networks. However, the matrix size grows as the square of the number of buses in SDP leads to a high computational need for large networks [104]. In addition, SDP formulations find a physically meaningful OPF solution if the line-flow limits are not binding [125]. However, SOCP relaxation-based OPF models are computationally efficient for large networks [117].

From the above discussion, the SOCP is computationally efficient but suffers from angle relaxation for meshed power networks due to the cyclic angle constraints. This motivates our proposed work to consider cyclic constraints directly in the SOCP AC-OPF formulation to obtain exact OPF solutions for meshed networks. With this premise, this chapter proposes a convex envelope to retrieve and include the bus voltage angle difference across the branches that satisfies the cyclic constraints in any mesh cycle in the power network. Additionally, the branches that do not belong to any mesh follow the radial network approach as [106,126] to determine the bus voltage phase difference for a tighter envelope. The bus voltage phase angle difference is recovered after the optimization if a wide envelope is considered. In the proposed approach, the voltage and current phase angles are first relaxed for converting the non-convex power flow equations into convex form. Then, a quadratic equation is relaxed as a second-order conic inequality constraint. Finally, a convex envelope is derived for the bus voltage angle difference, adhering to the cyclic constraints in the network.

5.1.1 Major Contributions

The main contributions of the proposed model are as follows:

- A convex envelope is proposed to retrieve the bus voltage angle difference for all the

branches in a power network. The envelope is determined based on the optimal power flow and the voltage limits. With the proposed OPF model, the bus voltage angle difference remains within the envelope and satisfies the mesh cyclic constraints.

- A theoretical framework, including the mathematical proof is developed for the relaxation of meshed power networks with the angle cyclic constraints.

- The approach also proposes a graph theory-based model for extracting the mesh cycles from a power network. The mesh cycles are determined from a network ex-ante of the SOCP-OPF analysis. Thus, the cycle information is a parameter for the proposed SOCP-OPF model.

The chapter is organized as follows. Section 5.2 discusses the proposed methodology, including the mathematical modeling in the relaxation framework and the graph theory-based cycle extraction method. The impacts of line flow limits on the SDP and SOCP-OPF models are illustrated in Section 5.3. Section 5.4 analyzes the exactness and global optimality of the proposed model. Section 5.5 discusses the model implementation and result evaluation, and Section 5.6 concludes the chapter with a summary.

The variable and parameters used in this chapter are as follows:

$\mathcal{N}$:	Set of all the buses in the network
$\mathcal{N}_g$:	Set of all the buses with generators in the network
$\mathcal{L}$:	Set of all the branches in the network
$\overline{()}$:	maximum limits of the variables and parameters
$\underline{()}$:	minimum limits of the variables and parameters
$\overline{V_i}$:	Voltage at the bus $i \in \mathcal{N}$
u_i:	Magnitude square of the voltage at the bus $i \in \mathcal{N}$
S_i^g:	Apparent power at the bus $i \in \mathcal{N}_g$
S_i^d:	Apparent power demand at the bus $i \in \mathcal{N}$
P_i^g:	Real power injection at the bus $i \in \mathcal{N}_g$
P_i^d:	Real power demand at the bus $i \in \mathcal{N}$
Q_i^g:	Reactive power injection at the bus $i \in \mathcal{N}_g$
Q_i^d:	Reactive power demand at the bus $i \in \mathcal{N}$
P_{ij}:	Real power flow through the branch $L_{ij} \in \mathcal{L}$ connecting the bus $(i,j) \in \mathcal{N}$
Q_{ij}:	Reactive power flow through the branch $L_{ij} \in \mathcal{L}$ connecting the bus $(i,j) \in \mathcal{N}$
S_{ij}:	Apparent power flow through the branch $L_{ij} \in \mathcal{L}$ connecting the bus $(i,j) \in \mathcal{N}$
I_{ij}:	Current flow through a branch $L_{ij} \in \mathcal{L}$ connecting the bus $(i,j) \in \mathcal{N}$
l_{ij}:	Magnitude square of the current flow through a branch $L_{ij} \in \mathcal{L}$
θ_{ij}:	Bus voltage angle difference between the bus $(i,j) \in \mathcal{N}$
z_{ij}:	Impedance of the branch $L_{ij} \in \mathcal{L}$ connecting the bus $(i,j) \in \mathcal{N}$
G_{ij}:	Real part of the off-diagonal components of the admittance matrix (Y)
B_{ij}:	Imaginary part of the off-diagonal components of the admittance matrix (Y)
c_2^i, c_1^i & c_0^i:	Cost coefficients for the generator at bus $i \in \mathcal{N}_g$

5.2 Proposed Methodology

It is well known that power transmission networks are generally in meshed orientation. Thus for generic model development, a small section of a meshed transmission network is considered as represented in the schematic diagram in Fig. 5.1. In this chapter, '$\mathcal{L}$' is considered as the set of all branches, and $\mathcal{N}$ is the set of all network buses. Further, i and $j \in \mathcal{N}$ denote the bus index, and $L_{ij} \in \mathcal{L}$ denotes the branch connecting the bus $i \in \mathcal{N}$ and bus $j \in \mathcal{N}$.

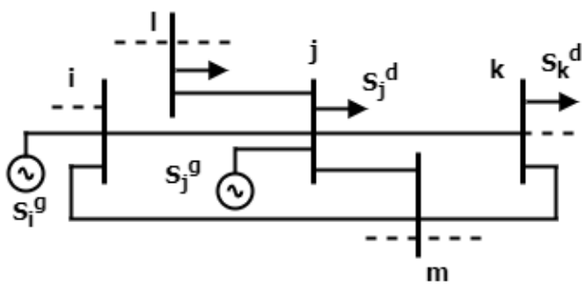

Figure 5.1: Schematic diagram of a simple meshed network.

5.2.1 Branch Flow Model (BFM) in Power System

Considering the above notations, the power flow relation through a branch $L_{ij} \in \mathcal{L}$ and voltage relations between the bus $i \in \mathcal{N}$ and bus $j \in \mathcal{N}$ can be represented as follows:

$$S_{ij} = V_i I_{ij}^* \tag{5.1}$$

$$V_j = V_i - \frac{z_{ij} S_{ij}^*}{V_i^*} \tag{5.2}$$

where z_{ij} is the impedance of the branch $L_{ij} \in \mathcal{L}$. S_{ij} and I_{ij} represent the apparent power and current flow from bus $i \in \mathcal{N}$ to bus $j \in \mathcal{N}$ through the branch $L_{ij} \in \mathcal{L}$, respectively. The power balance equation at the bus $j \in \mathcal{N}$ is as follows:

$$S_j^g - S_j^d = \sum_{k:j\to k} S_{jk} - \sum_{i:i\to j} (S_{ij} - z_{ij}|I_{ij}|^2) + y_j^*|V_j|^2 \tag{5.3}$$

where $y_j = g_j + jb_j$ is the half lump shunt admittance equivalent of the line at the bus $j \in \mathcal{N}$. Let Y denotes the admittance matrix of a power network, which has off-diagonal components as $Y_{ij} = G_{ij} + jB_{ij}$ for each branch $L_{ij} \in \mathcal{L}$ of the network. The real and reactive power flow through a branch $L_{ij} \in \mathcal{L}$ between two buses $i \in \mathcal{N}$ and $j \in \mathcal{N}$ can be represented as:

$$P_{ij} = -G_{ij}V_i^2 + G_{ij}V_iV_j\cos(\theta_{ij}) + B_{ij}V_iV_j\sin(\theta_{ij}) \tag{5.4}$$

$$Q_{ij} = B_{ij}V_i^2 - B_{ij}V_iV_j\cos(\theta_{ij}) + G_{ij}V_iV_j\sin(\theta_{ij}) \tag{5.5}$$

where $\theta_{ij} = \theta_i - \theta_j$; θ_i and θ_j are the bus voltage phase angle at the bus i and $j \in \mathcal{N}$ respectively. Further, from (5.4) and (5.5):

$$V_iV_j\sin\theta_{ij} = \frac{B_{ij}P_{ij} + G_{ij}Q_{ij}}{G_{ij}^2 + B_{ij}^2} \tag{5.6}$$

Eqn. (5.6) shows the dependency of the bus voltage angle difference on the power flow through a branch in the network.

5.2.2 Relaxations and Inclusion of the Cyclic Constraints

5.2.2.1 Angle Relaxation

In the proposed convex model, to convexify (5.1)-(5.3), the phase angle of the voltage and the current are relaxed as, $I_{ij} \Rightarrow |I_{ij}|$ and $V_i \Rightarrow |V_i|$. New variables have been introduced as $|I_{ij}|^2 = l_{ij}$; $|V_i|^2 = u_i$ and $|V_j|^2 = u_j$. The equation in (5.1) is converted as follows:

$$u_i l_{ij} = S_{ij}^2 \tag{5.7}$$

Considering the magnitude squared in (5.2), the voltage relationship between the bus $i \in \mathcal{N}$ & bus $j \in \mathcal{N}$ is as follows:

$$|V_j|^2 = |V_i|^2 + |z_{ij}|^2|I_{ij}|^2 - (z_{ij}S_{ij}^* + z_{ij}^*S_{ij}) \tag{5.8}$$

With the new variable as $|I_{ij}|^2 = l_{ij}$; $|V_i|^2 = u_i$ and $|V_j|^2 = u_j$ for the squared terms and with further simplification in (5.8):

$$u_j = u_i - 2(r_{ij}P_{ij} + x_{ij}Q_{ij}) + (r_{ij}^2 + x_{ij}^2)l_{ij} \tag{5.9}$$

With the angle relaxation and new-defined variables, the apparent power balance relationship from (5.3) at the bus j is:

$$s_j^g - s_j^d = \sum_{k:j\to k} S_{jk} - \sum_{i:i\to j}(S_{ij} - z_{ij}l_{ij}) + y_j u_j \tag{5.10}$$

Splitting the (5.10) in terms of real and reactive power, the power balance at bus $j \in \mathcal{N}$ is as follows:

$$P_j^g - P_j^d = \sum_{k:j\to k} P_{jk} - \sum_{i:i\to j}(P_{ij} - r_{ij}l_{ij}) + g_j u_j \tag{5.11}$$

$$Q_j^g - Q_j^d = \sum_{k:j\to k} Q_{jk} - \sum_{i:i\to j}(Q_{ij} - x_{ij}l_{ij}) + b_j u_j \tag{5.12}$$

where $z_{ij} = r_{ij} + jx_{ij}$; r_{ij} and x_{ij} are the resistance and reactance of the line $L_{ij} \in \mathcal{L}$ respectively. $S_{ij} = P_{ij} + jQ_{ij}$, $y_j = g_j + jb_j$, $S_j^g = P_j^g + jQ_j^g$, and $S_j^d = P_j^d + jQ_j^d$.

5.2.2.2 Conic Relaxation

For each of the branches in the network, the OPF model is still non-convex due to the quadratic equation in (5.7) as:

$$l_{ij} = \frac{S_{ij}^2}{u_i} \Rightarrow l_{ij} = \frac{P_{ij}^2 + Q_{ij}^2}{u_i} \tag{5.13}$$

With the conic-relaxation, the non-convex solution space is enclosed within a feasible conic convex space [107]. For the proposed model, further convexification is done by conic relaxation in (5.13) with a conic inequality as follows in (5.14):

$$u_i + l_{ij} \geq \left\| \begin{matrix} 2P_{ij} \\ 2Q_{ij} \\ u_i - l_{ij} \end{matrix} \right\|_2 \tag{5.14}$$

Fig. 5.2(a) represents the conic space for the OPF solution. The solution gap is minimum if the OPF solution is on the surface and the solution gap increases if it moves away from the surface, as demonstrated in Fig.5.3. The difference between solution points A and B is the solution gap of the SOCP-OPF analysis.

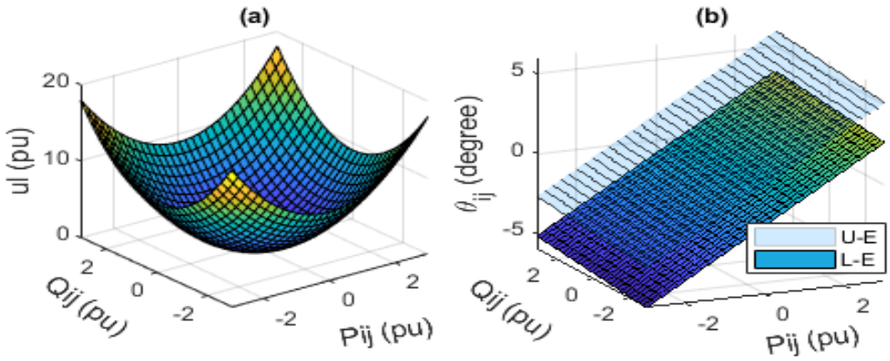

Figure 5.2: (a) Representation of the conic space; (b) the envelope for θ_{ij}, where U-E indicates the upper level and L-E indicates the lower level of the envelope.

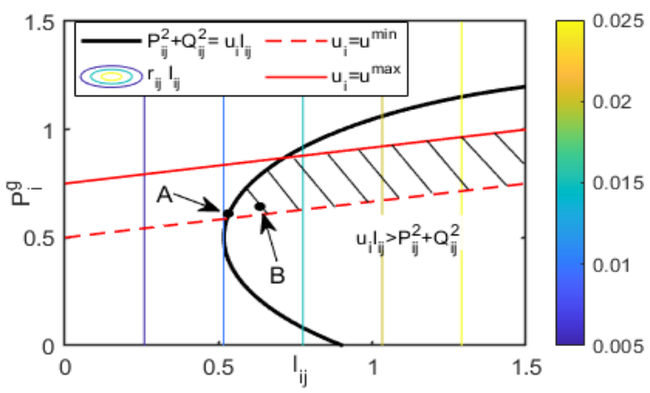

Figure 5.3: Feasible zone: NLP vs. SOCP. The feasible space for the NLP lies at the boundary of the $P_{ij}^2 + Q_{ij}^2 = u_i l_{ij}$ curve, while the feasible space for the SOCP is the shaded area right of the curve. Solution gap, $\sigma = |B - A|$.

5.2.2.3 Cyclic Constraints

It is stated in the earlier discussion that for an exact SOCP-OPF analysis, cyclic constraints are needed to be satisfied for meshed networks as shown below:

$$\sum_{(i,j,\ldots x)\in\mathcal{C}} \theta_{ij} + \theta_{jk} + \ldots + \theta_{xi} = 0 \tag{5.15}$$

where suffixes i, j, and x are the buses engaged with a particular mesh cycle ($\mathcal{C}$) in a power network. In the proposed OPF model, the bus voltage angle difference is retrieved based on (5.6), and the cyclic constraints in (5.15) are satisfied within the convex solution space. For this purpose, (5.6) is relaxed within an envelope comprising (5.16) and (5.17) as boundary conditions.

$$\theta_{ij} \geq \frac{M}{\overline{V}_i \overline{V}_j \cos\frac{\theta_{ij}^m}{2}} - \tan\frac{\theta_{ij}^m}{2} + \frac{\theta_{ij}^m}{2} \tag{5.16}$$

$$\theta_{ij} \leq \frac{M}{\underline{V}_i \underline{V}_j \cos\frac{\theta_{ij}^m}{2}} + \tan\frac{\theta_{ij}^m}{2} - \frac{\theta_{ij}^m}{2} \tag{5.17}$$

where $M = V_i V_j \sin(\theta_{ij}) = \frac{B_{ij}P_{ij} - G_{ij}Q_{ij}}{G_{ij}^2 + B_{ij}^2}$. A visual representation of the proposed envelope is illustrated in Fig. 5.2 (b), and the derivation of the envelope is shown in the following sub-section 5.2.3.

5.2.3 Derivation of the Envelope for the θ_{ij}:

The following convex envelope in (5.18)-(5.19) encloses the sine function in a polyhedral set as follows [107]:

$$\sin\theta_{ij} \leq \cos(\frac{\theta_{ij}^m}{2})(\theta_{ij} - \frac{\theta_{ij}^m}{2}) + \sin(\frac{\theta_{ij}^m}{2}) \tag{5.18}$$

$$\sin\theta_{ij} \geq \cos(\frac{\theta_{ij}^m}{2})(\theta_{ij} + \frac{\theta_{ij}^m}{2}) - \sin(\frac{\theta_{ij}^m}{2}) \tag{5.19}$$

where $\theta_{ij}^m = max[|\underline{\theta_{ij}}|, |\overline{\theta_{ij}}|]$.

Power transmission system networks are commonly in mesh orientation. For transmission networks, as the bus voltage (p.u) maximum and minimum limits are near unity and usually, the voltage (p.u) maximum and minimum limit of $[\underline{V}, \overline{V}] = [0.9, 1.1]$. If, $V_i V_j \sin\theta_{ij} = M$, then within the voltage limit, the $\sin\theta_{ij}$ function is relaxed as, $\sin\theta_{ij} \geq \frac{M}{\overline{V}_i \overline{V}_j}$ and $\sin\theta_{ij} \leq \frac{M}{\underline{V}_i \underline{V}_j}$. Then from (5.18):

$$\begin{aligned}
\frac{M}{\overline{V}_i \overline{V}_j} &\leq \cos(\frac{\theta_{ij}^m}{2})(\theta_{ij} - \frac{\theta_{ij}^m}{2}) + \sin(\frac{\theta_{ij}^m}{2}) \\
&\Rightarrow \theta_{ij} - \frac{\theta_{ij}^m}{2} \geq \frac{M}{\overline{V}_i \overline{V}_j \cos\frac{\theta_{ij}^m}{2}} - \tan\frac{\theta_{ij}^m}{2} \\
&\Rightarrow \theta_{ij} \geq \frac{M}{\overline{V}_i \overline{V}_j \cos\frac{\theta_{ij}^m}{2}} - \tan\frac{\theta_{ij}^m}{2} + \frac{\theta_{ij}^m}{2}
\end{aligned} \tag{5.20}$$

From (5.19):

$$\begin{aligned}
\frac{M}{\underline{V}_i \underline{V}_j} &\geq \cos(\frac{\theta_{ij}^m}{2})(\theta_{ij} + \frac{\theta_{ij}^m}{2}) - \sin(\frac{\theta_{ij}^m}{2}) \\
&\Rightarrow \theta_{ij} + \frac{\theta_{ij}^m}{2} \leq \frac{M}{\underline{V}_i \underline{V}_j \cos\frac{\theta_{ij}^m}{2}} + \tan\frac{\theta_{ij}^m}{2} \\
&\Rightarrow \theta_{ij} \leq \frac{M}{\underline{V}_i \underline{V}_j \cos\frac{\theta_{ij}^m}{2}} + \tan\frac{\theta_{ij}^m}{2} - \frac{\theta_{ij}^m}{2}
\end{aligned} \tag{5.21}$$

where $M = V_i V_j \sin(\theta_{ij}) = \frac{(B_{ij}P_{ij} - G_{ij}Q_{ij})}{(G_{ij}^2 + B_{ij}^2)}$.

5.2.4 Convexity of the Proposed Envelope

The envelope in (5.20) and (5.21) are represented as follows:

$$f_1(P,Q) = \alpha(B_{ij}P_{ij} - G_{ij}Q_{ij}) + \beta_1$$
$$f_2(P,Q) = \alpha(B_{ij}P_{ij} - G_{ij}Q_{ij}) + \beta_2$$

where $\alpha = \frac{1}{\underline{V}_i\underline{V}_j \cos\frac{\theta_{ij}^m}{2}}$; $\beta_1 = -\tan\frac{\theta_{ij}^m}{2} + \frac{\theta_{ij}^m}{2}$ and $\beta_2 = \tan\frac{\theta_{ij}^m}{2} - \frac{\theta_{ij}^m}{2}$. $f(P,Q)$ can be split into two first-order functions as, $f(P,Q) = f(P) + f(Q)$. From the definition, a first-order equation can be considered as convex. In this article the envelope formed by $f(P,Q)$ is used for the relaxation of θ_{ij} from (5.6) as, $f_1(P,Q) \leq \theta_{ij} \leq f_2(P,Q)$.

5.2.5 Proposed SOCP-OPF Architecture

The primary goal of an OPF analysis is to provide a supply-demand balance based on an objective while satisfying the imposed network constraints. The proposed OPF model can be applied with different objective functions $f(x)$, such as network loss minimization, generation cost minimization, bus voltage regulation, or a combination of these. We have considered only convex objective functions for the proposed SOCP-OPF model in this article. The following objective functions are analyzed with the proposed OPF model.

a) Network power loss minimization:

$$min \sum_{L_{ij}\in\mathcal{L}} r_{ij}|I_{ij}|^2 \Rightarrow min \sum_{L_{ij}\in\mathcal{L}} r_{ij}l_{ij} \tag{5.22}$$

b) Real power generation cost minimization:

$$min \sum_{i\in\mathcal{N}_g} [c_2^i(P_i^g)^2 + c_1^i P_i^g + c_0^i] \tag{5.23}$$

where $c_2^i(\$/MWh^2)$, $c_1^i(\$/MWh)$ and $c_0^i(\$/h)$ represent the quadratic cost coefficients of the generator at the bus $i \in \mathcal{N}_g$. For considering the cost function as a convex equation $c^i \geq 0$. Finally, the proposed SOCP-OPF model with a convex objective function is as follows:

$$min \sum f(x_i) \tag{5.24}$$

Subject to: (5.9), (5.11), (5.12) and (5.14)- (5.17); along with the following imposed con-

straints on the control variables:

$$\begin{cases} \underline{P}_i^g \leq P_i^g \leq \overline{P}_i^g \\ \underline{Q}_i^g \leq Q_i^g \leq \overline{Q}_i^g \\ l_{ij} \leq \bar{l}_{ij} \\ \underline{u}_i \leq u_i \leq \overline{u}_i \end{cases} \tag{5.25}$$

where P_i^g and Q_i^g are the real and reactive power generation of the generator at the bus $i \in \mathcal{N}_g$. Voltage limits are defined as, $\underline{u}_i = |\underline{V}_i|^2$ and $\overline{u}_i = |\overline{V}_i|^2$ for the bus $i \in \mathcal{N}$. Current flow limit is defined as $\bar{l}_{ij} = |\overline{I}_{ij}|^2$. $\overline{I}_{ij}$ is the rated current flow limit for the branch $L_{ij} \in \mathcal{L}$.

5.2.6 Graph Theory-Based Mesh Cycle Extraction

The proposed OPF analysis process starts with determining all the mesh cycles in a network. A graph theory-based methodology is proposed to find all the mesh cycles. The mesh cycles are determined from a network ex-ante of the SOCP-OPF analysis. The bus voltage angle difference between the buses is determined within the envelope defined by (5.16) & (5.17), which satisfies the cyclic angle constraints in the network with the imposed (5.15). An Adjacency matrix ($\mathcal{A}$) is generated for the network branches to find the cycles. If the bus number in a network is "N_b", then the size of the Adjacency matrix is $(N_b \times N_b)$. Graph vertices label the rows and columns of the matrix. If bus $i \in \mathcal{N}$ and bus $j \in \mathcal{N}$ are adjacent connected, then in position (i, j) of $\mathcal{A}$ is 1 otherwise 0. Then with the interconnected branches, mesh cycles are traced. The shortest mesh cycle is considered for the model if a branch engages with multiple mesh cycles. The shortest mesh cycle has the least number of edges and buses engaged with the mesh. For example as shown in Fig. 5.6, the branch L_{12} is engaged with multiple mesh cycles as $MC_1(1, 2, 5, 1)$, $MC_2(1, 2, 4, 5, 1)$ and $MC_3(1, 2, 3, 4, 5, 1)$. However, the mesh cycle MC_1 is considered the shortest for the branch L_{12}. If a branch L_{ij} is already within a previous mesh cycle, then it does not need to find for another cycle. This approach is continued until all branches' mesh cycles are determined. If a network branch is not engaged with any mesh cycles, then that is listed as a dangling branch. The algorithm for the cycle extraction is illustrated in Algorithm 2. Worth to note that, in the meshed branches, power transmission networks usually have a few dangling branches forming a radial-type network part. For those radial type branches, the phase angle difference depends on the width of the envelopes derived in (5.16) and (5.17). If a tight envelope is considered with a smaller θ_{ij}^m (i.e., $10^o - 20^o$), the phase angle difference (θ_{ij}) is retrieved during the OPF execution. However, if a broader range of θ_{ij}^m is considered for the envelope, θ_{ij} is recovered after the optimization process from (5.6). Algorithm 2 is also used to determine the radial-type dangling branches of the network. The execution

Algorithm 2 Network Mesh Cycle Extraction

-Determine the total bus number N_b and branch number N_L in the power network.
-Get data input for "from bus (f_b)" and "to bus (t_b)", $\{f_b, t_b\} \in \mathcal{N}$ and form the Adjacency matrix ($\mathcal{A}$) of size ($N_b \times N_b$).
-Define a matrix **A** for the vertices engaged with mesh cycles in the network.
-Define a matrix **B** for the vertices of the dangling branches.
for $n = 1 : N_L$ **do**
  if *branch* $L_{ij}(n)$ *is not already in matrix "**A**" or "**B**"* **then**
    -Trace for the inter-connected branches from the branch $L_{ij}(n)$ for any mesh cycles ($\mathcal{C}$) engaged with $L_{ij}(n)$.
    if *branch* $L_{ij}(n)$ *is in* $'k'$ *number of mesh cycles:* **then**
      Find the total number of buses in each mesh cycle from $\mathcal{C}_k$.
      Find the shortest path mesh cycle $\mathcal{C}_k^{shortest}$ engaged with the branch $L_{ij}(n)$ from $\mathcal{C}_k$.
      Find the total bus no. N_{ij}^{mesh} in the shortest mesh cycle $\mathcal{C}_k^{shortest}$.
      for $m = 1$ *to* N_{ij}^{mesh} **do**
        Find all of the bus indexes $i, j..x$ of the mesh cycle $\mathcal{C}_k^{shortest}$ and store them in the matrix **A**.
      end
    end
    else if *branch* $L_{ij}(n)$ *is not in a mesh* **then**
      Store the bus indexes i & j engaged with the dangling branch L_{ij} in the matrix **B**.
    end
  end
end
-The matrix **A** returns the cycles, and the matrix **B** returns the radial branches of the network.
-Here, $\mathcal{C}_k^{shortest}$ is the shortest mesh cycle among the mesh cycles $\mathcal{C}_k$ for branch L_{ij} with minimum edges.

time of Algorithm 2 for different test cases is shown in Table 5.7. Information regarding the cycles is included as a parameter in the proposed SOCP-OPF model after completing the mesh cycle extracting process before the optimization begins.

5.3 Line Flow Limits and Bi-directional Flow

5.3.1 Impact of Line Flow Limits

This section discusses the impact of the line flow limits on the SDP-OPF models compared to the proposed SOCP-OPF model. The SDP-OPF models fail to determine a feasible and physically meaningful solution for a tighter line-flow limit [3, 125]. To evaluate the impact of line flow limits on SDP, consider the power flow representation as follows:

$$P_i^g - P_i^d = \sum_{(i,j)\in\mathcal{N}} Re\{(W_{ii} - W_{ij})y_{ij}^*\} \tag{5.26}$$

$$Q_i^g - Q_i^d = \sum_{(i,j)\in\mathcal{N}} Im\{(W_{ii} - W_{ij})y_{ij}^*\} \tag{5.27}$$

where $W_{ii} = V_i V_i^*$ and $W_{ij} = V_i V_j^*$. V_i and V_j are the bus voltage at the bus $i \in \mathcal{N}$ and bus $j \in \mathcal{N}$ respectively. The inequality constraints are defined as follows:

$$\begin{aligned} \underline{P}_i^g \leq P_i^g \leq \overline{P}_i^g \\ \underline{Q}_i^g \leq Q_i^g \leq \overline{Q}_i^g \\ \underline{V}_i^2 \leq W_{ii} \leq \overline{V}_i^2 \end{aligned} \tag{5.28}$$

For a branch $L_{ij} \in \mathcal{L}$ connecting the buses $i \in \mathcal{N}$ and $j \in \mathcal{N}$, the line constraints can be imposed in a convex form as:

$$|S_{ij}| = |(W_{ii} - W_{ij}) y_{ij}^*| \leq \overline{S}_{ij} \tag{5.29}$$

Splitting (5.29) in terms of real and reactive flow, the power flow relation can be represented as follows:

$$|P_{ij}| = |Real[|(W_{ii} - W_{ij}) y_{ij}^*|]| \leq \overline{P}_{ij} \tag{5.30}$$

$$|Q_{ij}| = |Imag[|(W_{ii} - W_{ij}) y_{ij}^*|]| \leq \overline{Q}_{ij} \tag{5.31}$$

where $W \in H^n$ is a semidefinite Hermitian matrix. The SDP-OPF formulation is tight and the solution is feasible optimal if $W \geq 0$ and $rank\{W\} = 1$.

Remark. *If narrow band line flow limits are imposed on (5.29), then the SDP-OPF solver computationally fails or leads to an incorrect solution.*

Proof. From (5.29) it can be written as, $|(W_{ii} - W_{ij}) y_{ij}^*| \leq \overline{S}_{ij} \Rightarrow |(V_i V_i^* - V_i V_j^*) y_{ij}^*| \leq \overline{S}_{ij}$. If $i \in \mathcal{N}$ and $j \in \mathcal{N}$ are two adjacent buses connected with a line $L_{ij} \in \mathcal{L}$; $V_i = V_m \angle \theta$; $V_j = (V_m + \Delta V) \angle (\theta + \Delta\theta)$ and $y_{ij} = \frac{1}{z_{ij} \angle \theta_{ij}}$, then

$$|\{V_m^2 - (V_m^2 + V_m \Delta V) \angle - \Delta\theta\} y_{ij}^*| \leq \overline{S}_{ij} \tag{5.32}$$

If the SDP OPF is characterized with a voltage range $[1 - \xi, 1 + \xi]$, where ξ is small, then $-2\xi \leq \Delta V \leq 2\xi$. Thus $V_m \Delta V \approx 0$ or negligible $\Rightarrow |(V_m^2 - V_m^2 \angle - \Delta\theta) y_{ij}^*| \leq \overline{S}_{ij}$.
This means $|V_m^2 (1 - 1 \angle - \Delta\theta) |y_{ij}| \angle \delta_{ij}| \leq \overline{S}_{ij}$. Then in terms of real power, it can be shown that:

$$|V_m^2 |y_{ij}| \{\cos \delta_{ij} - \cos (\delta_{ij} - \Delta\theta)\}| \leq \overline{P}_{ij} \tag{5.33}$$

For a branch $L_{ij} \in \mathcal{L}$ the line impedance is $z_{ij} = r_{ij} + jx_{ij}$. Considering that for a transmission network, $x_{ij} >> r_{ij}$ and $y_{ij} = \frac{1}{z_{ij}\angle\delta_{ij}}$; $\delta_{ij} \approx \frac{\pi}{2}$. So for a transmission network (5.33) can be represented as follows:

$$||y_{ij}|V_m^2 \sin(\Delta\theta)| \leq \overline{P}_{ij} \tag{5.34}$$

If the voltage phase angle difference $\Delta\theta$ between two adjacent connected buses is not significantly low, the lower line flow constraint shown in (5.34) fails. So, the solution from the SDP formulation becomes infeasible or inaccurate.

The SOCP-OPF model is relaxed with the conic relaxation as $u_i l_{ij} \geq S_{ij}^2$. The current flow $l_{ij} = |I_{ij}|^2$ is proportional to the apparent power flow S_{ij}. So, in contrast with the SDP-OPF models, the SOCP-OPF models do not suffer from the line flow limit issue. □

5.3.1.1 Example

The impact of the line flow limit on the SOCP-OPF and SDP-OPF analysis is illustrated with an example of a 5-bus network [127], shown in Fig. 5.4. Line flow limits are imposed

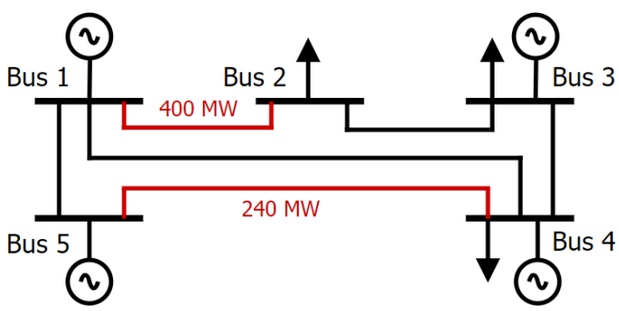

Figure 5.4: Schematic diagram of the 5-bus network.

on the two branches $L_{1,2}$ and $L_{4,5}$, as $\overline{P}_{(1,2)} = 400MW$ and $\overline{P}_{(4,5)} = 240MW$ respectively. It is observed that the SDP-OPF model became infeasible with these network constraints. Further, the two-line flow limits have been increased by a multiplying factor ϵ. For a range of $\epsilon\overline{P}_{(1,2)}$ and $\epsilon\overline{P}_{(4,5)}$; the network has been solved with different OPF models, and the results are illustrated in Fig. 5.5. With the increase of the value of ϵ, the line limit increases (i.e., when $\epsilon = 2$, the flow limit is increased by 100%). The total load is 1000 MW in the network, and a feasible solution occurs when the total generation meets the total demand. Besides the 5-bus network, tighter line limits are also imposed and tested for different branches in the IEEE 57-bus and 118-bus networks. Because of the stricter line limits, the SDP-OPF model computationally fails to provide a feasible solution as opposed to the SOCP-OPF model.

5.3.2 Bi-directional Flow in SOCP-OPF

The SOCP-based OPF models are widely used for radial-type power networks, and the conditions for the exact solution for any reverse power flow are discussed in [128]. However, it is necessary to check the feasibility of the SOCP-OPF model for possible bi-directional power

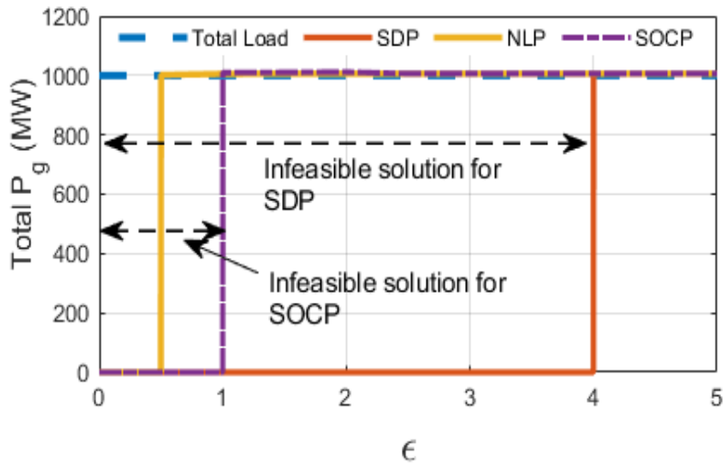

Figure 5.5: Impact of the branch flow limits on different OPF models.

flow conditions for meshed network systems. Consider bus $j \in \mathcal{N}$ in Fig. 5.1 with connected two adjacent buses $i \in \mathcal{N}$ & $k \in \mathcal{N}$. The power flow through the branches connected with the bus $j \in \mathcal{N}$ is as follows:

$$P_{ij} = r_{ij}l_{ij} - P_{ji}P_{jk} = r_{jk}l_{jk} - P_{kj}P_{lj} = r_{lj}l_{lj} - P_{jl}P_{jm} = r_{jm}l_{jm} - P_{mj}$$

These relations can be derived for reactive power flow as well. From Fig. 5.1, the real power balance at the bus $j \in \mathcal{N}$ is as:

$$P_j^g - P_j^d = \sum_{k:j\to k} P_{jk} - \sum_{i:i\to j}(P_{ij} - r_{ij}l_{ij}) + g_j u_j \tag{5.35}$$

If the power flows in at bus j from the bus i and l and goes out to the bus k and m then from (5.35):

$$P_j^g - P_j^d = P_{jk} + P_{jm} - (P_{ij} - r_{ij}l_{ij}) - (P_{lj} - r_{lj}l_{lj}) \tag{5.36}$$

If the direction of power flow at bus j is reversed, then:

$$P_j^g - P_j^d = P_{jl} + P_{ji} - (P_{kj} - r_{kj}l_{kj}) - (P_{mj} - r_{mj}l_{mj}) \tag{5.37}$$

From (5.36) and (5.37); $l_{jk} = l_{kj}$ and $l_{jm} = l_{mj}$. If the solution gap from the proposed SOCP model is minimal for the forward flow from bus i to bus j, then $S_{ij}^2 \cong u_i l_{ij}$. If the power flows from bus j to bus i, the solution will also be considered exact if it satisfies $S_{ji}^2 \cong u_j l_{ij}$, which can be extended as follows:

$$S_{ij}^2 + (r_{ij}^2 + x_{ij}^2)l_{ij}^2 - 2l_{ij}(P_{ij}r_{ij} - Q_{ij}x_{ij}) \cong u_j l_{ij} \tag{5.38}$$

As the optimal solution for the forward flow is considered with a minimal solution gap as $S_{ij}^2 \cong u_i l_{ij}$, then from (5.38):

$$(r_{ij}^2 + x_{ij}^2)l_{ij} - 2(P_{ij}r_{ij} - Q_{ij}x_{ij}) \cong 0 \tag{5.39}$$

For the proposed SOCP-OPF model the voltage relation between bus $i \in \mathcal{N}$ and bus $j \in \mathcal{N}$ is expressed as follows:

$$u_j = u_i - 2(r_{ij}P_{ij} + x_{ij}Q_{ij}) + (r_{ij}^2 + x_{ij}^2)l_{ij} \tag{5.40}$$

From (5.39) and (5.40) for a reverse flow, the solution gap is also minimal if $u_i \cong u_j$. For the reverse flow in the branch $L_{jk} \in \mathcal{L}$, it can also be shown that for minimal gap solution, $u_j \cong u_k$. Suppose there is any possible bi-directional flow through a branch in a mesh network; the OPF solution gap will be minimal if the bus voltage difference between the two connected buses with that particular branch is minimal.

5.4 Exactness and the Optimality of the Proposed SOCP-OPF Model

The exactness and the global optimality of the proposed SOCP-OPF model are discussed in this section. The feasible set of the OPF problem is convex with the angle relaxation and conic relaxation of the non-linear equality in (5.13) within a conic space. The exactness of an OPF solution from the proposed model depends on the conic space formed by (5.14) and the cyclic angle constraints. The solution gap is defined as, $\sigma = |u_i l_{ij} - S_{ij}^2|$ in this article.

For the proposed OPF model, we have considered the objective function $f(x)$ as convex and increasing with the current flow I_{ij}. Let us consider an optimal solution set from the proposed OPF model as, $\tilde{\psi} = (\tilde{S}_{ij}, \tilde{l}_{ij}, \tilde{u}, \tilde{S}_g)$. Further, assume there exist another feasible solution set as $\hat{\psi} = (\hat{S}_{ij}, \hat{l}_{ij}, \hat{u}, \hat{S}_g)$, where $\hat{l}_{ij} = \tilde{l}_{ij} - \epsilon$, $\hat{S}_{ij} = \tilde{S}_{ij} - \epsilon z_{ij}$, $\hat{u}_i = \tilde{u}_i$, $\hat{S}_i^g = \tilde{S}_i^g$, $\hat{S}_i^d = \tilde{S}_i^d + \epsilon z_{ij}$ and $\hat{S}_j^d = \tilde{S}_j^d$ for a $\epsilon \geq 0$. Also, the solution $\hat{\psi}$ satisfies the angle cyclic constraints. The OPF objective value $f(\hat{\psi})$ is smaller than the objective value $f(\tilde{\psi})$ as, $\hat{l}_{ij} = \tilde{l}_{ij} - \epsilon$, has a strict smaller value. This contradicts the optimality of the solution set $\tilde{\psi}$ from the proposed OPF model. The proposed model will be proved as tight, and the solution is globally optimal if the cyclic constraints are satisfied and there is no other solution set lower than $\tilde{\psi}$. It is sufficient to show $\epsilon = 0$ for proving the global optimality. The following remarks validate the global optimality and the tightness of the model when cyclic constraints are satisfied in a mesh network.

Remark. *An optimal solution set is within the conic convex solution space if the solution satisfies (5.9), (5.11), (5.12), and (5.14).*

Proof. As $\tilde{\psi}$ is the optimal solution from the proposed OPF model, it satisfies (5.9), (5.11),

(5.12) and (5.14). The (5.11) and (5.12) are derived in terms of real and reactive power by splitting the (5.10). For analyzing (5.11)-(5.12) together, the power flow equation (5.10) with the apparent power S_i^g, apparent power flow S_{ij}, and current flow l_{ij} are considered here for the bus i & $j \in \mathcal{N}$. For the solution set $\hat{\psi}$ at the bus $i \in \mathcal{N}$:

$$\begin{aligned}
&\hat{S}_i = \hat{S}_i^g - \hat{S}_i^d = \tilde{S}_i^g - \tilde{S}_i^d - \epsilon z_{ij} \\
&= \sum_{j:i\to j} \tilde{S}_{ij} - \sum_{k:k\to i} (\tilde{S}_{ki} - z_{ki}\tilde{l}_{ki}) + y_i\tilde{u}_i - \epsilon z_{ij} \\
&= \sum_{j':i\to j', j\neq j'} \hat{S}_{ij'} + (\hat{S}_{ij} + \epsilon z_{ij}) - \sum_{k:k\to i} (\hat{S}_{ki} - z_{ki}\hat{l}_{ki}) + y_i\hat{u}_i - \epsilon z_{ij} \\
&= \sum_{j:i\to j} \hat{S}_{ij} - \sum_{k:k\to i} (\hat{S}_{ki} - z_{ki}\hat{l}_{ki}) + y_i\hat{u}_i
\end{aligned}$$

At the bus $j \in \mathcal{N}$:

$$\begin{aligned}
&\hat{S}_j = \hat{S}_j^g - \hat{S}_j^d = \tilde{S}_j^g - \tilde{S}_j^d \\
&= \sum_{k:j\to k} \tilde{S_{jk}} - \sum_{i:i\to j} (\tilde{S_{ij}} - z_{ij}\tilde{l_{ij}}) + y_j\tilde{u}_j \\
&= \sum_{k:j\to k} \hat{S_{jk}} - \sum_{i':i'\to j, i'\neq i} (\hat{S_{i'j}} - z_{i'j}\hat{l_{i'j}}) + y_j\hat{u}_j - [(\hat{S_{ij}} + \epsilon z_{ij}) - z_{ij}(\hat{l_{ij}} + \epsilon)] \\
&= \sum_{k:j\to k} \hat{S_{jk}} - \sum_{i:i\to j} (\hat{S_{ij}} - z_{ij}\hat{l_{ij}}) + y_j\hat{u}_j
\end{aligned}$$

For the solution set $\tilde{\psi}$, the voltage relation (5.9) is as follows considering the branch $L_{ij} \in \mathcal{L}$:

$$\begin{aligned}
&\tilde{u_j} = \tilde{u_i} - 2(r_{ij}\tilde{P}_{ij} + x_{ij}\tilde{Q}_{ij}) + (r_{ij}^2 + x_{ij}^2)\tilde{l}_{ij} \\
&\Rightarrow \hat{u_j} = \hat{u_i} - 2[r_{ij}(\hat{P}_{ij} + \epsilon r_{ij}) + x_{ij}(\hat{Q}_{ij} + \epsilon x_{ij})] + (r_{ij}^2 + x_{ij}^2)(\hat{l}_{ij} + \epsilon) \\
&\Rightarrow \hat{u_j} = \hat{u_i} - 2(r_{ij}\hat{P}_{ij} + x_{ij}\hat{Q}_{ij}) + (r_{ij}^2 + x_{ij}^2)\hat{l}_{ij} - \epsilon(r_{ij}^2 + x_{ij}^2)
\end{aligned}$$

The solution $\hat{\psi}$ satisfies (5.9) if $\epsilon(r_{ij}^2 + x_{ij}^2) \approx 0$. As for a branch $L_{ij} \in \mathcal{L}$, $(r_{ij}^2 + x_{ij}^2) \neq 0$. So $\hat{\psi}$ satisfies (5.9) only if $\epsilon = 0$.

As, $\tilde{\psi}$ is the optimal solution from the proposed OPF model, it is within the conic space as follows:

$$\begin{aligned}
&\tilde{u}_i\tilde{l}_{ij} - \tilde{S}_{ij}^2 \geq 0 \\
&\Rightarrow \hat{u_i}(\hat{l}_{ij} + \epsilon) - (\hat{S}_{ij} + z_{ij}\epsilon)^2 \geq 0 \\
&\Rightarrow \hat{u_i}\hat{l}_{ij} - \hat{S}_{ij}^2 + \epsilon[\hat{u}_i - z_{ij}^2\epsilon - 2\hat{S}_{ij}z_{ij}] \geq 0
\end{aligned}$$

If $\epsilon = 0$; $\hat{u_i}\hat{l_{ij}} - \hat{S_{ij}^2} \geq 0$. The solution set $\hat{\psi}$ is within the conic space and the solution gap $\epsilon[\hat{u}_i - z_{ij}^2\epsilon - 2\hat{S}_{ij}z_{ij}]$ is minimal. □

Remark. *When the solution satisfies the cyclic angle constraints, the OPF model is tight,*

along with when $\epsilon = 0$ the solution from the proposed OPF model is globally optimal.

Proof. $\hat{\psi}$ is the optimal solution with a minimal solution gap satisfying the cyclic angle constraints in the network. So for a mesh including the branch $L_{ij} \in \mathcal{L}$:

$$\sin^{-1}\frac{B_{ij}\hat{P}_{ij}+G_{ij}\hat{Q}_{ij}}{\hat{V}_i\hat{V}_j(G_{ij}^2+B_{ij}^2)}+\sin^{-1}\frac{B_{jk}P_{jk}+G_{jk}Q_{jk}}{V_jV_k(G_{jk}^2+B_{jk}^2)}+...+\sin^{-1}\frac{B_{j'i}P_{j'i}+G_{j'i}Q_{j'i}}{V_{j'}V_i(G_{j'i}^2+B_{j'i}^2)}=0 \quad (5.41)$$

As the cyclic angle constraint is imposed on the proposed SOCP-OPF model for the solution $\tilde{\psi}$ in the mesh cycle consisting of the branch $L_{ij} \in \mathcal{L}$. Then for the solution set of $\tilde{\psi}$:

$$\begin{aligned}&\sin^{-1}\frac{B_{ij}\tilde{P}_{ij}+G_{ij}\tilde{Q}_{ij}}{\tilde{V}_i\tilde{V}_j(G_{ij}^2+B_{ij}^2)}+\sin^{-1}\frac{B_{jk}P_{jk}+G_{jk}Q_{jk}}{V_jV_k(G_{jk}^2+B_{jk}^2)}+...+\sin^{-1}\frac{B_{j'i}P_{j'i}+G_{j'i}Q_{j'i}}{V_{j'}V_i(G_{j'i}^2+B_{j'i}^2)}=0\\ &\Rightarrow\sin^{-1}\frac{B_{ij}\hat{P}_{ij}+G_{ij}\hat{Q}_{ij}+\epsilon(B_{ij}r_{ij}+G_{ij}x_{ij})}{\hat{V}_i\hat{V}_j(G_{ij}^2+B_{ij}^2)}+\sin^{-1}\frac{B_{jk}P_{jk}+G_{jk}Q_{jk}}{V_jV_k(G_{jk}^2+B_{jk}^2)}+.....\\ &\qquad+\sin^{-1}\frac{B_{j'i}P_{j'i}+G_{j'i}Q_{j'i}}{V_{j'}V_i(G_{j'i}^2+B_{j'i}^2)}=0\end{aligned} \quad (5.42)$$

$\hat{\psi}$ is the optimal solution with a minimal solution gap. So, comparing (5.41) and (5.42) if $\epsilon \approx 0$; the cyclic constraints are satisfied similarly for $\tilde{\psi}$ as $\hat{\psi}$. The solution gap for $\tilde{\psi}$ is also minimal. The solution gap, defined as $\sigma = |u_i l_{ij} - S_{ij}^2|$ is measured after the OPF analysis. The solution gap (σ) is very small from the proposed model for the test cases in this article.

Further, for the two solution set $\tilde{\psi}$ and $\hat{\psi}$, it is assumed $f(\hat{\psi}) \leq f(\tilde{\psi})$. From the definition of the convexity for convex objective functions:

$$f(a\hat{\psi}+(1-a)\tilde{\psi}) \leq af(\hat{\psi})+(1-a)f(\tilde{\psi}) \quad (5.43)$$

where $a \in [0,1]$. Then:

$$af(\hat{\psi})+(1-a)f(\tilde{\psi}) \leq af(\tilde{\psi})+(1-a)f(\tilde{\psi}) \Rightarrow af(\hat{\psi})+(1-a)f(\tilde{\psi}) \leq f(\tilde{\psi})$$

From (5.43) and (5.44):

$$f(a\hat{\psi}+(1-a)\tilde{\psi}) \leq f(\tilde{\psi}) \quad (5.44)$$

Since $f(\tilde{\psi})$ is the optimal solution, so for any other solution within the convex space is $f(\psi) > f(\tilde{\psi})$, which contradicts with (5.44). To satisfy both conditions it must be $\tilde{\psi} = \hat{\psi}$, thus $\epsilon = 0$. So for a convex objective function, it is impossible to have another solution set lower than $\tilde{\psi}$. So the solution from the proposed OPF model is globally optimal and satisfies the cyclic angle constraints in the mesh network. □

5.5 Simulation and Evaluation

The proposed OPF model has been simulated and tested in the MATLAB® with the MOSEK® solver platform. The proposed OPF model is simulated in multiple standard test cases (i.e., IEEE 14-bus, 57-bus, 118-bus, and 2736-bus network systems [127]) and a synthetic 500-bus network [129]. The results from the proposed SOCP-OPF model are compared with the NLP-OPF and SDP-OPF solutions from MATPOWER® [127]. The solution from the SDP-OPF in MATPOWER® for the 118-bus network is globally optimal and feasible with a minimum branch resistance of 1×10^{-4} per unit [124]. Thus, The same network conditions are applied in the proposed SOCP-OPF model. It has been observed that the solution from the SOCP-OPF model matches with the solution from the SDP-OPF proven to yield global optimal solutions [124] for the test systems considered.

5.5.1 Implementation of the Proposed SOCP-OPF Model

The model implementation starts with the identification of the mesh cycles in the network using Algorithm 2. Then the optimization process is executed with the proposed SOCP-OPF model, where the cyclic constraints for all the meshes are satisfied. This improves the exactness of the SOCP-OPF model for mesh networks and provides a globally optimal solution.

As an illustrative example, in Fig. 5.6, the schematic diagram of the IEEE 14-bus network shows the mesh cycles with all of the branches associated with any loop. In the network, bus no. 8 is not associated with any mesh cycle and is considered as a radial type dangling branch from the Algorithm 2.

Table 5.1: Comparison of the angle difference summation over cycles between SOCP with cyclic constraints (CC) and without cyclic constraints (WCC) on the IEEE 14-bus network

Loop No.	SOCP-WCC 100% load (Degree)	SOCP-CC 100% load (Degree)	SOCP-WCC 200% load (Degree)	SOCP-CC 200% load (Degree)
1	2.1347	3.803e-07	4.4935	1.007e-06
2	-2.9525	0	-4.9639	0
3	0.0272	1.493e-07	-0.5300	6.981e-08
4	-0.3881	0	-2.2302	0
5	-0.5042	-9.94e-17	1.7143	1.988e-16
6	0.0999	0	0.8921	0
7	-0.1146	0	-0.394	0

Table 5.1 shows the comparison of the bus voltage phase difference summation over mesh cycles between SOCP-OPF with cyclic constraints (CC) and without cyclic constraints (WCC) for different loading conditions. For the WCC, the sum of the angle difference increases with the higher loading conditions. As a convex OPF model, the proposed model promises a globally optimal solution for convex objectives with the imposed cyclic constraints. The OPF solution from the proposed model for the IEEE 14-bus network is compared with

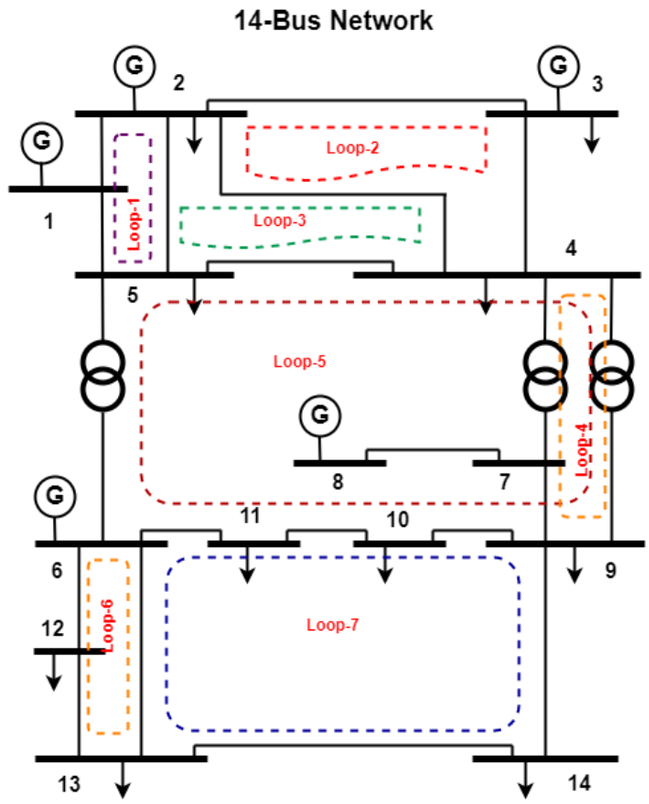

Figure 5.6: Single line schematic diagram of the IEEE 14-bus network.

Table 5.2: Generation comparison in IEEE 14-bus network (linear cost function)

Bus No.	C_1	Pg (MW) (SOCP)	Qg (MVAR) (SOCP)	Pg (MW) (NLP)	Qg (MVAR) (NLP)
1	20	128.58	0	128.58	0
2	20	139.99	21.72	140.00	21.70
3	40	0	30.04	0	30.04
6	40	0	10.22	0	10.15
8	40	0	8.05	0	8.05

the benchmark results from NLP-OPF and SDP-OPF models in MATPOWER. The real and reactive power generation for the minimum generation cost objective function is shown in Table 5.2 and Table 5.3. It is observed that the power generation in different buses is same as the NLP-OPF model.

The proposed OPF model is further simulated on more extensive networks to check the scalability. Table. 5.4 shows the generation comparisons of the proposed SOCP-OPF model with NLP-OPF and a convex SDP-OPF model. The network conditions for the proposed SOCP-OPF model are the same as the MATPOWER models. The percent of generation mismatch between the proposed SOCP-OPF vs. NLP-OPF and SOCP-OPF vs. SDP-OPF model is illustrated in Table 5.4. MATPOWER uses an interior point solver. Due to the solver difference, there is a negligible generation discrepancy between the OPF models. The maximum real power difference for the SOCP-OPF vs. NLP-OPF is 0.09% (2736-Bus Network), and the reactive power difference is 0.84% (118-Bus Network). For the SOCP-OPF vs. SDP-OPF, the maximum real power difference is 0.11%, and the reactive power

Table 5.3: Generation comparison in IEEE 14-bus network (quadratic cost function)

Bus No.	C_2	C_1	C_0	Pg (MW) (SOCP)	Qg (MVAR) (SOCP)	Pg (MW) (NLP)	Qg (MVAR) (NLP)
1	0.04	20	0	194.40	0	194.43	0
2	0.25	20	0	36.78	23.70	36.80	23.67
3	0.01	40	0	28.74	25.12	28.75	25.13
6	0.01	40	0	0	12.71	0	12.63
8	0.01	40	0	8.52	8.51	8.50	8.51

difference is 0.81% (2736-Bus Network). Due to space constraints, only the voltage profile of the IEEE 118-bus network is demonstrated in Fig.5.7. The power loss from the proposed SOCP-OPF model and the voltage profile mismatch between the proposed OPF model and the NLP-OPF model is illustrated in Table 5.6. The tightness of the OPF model has been analyzed using the solution gap from (5.14) represented as $\sigma = |u_i l_{ij} - S_{ij}^2|$. The solution gap ($\sigma$) for all the branches is measured, and the average value is presented in Table 5.6. For all of the test cases, the σ and % of voltage deviation (Δv) are minimal for the proposed OPF model compared to the NLP counterpart. The convergence time of the proposed SOCP-OPF is compared with the SDP-OPF and NLP-OPF models as shown in Table 5.7. The test system is an Intel(R) Core(TM) i7-10510U CPU, 2.30 GHz processor, and 16 GB RAM machine. From the results shown in Table 5.7, it is observed that the convergence time for the proposed SOCP-OPF model is significantly lower than the NLP-OPF and SDP-OPF models.

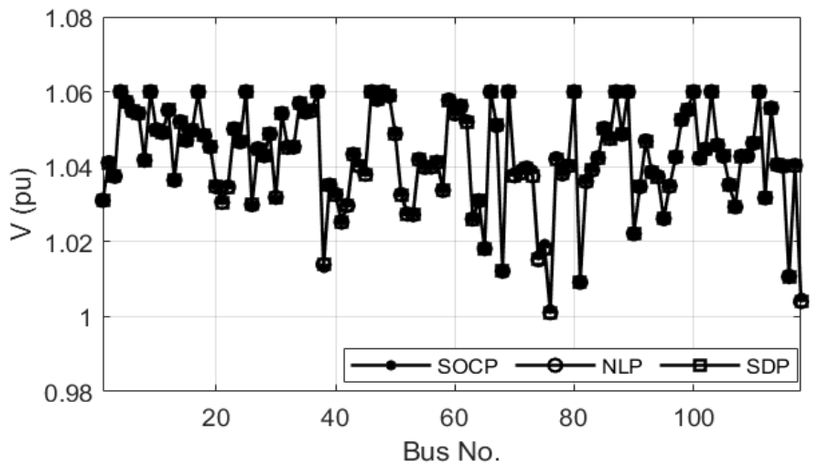

Figure 5.7: Voltage profile for the IEEE 118-bus network.

5.5.2 Impact of the Envelope Width on the SOCP-OPF

This section evaluates one of the major contributions to deriving a convex envelope based on (5.16) and (5.17). The optimal solution from the proposed model includes an optimal bus voltage angle difference within the envelope based on the power flow and satisfies the cyclic angle constraints as (5.15). The impact of the envelope width on the θ_{ij} is illustrated in Fig.

Table 5.4: Comparison of different OPF models with the Proposed SOCP-OPF model

Test Case	Connected Load		SOCP		NLP		SDP		SOCP vs NLP		SOCP vs SDP	
	Pd (MW)	Qd (MVAR)	Pg (MW)	Qg (MVAR)	Pg (MW)	Qg (MVAR)	Pg (MW)	Qg (MVAR)	ΔP_g	ΔQ_g	ΔP_g	ΔQ_g
14-Bus Network	259.00	73.50	268.44	70.44	268.58	69.94	268.58	69.94	0.05%	0.70%	0.05%	0.70%
57-Bus Network	1250.80	336.40	1266.61	273.60	1267.00	272.24	1267.00	272.24	0.03%	0.50%	0.03%	0.50%
118-Bus Network	4242.00	1438.00	4328.47	455.67	4329.05	451.84	4329.05	457.73	0.01%	0.84%	0.01%	0.45%
500-Bus Network	3692.69	984.73	3750.68	608.31	3750.43	607.40	3750.41	607.58	.006%	0.15%	.007%	0.12%
2736-Bus Network	18074.5	5837.2	18419.3	3042.4	18437.4	3056.5	18439.7	3067.2	0.09%	0.46%	0.11%	0.81%

Table 5.5: Impact of the width of the proposed envelope on the θ_{ij} from the proposed SOCP-OPF model

Test Case	θ_{ij}^{m} (Degree)	Branch No. with Maximum θ_{ij}	Connected Buses (From-To)	Envelope Lower Limit (Degree)	Envelope Upper Limit (Degree)	θ_{ij} From the Model (Degree)	Standard Deviation $\Delta\theta_{ij}$ (Degree)
14-Bus Network	20°	3	2-3	8.6447	8.9503	8.6562	0.2969
	30°	3	2-3	8.5482	9.6529	8.8552	0.3951
57-Bus Network	20°	8	8-9	5.1142	5.4198	5.1611	0.1330
	30°	8	8-9	5.0916	5.7963	5.2189	0.2487
118-Bus Network	20°	68	49-42	18.575	18.781	18.594	0.3507
	30°	68	49-42	18.086	18.791	18.607	0.4451
500-Bus Network	20°	521	247-246	14.580	14.620	14.591	0.2061
	30°	521	247-246	14.570	14.621	14.593	0.3472
2736-Bus Network	20°	74	28-25	12.087	12.292	12.170	0.2601
	30°	74	28-25	12.076	12.781	12.657	0.3670

Table 5.6: Voltage comparison between SOCP-OPF vs NLP-OPF

Test case	Voltage Mismatch (SOCP vs NLP)	Power Loss (SOCP)	Avg. Solution Gap (SOCP)
14-Bus Network	0.000 %	3.56 %	5.1e-09
57 Bus Network	0.008 %	1.28 %	9.4e-09
118-Bus Network	0.015 %	1.99 %	2.3e-09
500-Bus Network	0.007 %	1.54 %	1.4e-08
2736-Bus Network	0.025 %	1.87 %	7.03e-09

Table 5.7: OPF solution convergence time comparison and execution time of Algorithm 2

Test Case	Run Time (sec) (Algorithm 2)	OPF Convergence Time (sec)		
		SOCP	NLP	SDP
14-Bus Network	0.34	0.31	0.34	0.39
57-Bus Network	1.52	0.34	0.56	0.44
118-Bus Network	2.04	0.41	0.64	0.48
500-Bus Network	6.24	0.52	1.05	6.47
2736-Bus Network	15.85	1.47	3.52	322.4

5.8 for the IEEE 14-bus, IEEE 57-bus, and IEEE 118-bus networks. In the figure, θ_{ij} is shown for the $\theta_{ij}^m = 20°$, and $30°$, where, θ_{ij}^m is defined as $\theta_{ij}^m = max[|\underline{\theta_{ij}}|, |\overline{\theta_{ij}}|]$ for the envelope in (5.16) and (5.17). While θ_{ij}^m increases, the width of the envelope increases, so the deviation of θ_{ij} from the optimal point increases, which is illustrated in Table 5.5. The $\theta_{ij}(NLP)$ is the reference value determined from the NLP-OPF solution in MATPOWER. Then the standard deviation of θ_{ij} is illustrated as $\Delta\theta_{ij}$, which is defined as $\Delta\theta_{ij} = \sqrt{\frac{[\theta_{ij}(NLP)-\theta_{ij}(SOCP)]^2}{N_L}}$, N_L is the total number of branches in the network. From the analysis, the standard deviations are considerably low even for $\theta_{ij}^m = 30^o$ for all the cases, which is an acceptable range for the envelope for most practical transmission networks. From this, it is observed that a reasonable width can be considered for the envelope with the proposed SOCP-OPF model for optimal operation. The impact of the envelope width on the solution gap (σ) is illustrated in Fig. 5.9 for the IEEE 118-bus network. It is observed as when the width of the envelope is smaller, and the cyclic constraints (CC) are considered, the solution gap (σ) is considerably lower than without considering (WCC). With the cyclic constraints, the solution gap (σ) is less than 1×10^{-7}. The figure shows the results in per-unit (pu) with a base of 100 MVA. This concludes that the proposed model's cyclic constraints significantly improve the exactness of the SOCP-OPF model for mesh networks.

5.5.3 Analysis of Voltage Difference on the Solution Gap

The effect of the voltage change for bi-directional flow is analyzed with the change of loading conditions. A load in a particular bus is changed with a multiplying factor $\lambda \in [0, 3]$ (i.e., when $\lambda = 1$ the load is increased by 100% and when $\lambda = 2$, increased by 200% and so on) for observing the impact of the bus voltage difference between two adjacent connecting buses and thus tightness of the proposed model. For the IEEE 14-bus network's overload condition, the voltage difference between bus no. 1 and bus no. 2 is low. Hence, the solution

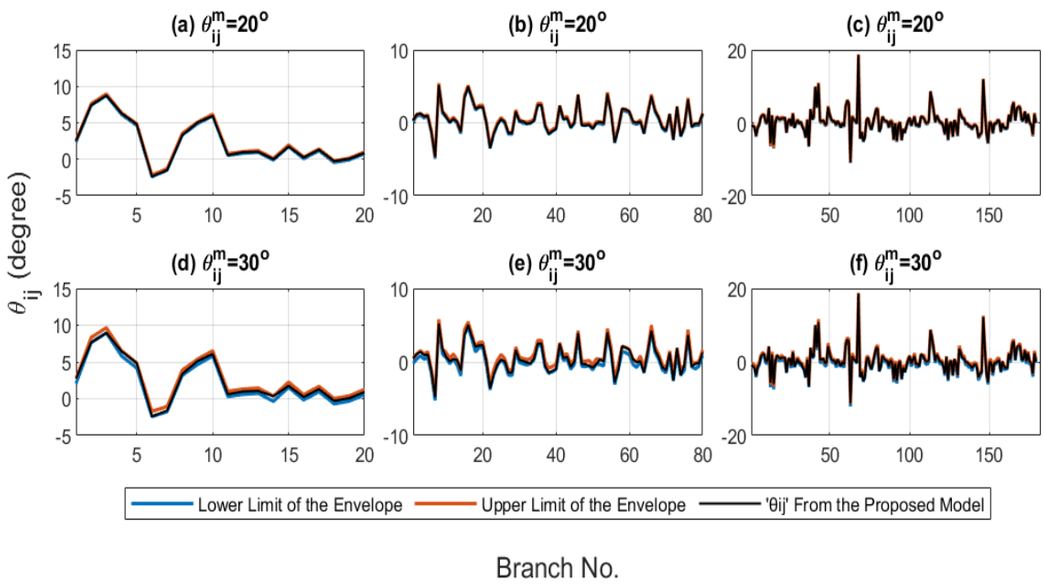

Figure 5.8: θ_{ij} from the proposed envelope satisfying the cyclic constraints. Here, (a) & (d) are for the IEEE 14-bus network, (b) & (e) are for the IEEE 57-bus network, and (c) & (f) are for the IEEE 118-bus network, respectively.

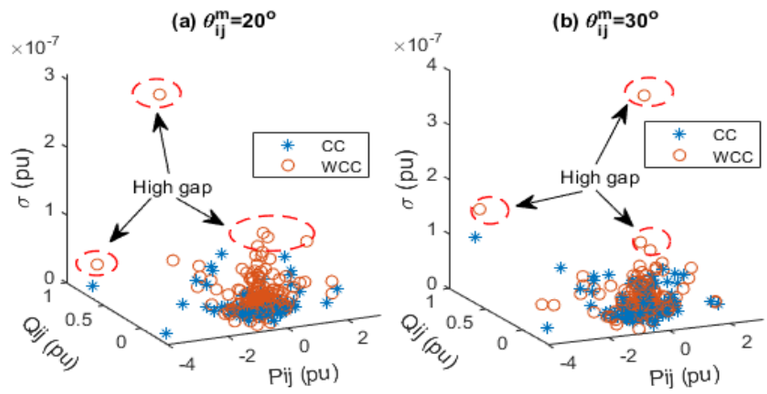

Figure 5.9: Impact of the envelope width on the solution gap (σ) for the IEEE 118-bus network (a) $\theta_{ij}^m = 20^o$ (b) $\theta_{ij}^m = 30^o$.

gap (σ) is low, and while the cyclic constraints are applied, the OPF model is tighter, which is shown in Fig. 5.10 (a)-(b). The metric σ presents the overall tightness, with close to zero being tighter and thus more accurate. To illustrate the effect of a more extensive network, bus no. 43 and bus no. 44 in the IEEE 118-bus network are considered. The solution gap is checked by assessing the voltage difference for both conditions (i.e., with and without imposing the cyclic constraints). When there is a load increase (considered as the multiplying factor $\lambda \in [0, 3]$). The results show that the model is tight with CC and WCC when the voltage difference between two adjacent buses is small. However, with a larger voltage difference between adjacent buses, the solution gap is comparatively higher when cyclic constraints are not considered. This impact is observed on other buses as well. The solution gap from the proposed SOCP-OPF model is significantly lower, as shown in Fig. 5.10 (c)-(d). These results show that the proposed architecture is tight even for bi-directional flow if the cyclic constraints are applied with the OPF model.

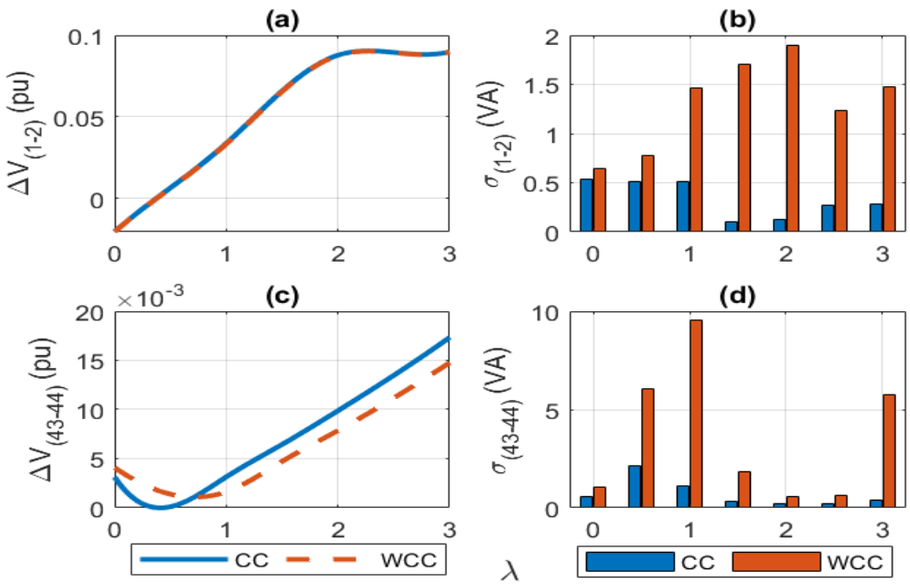

Figure 5.10: Impact of the bus voltage difference on the solution gap (σ). Here, (a) & (b) and (c) & (d) are for the IEEE 14-bus and 118-bus networks, respectively. (CC: Cyclic constraints, WCC: Without cyclic constraints.)

5.6 Summary

This chapter represents a novel branch flow-based SOCP-OPF model for meshed power transmission networks. A convex envelope is derived to satisfy cyclic angle constraints in meshed power networks. The tightness of the proposed OPF model and the solution gap is improved when the cyclic angle constraints are imposed. The condition for the proposed SOCP-OPF model's tightness for bi-directional power flow through a branch is also analyzed. The OPF model has been simulated and evaluated for several IEEE standard meshed transmission test networks and compared with NLP-OPF and SDP-OPF models. From the simulation analysis, the proposed model is tight and provides a globally optimal solution. Furthermore, the computational efficiency and solution time for convergence of the proposed SOCP-OPF is improved by up to 58% when compared to the NLP-OPF and SDP-OPF models for large networks. The proposed OPF model is extendable for the mixed-integer version of OPF analysis and contingency analysis for unbalanced power networks.

CHAPTER 6: OPTIMAL POWER FLOW (OPF) ANALYSIS FOR AC-DC TYPE ACTIVE DISTRIBUTION NETWORKS WITH SECOND ORDER CONE PROGRAMMING (SOCP) MODEL

6.1 Introduction and Contribution

Power system network grids are mainly based on alternating current (AC) [130, 131]. Due to the invention of modern power converters with renewable-based distributed energy resources (DERs) and increased use of modern DC-type loads, DC grid systems are getting incorporated with the conventional AC grid system [27, 28]. Though DC grid-systems have several advantages over AC grid-systems [132, 133], complete replacement of AC grid with DC systems is not feasible [134]. Hence, the researcher proposes the AC-DC power network system leveraging the benefits of the DC systems connected with AC grid systems [135, 136].

Under different constraints (i.e., network thermal and reactive power limits), the optimal power flow (OPF) analysis is a salient tool for system operation and planning. Due to the nonlinearity of Conventional AC-OPF formulations, AC-OPF analysis is nondeterministic polynomial (NP) hard (NP-hard) in its original form [13]. Due to this complexity, linear approximated models (i.e., DC-OPF [21]) are used, which compromise the solution accuracy [137]. The conventional OPF models fail to perform the OPF analysis of the AC-DC network accurately as the AC-DC network has additional components such as converters, additional types of buses, etc. The solution to the OPF analysis of the AC-DC networks through conventional OPF models may lead to computational infeasibility. Hence, researchers have focused on developing efficient OPF models for AC-DC power distribution networks.

Few works of literature have discussed the OPF analysis for the AC-DC distribution networks. An AC-DC load flow model based on the Newton Raphson (NR) OPF has been proposed in [138] with voltage source converter (VSC) HVDC links but did not consider the DC grid. The net active power injection into the DC system area accounts for the DC links. A generalized approach to the load flow analysis considering the converters and DC grid of AC–DC distribution systems is discussed in [139]. But, these load flow models also do not consider the optimal operation of the network. An OPF model for transmission systems with volatile renewable resources is presented in [140] with AC-DC network structure. But, the non-convexity in OPF equations do not guarantee a globally optimal solution [141], [142].

As the convex relaxation of AC-OPF problems is computationally efficient [22], [106], and conditionally exact [57, 90, 143] (hence, AC-feasible). Hence, a modified second-order cone (SOC) [68] based convex model will be an efficient approach for the OPF analysis in a dis-

tribution network with AC-DC structural orientation. The research work presented in [144] validates the above statement by using SOCP-based formulation with voltage source converters (VSC) for AC-DC type power distribution systems. Nevertheless, the model does not consider radial distribution networks and DERs. Hence, this article proposes an OPF model using SOCP for AC-DC-type distribution networks with DERs. Then a modified interior point method (IPM) based non-linear NLP-OPF model is considered to compare the performance of the proposed AC-DC SOCP-OPF model. NLP-OPF models are computationally challenging [61, 62]. The SOCP-OPF model proposed in this article is based on branch flow-based power flow equations.

6.1.1 Major Contributions

The contributions of the proposed approach are as follows:

- Even though with the angle and conic relaxations of the power flow relations and the relaxation of the non-linear relations of the power converters (i.e., AC-DC rectifiers, DC-AC inverters) with McCormick envelopes the SOCP-OPF model provides an exact optimal solution for AC-DC distribution networks. Being convex in nature, the OPF model guarantees the globally optimal solution.

- The proposed model determines the optimal modulation index of the converters (i.e., AC/DC rectifiers and DC/AC inverters) based on the objective functions, converter ratings, and network constraints.

- A minimum voltage deviation condition is considered with the objective functions using a participation factor variable. With different participation factors and DERs penetration, the OPF model provides optimal solutions providing the robustness of the OPF analysis approach.

- The computational efficiency of the SOCP-OPF model for AC-DC networks has been verified by comparing it with an IPM-based NLP-OPF model in this article. The simulation analysis proves that the SOCP-OPF model is computationally superior to the NLP-OPF model.

The organization of this chapter is as follows. Section 6.2 discusses the AC-DC distribution network, and Section 6.3 discusses the proposed OPF methodology. An interior point-based NLP-OPF model is discussed in Section 6.4. Then, Section 6.5 discusses the model result analysis from the simulated test cases. Finally, the summary is discussed in Section 6.6 of this chapter.

The variable and parameters used in this chapter are as follows:

$\mathcal{N}$:	Set of all the buses in the network
VD_{max}:	Max voltage deviation from the reference voltage
σ_{ij}:	solution-gap
M:	Modulation index of a converter
K:	Participation factor of the objectives
$\mathcal{N}$:	Set of the buses
$\mathcal{N}_g$:	Set the buses with DERs
$\mathbb{L}$:	Set of the branches
v_i:	Bus voltage at $i \in \mathcal{N}$
u_i:	voltage magnitude square at $i \in \mathcal{N}$
s_i^g:	Injection of power (apparent) at $i \in \mathcal{N}_g$
s_i^d:	Load at $i \in \mathcal{N}$
p_i^g:	Injection of power (real) at $i \in \mathcal{N}_g$
p_i^d:	Load (real) at $i \in \mathcal{N}$
q_i^g:	Injection of power (reactive) at $i \in \mathcal{N}_g$
q_i^d:	Load (real) at $i \in \mathcal{N}$
P_{ij}:	Power flow (real) in $L_{ij} \in \mathbb{L}$
Q_{ij}:	Power flow (reactive) in $L_{ij} \in \mathbb{L}$
S_{ij}:	Power flow (apparent) in $L_{ij} \in \mathbb{L}$
I_{ij}:	Current through $L_{ij} \in \mathbb{L}$
l_{ij}:	Square of current magnitude through $L_{ij} \in \mathbb{L}$
z_{ij}:	Line impedance of $L_{ij} \in \mathbb{L}$
c_i:	DER's cost-coefficients at $i \in \mathcal{N}_g$

6.2 AC-DC Structure of Distribution Network

The hybrid structure of AC-DC distribution systems consist different AC and DC components which includes conventional AC loads, DC loads (i.e., Electric vehicles (EVs)), AC generators, and DC generating units (i.e., PV farms), as shown in Fig. 6.1. In the OPF analysis, the inclusion of the converter model is challenging because of its nonlinear characteristics. This chapter utilizes the per-unit equivalent mathematical model of the power converter developed by the authors in [145] [146].

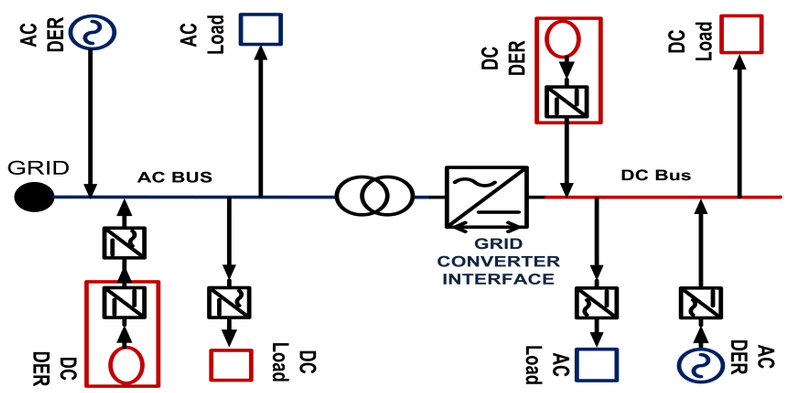

Figure 6.1: Single line representation of an AC-DC distribution network.

Per Unit relation of converters (PWM Inverter & Rectifiers): The input-output voltage and power relationships (in per-unit) of the converters can be represented using (6.1) and (6.2), respectively.

$$v_j = v_i M \tag{6.1}$$

$$P_{out} = \eta P_{in} \tag{6.2}$$

where η is the efficiency co-efficient of the converter and M is the modulation index. The base value relation on input and output sides of the converters is provided in Table 6.1.

Table 6.1: Converter input-output base relation

PWM Rectifier	PWM Inverter
$V_{dc} = \frac{2\sqrt{2}}{\sqrt{3}} V_{ac}$	$V_{ac} = \frac{\sqrt{3}}{2\sqrt{2}} V_{dc}$
$I_{dc(B)} = \frac{3}{2\sqrt{2}} I_{ac}$	$I_{ac} = \frac{2\sqrt{2}}{3} I_{dc}$

6.3 Proposed Methodology for SOCP-OPF

6.3.1 Branch Flow Model

In this article, we have considered radial distribution networks with n number buses. $\mathcal{N}$ is the set of all buses in the network with $\mathcal{N} = \{1, 2, 3....., n\}$. $\mathbb{L}$ represents the set of the branches with $n-1$ number of branches. The branches are denoted as L_{ij} connecting the pair of buses (i, j). v_i denotes the bus voltage at $i \in \mathcal{N}$. With the apparent power S_{ij} and current flow I_{ij} in $L_{ij} \in \mathbb{L}$, the power flow relations are represented as follows:

$$S_{ij} = v_i I_{ij}^* \tag{6.3a}$$

where the distribution lines are modeled with a series impedance of $z_{ij} = r_{ij} + jx_{ij}$ for the branch $L_{ij} \in \mathbb{L}$. As a radial-type network, any bus of the network has only one incoming branch. So, the apparent power at $j \in \mathcal{N}$ is as:

$$s_j^g - s_j^d + S_{ij} - z_{ij}|I_{ij}|^2 = \sum_{j \to k} S_{jk} \tag{6.3b}$$

where s_j^g is the apparent power injected by DERs, and s_j^d is the apparent load associated with the bus $j \in \mathcal{N}$.

If a converter is located at the bus j of the network, then a dummy bus is considered as $j^{'}$ at the input of the converter. Therefore, the input/output relation of the voltage for the converter is represented as follows:

$$v_j = v_{j'} M \tag{6.3c}$$

The benefits of the convex OPF analysis are already discussed in the introduction section of this article. Angle and conic relaxation are considered for the convexification for the SOCP-OPF model, which is discussed in the following subsection.

6.3.2 Angle, Conic and McCormick Relaxation

6.3.2.1 Angle and Conic relaxation

For convexification, the phase angle of the voltage and current phase is relaxed. Then, new variables are defined as, $|v_i|^2 = u_i$ and $|I_{ij}|^2 = l_{ij}$. With the new-defined variables, the power flow relationships are as follows:

$$u_i l_{ij} = S_{ij}^2 \tag{6.4}$$

Considering the voltage magnitude square and using the new-define variables for the squared terms, the voltage drop between the bus pair $(I, j) \in \mathcal{N}$ is as follows:

$$u_j = u_i + |z_{ij}|^2 l_{ij} - (z_{ij} S_{ij}^* + z_{ij}^* S_{ij}) \tag{6.5}$$

With the new variables, at bus $j \in \mathcal{N}$ the power balance is:

$$s_j^g + S_{ij} - z_{ij} l_{ij} - s_j^d = \sum_{j \to k} S_{jk} \tag{6.6}$$

Along the angle relaxation, the relation in (6.4) is convexified with conic relaxation with the following inequality:

$$u_i l_{ij} \geq P_{ij}^2 + Q_{ij}^2 \tag{6.7}$$

For the AC-DC network, the proposed OPF model considers multiple power converters. For the converters, the voltage relation is as follows:

$$|v_j|^2 = |v_{j'}|^2 M^2 \Rightarrow u_j = u_{j'} m (6.8)$$

where $m = M^2$. (6.8) is still non-convex, which is convexified with the McCormick envelopes.

6.3.2.2 McCormick Relaxation for the Converters

AC-DC networks contain multiple converters. In this article, the AC-DC and DC-AC converters are considered only. As the modulation index (M) is an optimization variable, (6.8) is non-convex. So the voltage relation (6.8) is convexified with McCormick envelopes [74]. For the converter at the bus $j \in \mathcal{N}$ if the input voltage relation is noted as $u_{j'} = u_{in}$ and the output as $u_j = u_{out}$, the voltage relationship is as follows:

$$u_{out} = u_{in} m \tag{6.9}$$

This non-convex relation in (6.9) is convexified with the following McCormick envelopes:

$$u_{out} \geq m^L u_{in} + m u_{in}^L - m^L u_{in}^L \tag{6.10a}$$

$$u_{out} \geq m^U u_{in} + m u_{in}^U - m^U u_{in}^U \tag{6.10b}$$

$$u_{out} \leq m^U u_{in} + m u_{in}^L - m^U u_{in}^L \tag{6.10c}$$

$$u_{out} \leq m^L u_{in} + m u_{in}^U - m^L u_{in}^U \tag{6.10d}$$

where $m^L = \underline{m}$, $m^U = \overline{m}$, $u_{in}^U = |\overline{v}_{in}|^2$ and $u_{in}^L = |\underline{v}_{in}|^2$, modulation index as $m_{_{AC-DC}} = M_{_{AC-DC}}^2$ and $m_{_{DC-AC}} = M_{_{DC-AC}}^2$ for AC-DC and DC-AC converters.

6.3.3 Operational Cases for a Network with AC-DC Structure

An AC-DC type distribution network structure forms with multiple network configurations, as illustrated in Fig. 6.2. This section evaluates the mathematical formulations of the proposed SOCP-OPF model for the network.

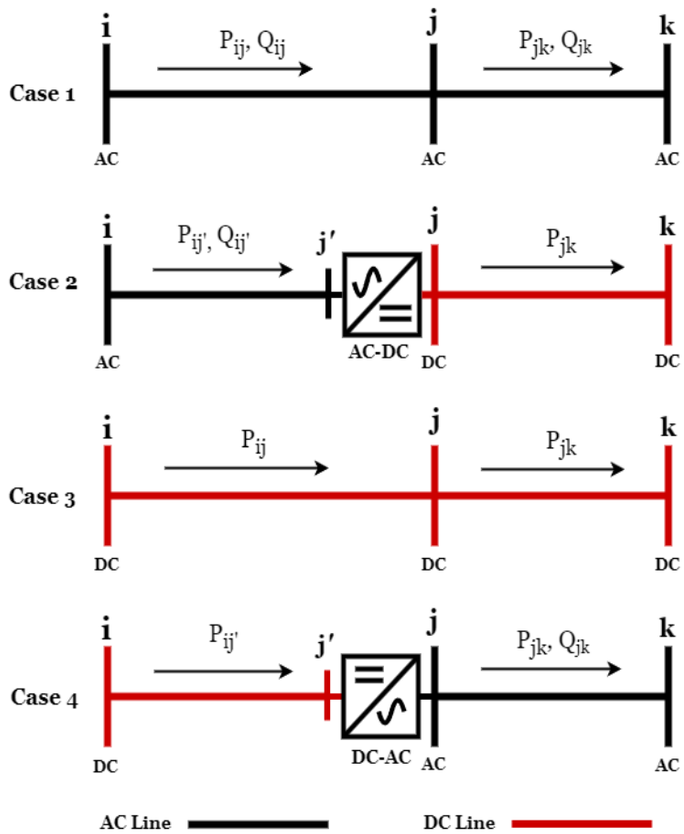

Figure 6.2: AC-DC network model with converters.

6.3.3.1 Case: 1 (AC-AC Network)

Only AC network sections of a network are considered for this case. So only the AC-AC convexified equations are considered for the power flow, which is illustrated as follows:

$$p_j^g + P_{ij} - r_{ij} l_{ij} - p_j^d = \sum_{j \to k} P_{jk} \tag{6.11a}$$

$$q_j^g + Q_{ij} - x_{ij} l_{ij} - q_j^d = \sum_{j \to k} Q_{jk} \tag{6.11b}$$

The (6.11a), and (6.11b) are derived by splitting (6.6) in terms of real and reactive power, using $S_{ij} = P_{ij} + jQ_{ij}$, $s_j^g = p_j^g + jq_j^g$, and $s_j^d = p_j^d + jq_j^d$. Further simplifying (6.5) and (6.7):

$$u_j = u_i - 2(r_{ij} P_{ij} + x_{ij} Q_{ij}) + (r_{ij}^2 + x_{ij}^2) l_{ij} \tag{6.11c}$$

$$u_i + l_{ij} \geq \left\| \begin{matrix} 2P_{ij} \\ 2Q_{ij} \\ u_i - l_{ij} \end{matrix} \right\|_2 \tag{6.11d}$$

6.3.3.2 Case: 2 (AC-DC converter)

Case: 2 is considered at the coupling buses where an AC section is connected with a DC section through a converter in the network. An example section of case: 2 is shown in Fig. 6.2. For an AC-DC converter at the bus j, a dummy node $j^{'}$ is considered at the input of the converter. Then the load flows through the branch $L_{ij'}$ before the AC-DC converter is as follows (6.11a)-(6.11d).

The voltage and power conversion relationships for the converters are as follows:

$$u_j = m_{_{AC-DC}} u_{j'} \tag{6.12a}$$

where $M_{_{AC-DC}}$ is the converter's (rectifier) modulation index and $m_{_{AC-DC}} = M_{_{AC-DC}}^2$. For the proposed analysis, (6.12a) is relaxed with the McCormick envelope as in (6.10). Then,

$$P_{out}^{DC} = \eta P_{in}^{AC} \tag{6.12b}$$

where P_{in}^{AC} is the input power at the dummy node $j^{'}$, and the converter efficiency is η.

6.3.3.3 Case 3 (DC-DC Network)

Only DC-DC network sections of an AC-DC network are considered for this case. So only the real power equations are considered for the load flow, which is illustrated as follows:

$$p_j^g - p_j^d + P_{ij} - r_{ij} l_{ij} = \sum_{k:j \to k} P_{jk} \tag{6.13a}$$

$$u_j = u_i - 2r_{ij} P_{ij} + r_{ij}^2 l_{ij} \tag{6.13b}$$

$$u_i + l_{ij} \geq \left\| \begin{matrix} 2P_{ij} \\ u_i - l_{ij} \end{matrix} \right\|_2 \tag{6.13c}$$

The (6.13a)-(6.13c) are derived from the (6.5), (6.6) and (6.7), where only the real power components are considered.

6.3.3.4 Case 4 (DC-AC Network)

This is considered at the coupling buses where a DC network section is connected with an AC section through a DC-AC converter. An example section of the case: 4 is demonstrated in Fig. 6.2. If the converter's (inverter) modulation index is $M_{_{DC-AC}}$, the power flow through the converter is as follows:

$$P_{out}^{AC} = \eta P_{in}^{DC} \tag{6.14a}$$

where P_{in}^{DC} is the DC input power to the converter at the dummy node $j^{'}$ and P_{out}^{AC} is the AC output power from the inverter at the bus j. The voltage relation of the converter is as follows:

$$u_j = m_{_{DC-AC}} u_{j'} \tag{6.14b}$$

where modulation index $m_{_{DC-AC}} = M_{_{DC-AC}}^2$. For the proposed analysis, (6.14b) is relaxed using the McCormick envelope as in (6.10).

6.3.4 Proposed SOCP-OPF Model

OPF analysis is performed to determine the optimal operating point (i.e., p_i^g, q_i^g, etc.) for an objective function $f(x, y)$ maintaining the network operational and control constraints. The objective function of the OPF analysis for an AC-DC type network is established as:

$$f(x_i, y_i) = f_{_{AC}}(x_i^{AC}, y_i^{AC}) + f_{_{DC}}(x_i^{DC}, y_i^{DC}) \tag{6.15}$$

where x is a vector of the control variables (i.e., the active and reactive power from the controllable shunts, etc.) and y is a vector of the state variables (i.e., the voltage magnitude). $f_{_{AC}}$ and $f_{_{DC}}$ stand for the AC and DC variables of the objective function $f(x, y)$, respectively. For an AC-DC network, the SOCP-OPF model is proposed as:

$$min \sum f(x_i, y_i) \tag{6.16}$$

Subject to $(s.t.) : \{(6.11a) - (6.14b)\}$ (case-wise) and,

$$s.t. \begin{cases} \underline{p}_i^g \leq p_i^g \leq \overline{p}_i^g \\ \underline{q}_i^g \leq q_i^g \leq \overline{q}_i^g \\ l_{ij} \leq \bar{l}_{ij} \\ \underline{u}_i \leq u_i \leq \overline{u}_i \\ \underline{M} \leq M \leq \overline{M} \end{cases} \tag{6.17}$$

where $\underline{p}_i^g$ and $\overline{p}_i^g$ are the minimum and maximum limit of real power injection and $\underline{q}_i^g$ and $\overline{q}_i^g$ are the minimum and maximum limit of reactive power injection from the DERs at $i \in \mathcal{N}_g$. $\underline{u}_i = |\underline{v}_i|^2$ and $\overline{u}_i = |\overline{v}_i|^2$ at $i \in \mathcal{N}$ and $\bar{l}_{ij} = |I_{ij}^{rated}|^2$ at $L_{ij} \in \mathbb{L}$. M is the modulation index for a converter with $\underline{M} = \underline{v}/\overline{v}$ and $\overline{M} = \overline{v}/\underline{v}$.

6.3.4.1 Objective Functions

This article considers different convex objective functions. For generation cost minimization or network loss minimization, the converters are prone to dispatch the maximum limit of reactive support. This results in the voltages hitting the maximum limits. So the system lacks the required reactive reserves during any contingencies in the network in a particular operating condition [147]. To avoid this situation, the voltage deviation value is included as a part of the objective function [148]. The objective function $f(x, y)$ considered with the proposed model is as follows:

a) Network loss:

$$f_1(x) = \sum_{L_{ij} \in \mathbb{L}} r_{ij} l_{ij} \tag{6.18}$$

or generation cost:

$$f_1(x) = \sum_{i \in \mathcal{N}_g} c_i p_i^g \tag{6.19}$$

where c_i is the cost-coefficients for the DERs at $i \in \mathcal{N}_g$ and for convex cost equation $c_i \geq 0$.

b) The deviation of voltage is included to the objective function as follows:

$$f_2(y) = \sum_{i \in \mathcal{N}} \frac{|u_i - u_i^r|}{n} \tag{6.20}$$

where $u_i^r = |v_i^r|^2$; v_i^r is the reference voltage of a bus at $i \in \mathcal{N}$ and n is the total bus in the network.

Finally, the objective is as follows:

$$f(x,y) = (1-K)f_1(x) + Kf_2(y) \qquad K \in [0,1] \tag{6.21}$$

where K is the participation factor for the objective function. The SOCP-OPF model is compared with an interior point method (IPM) based NLP-OPF model.

6.4 Interior Point Method-based NLP-OPF Model

The injected active power (p_i) and reactive power (q_i) at a bus $i \in \mathcal{N}$ can be written as follows [59]:

$$p_i = v_i^2 G_{ii} + \sum_{j=1}^{n} v_i v_j [G_{ij} cos(\theta_i - \theta_j) + B_{ij} sin(\theta_i - \theta_j)] \tag{6.22}$$

$$q_i = -v_i^2 B_{ii} + \sum_{j=1}^{n} v_i v_j [G_{ij} sin(\theta_i - \theta_j) - B_{ij} cos(\theta_i - \theta_j)] \tag{6.23}$$

where θ_i is the voltage phase angle at $i \in \mathcal{N}$ and $i \neq j$. Y_{ij} denotes the off-diagonal elements of the Y bus matrix, which is defined as $Y_{ij} = G_{ij} + jB_{ij}$ for the network. For the OPF analysis, equality constraints regarding the power balance are as follows:

$$\sum p_i^g - \sum p_i^d - p_i = 0 \tag{6.24}$$

$$\sum q_i^g - \sum q_i^d - q_i = 0 \tag{6.25}$$

Here, p_i^g and q_i^g are the power injection and p_i^d and q_i^d are the connected load at $i \in \mathcal{N}$. For a converter at $j \in \mathcal{N}$:

$$v_j = V_{in} M \tag{6.26}$$

Here, $x = [\theta_i, v_i, p_i^g, q_i^g, M]^T$ is defined for the unknown variables. The inequality box constraints related to the variables in x are defined as follows:

$$\underline{x} \leq x \leq \overline{x} \tag{6.27}$$

where $\overline{x}$ and $\underline{x}$ represent the maximum and minimum limit of x, respectively.

Two non-negative slack variables are defined as $a = [a_1, a_2, ..., a_r]^T$ and $b = [b_1, b_2, ..., b_r]^T$. Here is the size of x. The inequality in (6.27) can be represented as follows:

$$\overline{x} = x + a \tag{6.28}$$

$$\underline{x} = x - b \tag{6.29}$$

With the logarithmic barrier functions, the new-defined objective function for the OPF analysis is as follows:

$$f(x,y) - \mu[\sum_{j=1}^{r} \ln(a_j) + \sum_{j=1}^{r} \ln(b_j)] \tag{6.30}$$

where $a_j \in a$ and $b_j \in b$ are positive and μ is a penalty factor. The Lagrangian function of the OPF analysis is as follows:

$$\mathcal{L} = f(x,y) - \mu[\sum_{j=1}^{r} \ln(a_j) + \sum_{j=1}^{r} \ln(b_j)] - \lambda^T \begin{bmatrix} \sum p_i^g - \sum p_i^d - p_i \\ \sum q_i^g - \sum q_i^d - q_i \end{bmatrix} - z^T(x + a - \overline{x}) - w^T(x - a - \underline{x})$$

where λ, z, w are Lagrange multipliers.

6.5 Simulation and Evaluation

The OPF models are implemented in an Intel(R)-Core(TM) i7-3770 @3.40 GHz, 16 GB RAM machine. The proposed OPF model determines the optimal (p_i^g, q_i^g) and the optimal modulation index (M) of the converters. The OPF model simulation and experimental analysis, a 32-bus (modified IEEE 33-bus) and an IEEE 123-bus network systems are modified to AC-DC type network structure. Power flow analysis is conducted for the validation purpose of the modified AC-DC networks. The power flow analysis (SOCP-PF) is conducted by excluding the objective function from the OPF model and compared with the results from the graph-theoretic-based AC-DC power flow model (G-PF) in [145] [146]. The percent of voltage error is illustrated in Fig. 6.3, which is less than 0.02%. Algorithm 3 illustrates the implementation of the proposed OPF model and the simulation results are compared with the IPM-NLP model.

Algorithm 3 AC-DC SOCP-OPF

The number of total branches $N_L = n - 1$.
for $k = 1 : N_L$ **do**
  if $L_{ij}(k) \in \mathbb{L}$ *is an AC-AC branch* **then**
    Run SOCP-OPF using (6.11a)-(6.11d)
  end
  if *An AC-DC converter is placed at the branch* $L_{ij}(k) \in \mathbb{L}$ **then**
    The converter is placed at the j bus
    Define a temporary node as $j^{'}$ at the converter
    Run SOCP-OPF using (6.12a)-(6.12b) along with (6.11a)-(6.11d)
  end
  if $L_{ij}(k) \in \mathbb{L}$ *is a DC-DC branch* **then**
    Run SOCP-OPF using (6.13a)-(6.13c)
  end
  if *An DC-AC converter is placed at the branch* $L_{ij}(k) \in \mathbb{L}$ **then**
    The converter is placed at the j bus
    Define a temporary node as $j^{'}$ at the converter
    Run SOCP-OPF using (6.14a)-(6.14b) along with (6.13a)-(6.13c)
  end
end

Table 6.2: Rating of the converters

Case	Converter ID	Converter Rating (KVA)
32-bus Network	M_1	1200
	M_2	500
	M_3	1200
123-bus Network	M_1	400
	M_2	1000
	M_3	100
	M_4	800

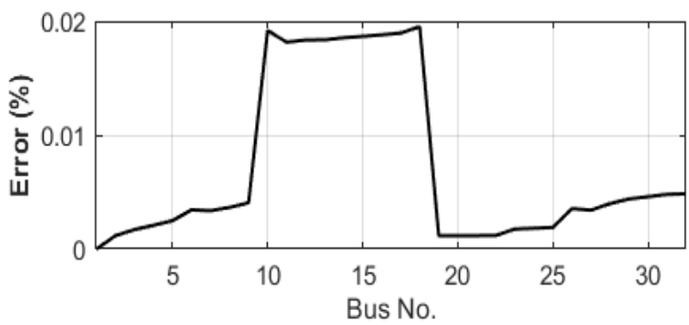

Figure 6.3: Percent of error of the voltage profile from the load flow analysis for the 32-bus AC-DC network structure.

6.5.1 Case 1 (32-Bus Network)

The 32-bus network is derived from the 33-bus network in [149]. The sub-station (bus no. '0') is excluded, and the tie-lines are disconnected for considering a radial type network. For converting an AC-DC network structure in this article, the reactive components are excluded from the DC-DC part of the network shown in Fig. 6.4. The placements of the AC/DC converters (rectifiers) and the DC/AC converter (inverter) are shown in Fig. 6.4 as well, and the ratings of the converters are in Table 6.2. The modulation index M for different converters are labeled as M_1 (bus no. 6-7), M_2 (bus no. 12-13), and M_3 (bus no. 26-27). There are two AC-DC converters between bus no. 6-7 and bus no. 26-27. The DC-AC converter is placed between bus no. 12-13. The base voltage of the AC side is 12.66 KV, and the DC side network is 17.90 KV for the 32-bus network. The OPF models are simulated for the base case and also as well as with high DERs (30% DGs of the total connected loads). For the experimental simulation, the maximum range of efficiency of the converters is 90%, and $v_i^* = 1\ (pu)$ is considered as the reference voltage. The profile of the voltage for the network with DERs is illustrated in Fig. 6.5. The voltage mismatch is less than 0.01%. With the increment of the participation factor (K), the weight of the objective function f_2 increases, and the voltage deviation decreases. From the SOCP-OPF and NLP-OPF models, the optimal modulation index (M) for the converters concerning the participation factor (K) is compared in Table 6.3. The modulation index (M) is comparable to the NLP-OPF model. The impact of the optimal index M on the network loss minimization objective function is illustrated in Fig. 6.6. The network loss increases if the converters do not operate with the

optimal modulation index. When the weight of the participation factor (K) increases, the voltage deviation from the reference voltage (v_i^r) decreases, which is demonstrated in Fig. 6.8 in terms of VD_{max}. Here voltage deviation is determined as $VD_i = |v_i - v_i^r|$ for all the buses in the network, and VD_{max} is the maximum voltage deviation among them. The time of convergence (ToC) of the OPF analysis in Table 6.5 shows the computational efficiency of the proposed SOCP-OPF model for the 32-bus network.

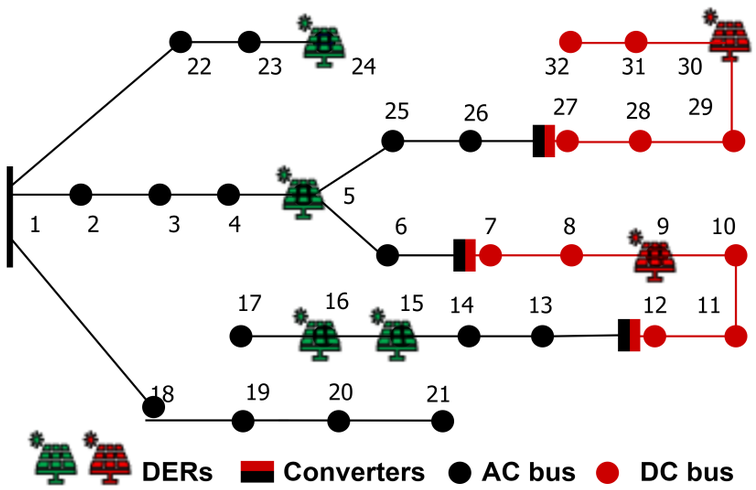

Figure 6.4: The modified 32-bus AC-DC network with converters.

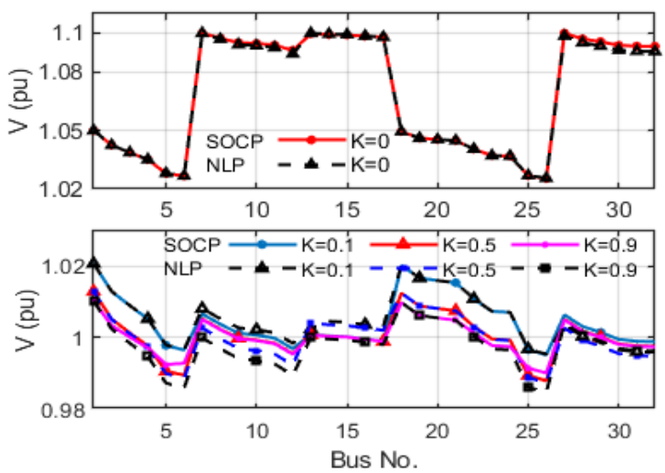

Figure 6.5: Voltage profile from the 32-bus network. Legend 'SOCP' indicates the SOCP-OPF model, and 'NLP' indicates the nonlinear-OPF results.

6.5.2 Case 2 (123-Bus Network)

For checking scalability and robustness, the proposed SOCP-OPF model is simulated on the IEEE 123-bus network (base case) and with high penetration of DERs (30% DERs of the total loads). The network is modified to create an AC-DC network structure, as shown in Fig. 6.7. Three AC/DC converters (rectifiers) and one DC/AC converter (inverter) are connected to the 123-bus network. The ratings of the converters are in Table 6.2, and the placements are shown in Fig. 6.7, including the DERs. The AC/DC converters are labeled as M_1 (bus no. 40-41), M_2 (bus no. 59-60), and M_4 (bus no. 116-117), and the

Table 6.3: Optimal 'M' and percent of network loss for the 32-bus network

Network	V_{base} (AC-KV)	V_{base} (DC-KV)	Part. Factor 'K '	Converter Connected Nodes	Converter Type	Converter ID	Optimal 'M' (SOCP)	Optimal 'M' (NLP)	Network Loss (%) (SOCP)	Network Loss (%) (NLP)
32-bus (Base case)	12.66	17.90	0.0	6-7	AC-DC	M_1	1.7524	1.7683	8.967%	8.436%
				12-13	DC-AC	M_2	0.6235	0.6218		
				26-27	AC-DC	M_3	1.7556	1.7614		
			0.5	6-7	AC-DC	M_1	1.6678	1.6729	9.115%	8.628%
				12-13	DC-AC	M_2	0.6206	0.6202		
				26-27	AC-DC	M_3	1.6667	1.6760		
			0.9	6-7	AC-DC	M_1	1.6618	1.6814	9.581%	8.757%
				12-13	DC-AC	M_2	0.6208	0.6200		
				26-27	AC-DC	M_3	1.6635	1.6741		
32-bus (30% DERs)	12.66	17.90	0.0	6-7	AC-DC	M_1	1.7350	1.7492	5.957%	5.847%
				12-13	DC-AC	M_2	0.6215	0.6183		
				26-27	AC-DC	M_3	1.7371	1.7490		
			0.5	6-7	AC-DC	M_1	1.6599	1.6561	6.097%	5.961%
				12-13	DC-AC	M_2	0.6192	0.6195		
				26-27	AC-DC	M_3	1.6621	1.6581		
			0.9	6-7	AC-DC	M_1	1.6551	1.6560	6.268%	6.169%
				12-13	DC-AC	M_2	0.6192	0.6188		
				26-27	AC-DC	M_3	1.6588	1.6650		

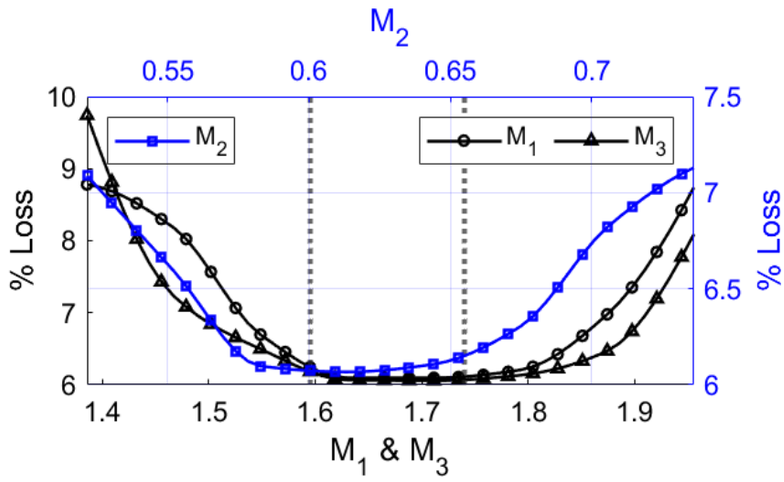

Figure 6.6: % Loss vs M for the 32-bus network (30% DERs), when K=0.5.

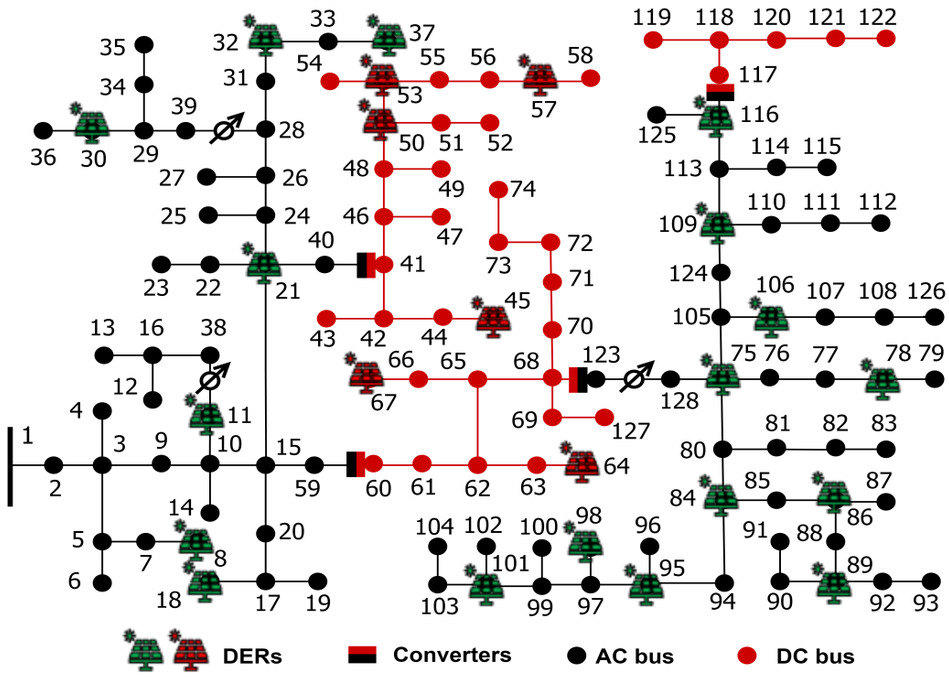

Figure 6.7: The modified 123-bus AC-DC network with converters.

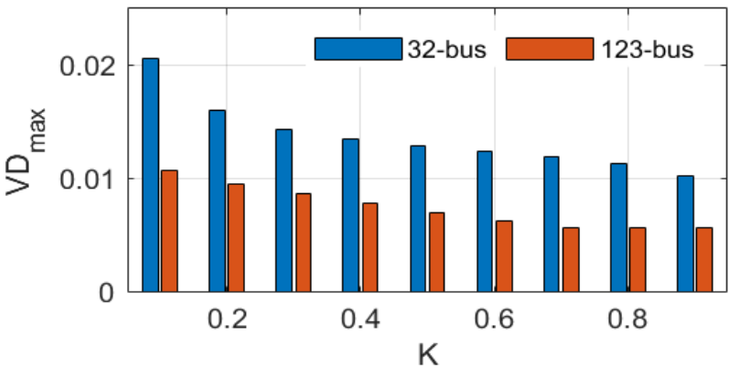

Figure 6.8: Maximum voltage deviation (VD_{max}) across a branch.

DC/AC converter is labeled as M_3 (bus no. 68-123), which makes the network structure as an AC-DC-AC network. The base voltage for the AC-AC and DC-DC sides is 4.16 KV and 6.8 KV, respectively. A maximum of 90% operating efficiency is considered for all of the converters in the network. The optimal point (modulation index) of operation for the

Table 6.4: Optimal 'M' and percent of network loss for the 123-bus network

Case	K	Conv. ID	Optimal 'M' (SOCP)	Optimal 'M' (NLP)	Loss (%) (SOCP)	Loss (%) (NLP)
Base case	0.0	M1	1.6343	1.6671	14.95%	14.37%
		M2	1.75233	1.7549		
		M3	0.5698	0.5675		
		M4	1.6817	1.6921		
	0.5	M1	1.6420	1.6590	15.34%	14.69%
		M2	1.6517	1.6584		
		M3	0.6182	0.6142		
		M4	1.6380	1.6333		
	0.9	M1	1.6400	1.6308	15.81%	15.24%
		M2	1.6504	1.6689		
		M3	0.6181	0.6132		
		M4	1.6325	1.6232		
30% DERs	0.0	M1	1.6862	1.7029	9.16%	9.35%
		M2	1.7461	1.7650		
		M3	0.5660	0.5644		
		M4	1.7581	1.7648		
	0.5	M1	1.6417	1.6350	9.34%	9.63%
		M2	1.6477	1.6405		
		M3	0.6177	0.6096		
		M4	1.6389	1.6340		
	0.9	M1	1.6402	1.6333	9.52%	10.02%
		M2	1.6471	1.6424		
		M3	0.6176	0.6138		
		M4	1.6356	1.6324		

converters is illustrated in Table 6.4 for both OPF models for different participation factor K values. With the increase of K, the network loss increases, and the voltage deviation from the reference voltage decreases. Though the network loss increases by a small portion, the objective function associated with the f_2 keeps the voltage within a stable limit. The voltage mismatch is less than 0.01% between the two OPF models. Besides that, the modulation index (M) from the OPF models is also compared. With the increase of the participation factor (K), the voltage-deviation (VD_{max}) from the reference voltage (v_i^*) decreases, which is demonstrated in Fig. 6.8 for the 123-bus network. The time of convergence (ToC) of the OPF analysis for the 123-bus network is illustrated in Table 6.5. This shows that the proposed SOCP-OPF model's computational efficiency is superior to the NLP-OPF model.

Table 6.5: OPF analysis convergence time comparison

Case	K	ToC (sec)	
		SOCP-OPF	NLP-OPF
32-bus Network (Base Case)	0.0	0.21	5.37
	0.5	0.19	3.11
32-bus Network (DERs)	0.0	0.16	3.84
	0.5	0.20	3.15
123-bus Network (Base Case)	0.0	0.25	24.20
	0.5	0.21	10.76
123-bus Network (DERs)	0.0	0.23	8.18
	0.5	0.17	8.11

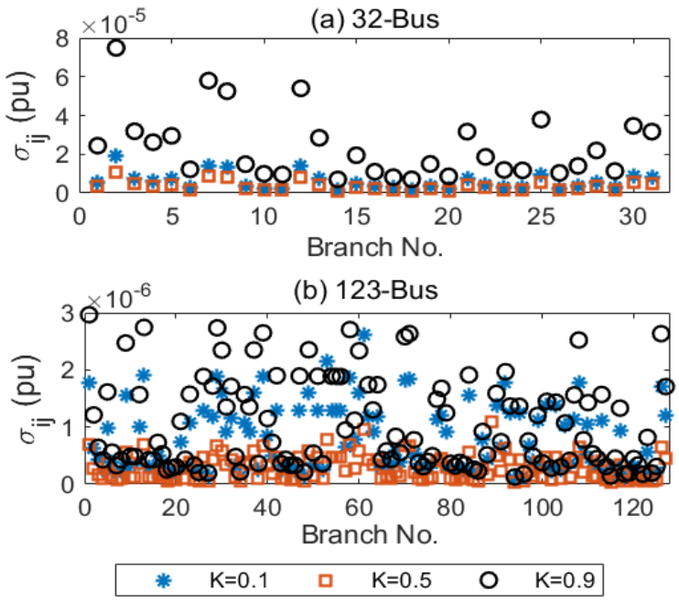

Figure 6.9: solution-gap (σ_{ij}) from the SOCP-OPF analysis.

6.5.3 Tightness and Robustness of the SOCP-OPF Model

For the OPF analysis with the SOCP, in this article relaxes the voltage and current phase angle and considers the McCormick relaxation for the optimal modulation index. The model also considers conic relaxation and convex objective function $f(x, y)$ for an OPF solution. The tightness of relaxation of the SOCP model is analyzed with the parameter of solution-gap defined as $\sigma_{ij} = |u_i l_{ij} - S_{ij}^2|$. The solution-gaps ($\sigma_{ij}$) for all the branches are measured in the 32-bus and 123-bus networks for different participation factors K and demonstrated in Fig. 6.9. When the participation factor is $K \approx 0.5$ for the net loss and voltage deviation minimization objective, the solution-gap (σ_{ij}) is minimum for the network. Fig. 6.9 illustrates that the solution-gap (σ_{ij}) is negligible for all the test values of K, so the relaxation for the proposed SOCP-OPF model is tight for radial distribution networks with AC-DC structure. The proposed model is tested with different participation factors K (i.e., 0.1 to 0.9) and with multiple levels of DERs penetration (i.e., base case, 10%, 20% & 30% DERs). For all the test cases, the SOCP-OPF model provides exact solutions, which are verified with the solution from the NLP-OPF model and the results are illustrated in Table 6.3 and Table 6.4. Due to space constraints, only the results for the base case and with 30% DERs are included in the tables. Thus the analysis proves the robustness of the proposed model.

6.6 Summary

This chapter proposes and analyzes a SOCP-OPF model for AC-DC structured radial power distribution networks. Besides the operating points of the DERs, the proposed model also determines the optimal modulation index of the converters in the network. The model is simulated and evaluated for several modified distribution networks with AC-DC structure.

Being convex, the AC-DC SOCP-OPF model always produces a globally optimal solution; from the analytical analysis, the solution gap is negligible. So the relaxation of the proposed model is tight, and the solution is exact. The solution from the AC-DC SOCP-OPF is compared with an IPM-based NLP-OPF model for validation. Because of the computational superiority, the time of convergence (ToC) of the AC-DC SOCP-OPF is significantly low compared to the NLP-OPF model for the AC-DC network.Besides that, the proposed model provides accurate OPF solutions for various participation factors in the objective functions and with various DERs penetration levels. Which proves the robustness of the OPF model.

CHAPTER 7: A DISTRIBUTED OPTIMAL POWER FLOW (D-OPF) MODEL AND A TIME-DEPENDENT REAL-TIME OPTIMAL POWER FLOW (R-OPF) MODEL WITH SECOND-ORDER CONE PROGRAMMING (SOCP)

7.1 Introduction and Contribution

Optimal Power Flow (OPF) analysis is fundamental in power system planning and operation for particular objectives [114]. The high penetration of distributed energy resources (DERs) has recently increased the complexity of modern power distribution system networks [6]. So the OPF analysis for modern power distribution networks (PDNs) is crucial for efficient and reliable grid operation. AC-OPF problem is naturally nondeterministic polynomial (NP)-hard because of the non-linearity of the original AC power flow equations [13]. So, linear approximations are commonly used, but linear approximated OPF formulations compromise with the solution accuracy [150]. Besides that, due to the non-convexity of the original non-linear OPF (NLP-OPF), globally optimal solutions are not always guaranteed [114]. Because of these reasons, due to the computational superiority and the capability of finding the global optimal solution convex, OPF models are extensively used in power systems [151–153]. One of the most commonly used convex models using second-order cone programming (SOCP) in power system analysis [22, 126]. In prior research, it is proven that the conic and angle relaxation are exact in radial-type power distribution networks with certain conditions [68]. So, SOCP-OPF is a good candidate for distributed OPF (D-OPF) analysis in radial distribution networks.

Traditionally OPF analysis of power distribution networks (PDNs) has been solved with centralized optimization techniques using a central distribution management system (CDMS) [44, 154]. High penetration of DERs forms active DNs [155, 156] with increased numbers of controllable devices and distributed active components. This makes the centralized OPF algorithms complex and sometimes computationally infeasible. Besides computational, maintenance, and operational issues, CDMS becomes a vulnerable target for cyber-physical attacks [157]. Also, in the CDMS, the entire network fails for single nodal mismanagement or operational failure. From these points of consideration, D-OPF is considered for centralized or decentralized operations for distribution networks.

Researchers have proposed and explored several approaches for solving OPF problems in a distributed fashion OPF analysis. The most commonly used techniques for D-OPF are based on the alternating direction method of multipliers (ADMM) [44]. Several D-OPF techniques based on the ADMM algorithm have been discussed in [17, 66, 88, 96]. For the

ADMM-based D-OPF models, micro-iterations are counted for local area OPF, while macro-iterations exchange information for the global variables among the decision-making agents. Micro and macro-iterations decide the actual time of convergence (ToC) for the algorithm for a distributed OPF. Even with multiple acceleration methods, the ADMM-based OPF models require a comparatively large number of iterations for convergence [22]. Thus the ToC increases for a moderate-size network [18,158]. Besides that, many iterations and a more significant communication channel are also required among the distributed areas, which makes the system impractical or more expensive. Real-time feedback-based methods [68, 69] and auxiliary problem principle-based [90] models have been explored. However, these methods also suffer from either a higher number of iteration issues or data exchanging communication channel latency issues. So, this chapter is motivated by the reduced equivalent network approximation (ENApp) approach for the D-OPF for radial networks [158].

Because of the computational efficiency and exactness [68, 90], the SOCP-based OPF model is considered for the proposed D-OPF analysis. For the D-OPF methodology, the networks are divided into several micro areas, and local OPF analysis is conducted for each area. Then the optimal operating information is shared among the areas for the optimal operation of the whole network.

7.1.1 Major Contributions

The main contributions of the proposed work are as follows:

- Proposed a novel distributed optimization approach using SOCP in radial power distribution systems, which leverages a computationally tractable and efficient OPF model for a globally optimal solution.
- The proposed D-OPF method converges to the solution with comparatively similar convergence time as centralized OPF analysis with a less computational burden. Also, it minimizes the effect of the cyber-physical attack on the whole power system network.
- The relaxation is tight for the SOCP D-OPF model, and the model provides an exact solution with the high penetration of DERs in the network.
- Proposed a time-dependent SOCP-based model for real-time OPF analysis which facilitates monitoring and control of the grid for an optimal and reliable operation.

In this chapter, the SOCP-OPF methodology in a relaxed framework is discussed in Section 7.2. Section 7.3 discusses the model implementation and the simulation result analysis. Section 7.4 proposes a real-time OPF model with simulation analysis and Section 7.5 concludes the chapter with a summary.

The variable and parameters used in this chapter are as follows:

$\mathcal{N}$:	Set of all the buses in the network
$\mathcal{N}$:	Set of the buses
$\mathcal{N}_g$:	Set the buses with DERs
$\mathcal{L}$:	Set of the branches
$\mathcal{T}$:	Set of the discrete-time instants
V_i:	Bus voltage at $i \in \mathcal{N}$
u_i:	voltage magnitude square at $i \in \mathcal{N}$
s_i^g:	Injection of power (apparent) at $i \in \mathcal{N}_g$
s_i^d:	Load at $i \in \mathcal{N}$
p_i^g:	Injection of power (real) at $i \in \mathcal{N}_g$
p_i^d:	Load (real) at $i \in \mathcal{N}$
q_i^g:	Injection of power (reactive) at $i \in \mathcal{N}_g$
q_i^d:	Load (real) at $i \in \mathcal{N}$
P_{ij}:	Power flow (real) in $L_{ij} \in \mathcal{L}$
Q_{ij}:	Power flow (reactive) in $L_{ij} \in \mathcal{L}$
S_{ij}:	Power flow (apparent) in $L_{ij} \in \mathcal{L}$
I_{ij}:	Current through $L_{ij} \in \mathcal{L}$
l_{ij}:	Square of current magnitude through $L_{ij} \in \mathcal{L}$
z_{ij}:	Line impedance of $L_{ij} \in \mathcal{L}$
c_i:	DER's cost-coefficients at $i \in \mathcal{N}_g$

7.2 Proposed Methodology (Relaxation and Convexification)

7.2.1 Angle and Conic Relaxation for SOCP-OPF

For the OPF analysis, we have considered the branch flow-based power flow model, which is discussed in this section. This section also elaborates on convexification with angle and conic relaxation. $\mathcal{N}$ is defined as a set of N number of elements for a radial network with N buses and $\mathcal{L}$ is the set of $(N-1)$ of branches. The set of DERs-connected buses is defined as $\mathcal{N}_g$. V_i denotes the voltage at a bus $i \in \mathcal{N}$ of the network. If S_{ij}, and I_{ij} are defined as the power (apparent) and the current flow, the power flow relations for a branch $L_{ij} \in \mathcal{L}$ concerning the bus pair $(i,j) \in \mathcal{N}$ are as follows:

$$S_{ij} = V_i I_{ij}^* \tag{7.1a}$$

$$V_j = V_i - \frac{z_{ij} S_{ij}^*}{V_i^*} \tag{7.1b}$$

where $z_{ij} = r_{ij} + jx_{ij}$ is the branch impedance of $L_{ij} \in \mathcal{L}$. For the bus $j \in \mathcal{N}$, the power balance relationship is as follows:

$$s_j^g - s_j^d + S_{ij} - z_{ij}|I_{ij}|^2 - y_j^*|V_j|^2 = \sum_{k:j\to k} S_{jk} \tag{7.1c}$$

where y_j is the half-lump shunt admittance and $y_j = g_j + jb_j$. s_j^g is the apparent power injection, and s_j^d is the apparent power of load associated with the bus $j \in \mathcal{N}$.

The non-convex equations concerning the network power flow in (7.13a) - (7.13c) are convexified with angle and conic relaxations. The angles for the proposed model are relaxed,

and new variables have been introduced as $|I_{ij}|^2 = l_{ij}$; $L_{ij} \in \mathcal{L}$ and $|V_i|^2 = u_i$; $i \in \mathcal{L}$. So the power flow equation (7.13a)- (7.13c) are converted as follows:

$$u_i l_{ij} = S_{ij}^2 \tag{7.2a}$$

$$u_i - u_j - (Z_{ij} S_{ij}^* + Z_{ij}^* S_{ij}) + |Z_{ij}|^2 l_{ij} = 0 \tag{7.2b}$$

Here (7.14b) is derived from the square magnitude in (7.13b). With the new-defined variables and further considering $S_{ij} = P_{ij} + jQ_{ij}$, $y_j = g_j + jb_j$, $s_j^g = p_j^g + jq_j^g$, and $s_j^d = p_j^d + jq_j^d$; (7.13c) is split in terms of real and reactive power as follows:

$$p_j^g - p_j^d + P_{ij} - r_{ij} l_{ij} - g_j u_j = \sum_{k:j\to k} P_{jk} \tag{7.3a}$$

$$q_j^g - q_j^d + Q_{ij} - x_{ij} l_{ij} - b_j u_j = \sum_{k:j\to k} Q_{jk} \tag{7.3b}$$

With further simplification in (7.14b) the voltage relationship is obtained as (7.15c).

$$u_i - u_j - 2(r_{ij} P_{ij} + x_{ij} Q_{ij}) + (r_{ij}^2 + x_{ij}^2) l_{ij} = 0 \tag{7.3c}$$

As (7.14a) is still a non-convex relation, the convex model is derived With further conic relaxation shown below:

$$u_i + l_{ij} \geq \left\| \begin{array}{c} 2P_{ij} \\ 2Q_{ij} \\ u_i - l_{ij} \end{array} \right\|_2 \tag{7.3d}$$

7.2.1.1 Convex SOCP-OPF Model

Primarily OPF analysis is performed on a network to find the optimal point of operation for an objective $f(x)$. For the exactness, we have considered convex objective functions $f(x)$ (i.e., loss minimization as, $min \sum r_{ij} l_{ij}$ and generation cost minimization as, $min \sum [c_2^i (p_i^g)^2 + c_1^i p_i^g + c_0^i]$) for the SOCP-OPF analysis in this article with $c^i \geq 0$. Here, $c_2^i (\$/MWh^2)$, $c_1^i (\$/MWh)$ and $c_0^i (\$/h)$ are the quadratic coefficients of the generators. The SOCP-OPF model is as follows:

$$min \;\; f(x) \tag{7.4}$$

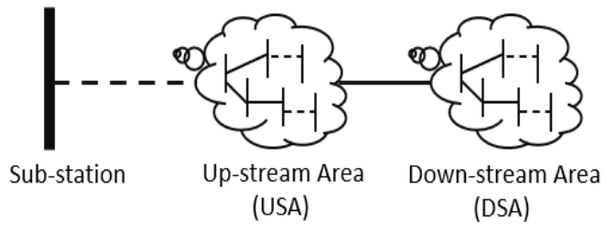

Figure 7.1: Distributed Area Configuration of radial distribution networks.

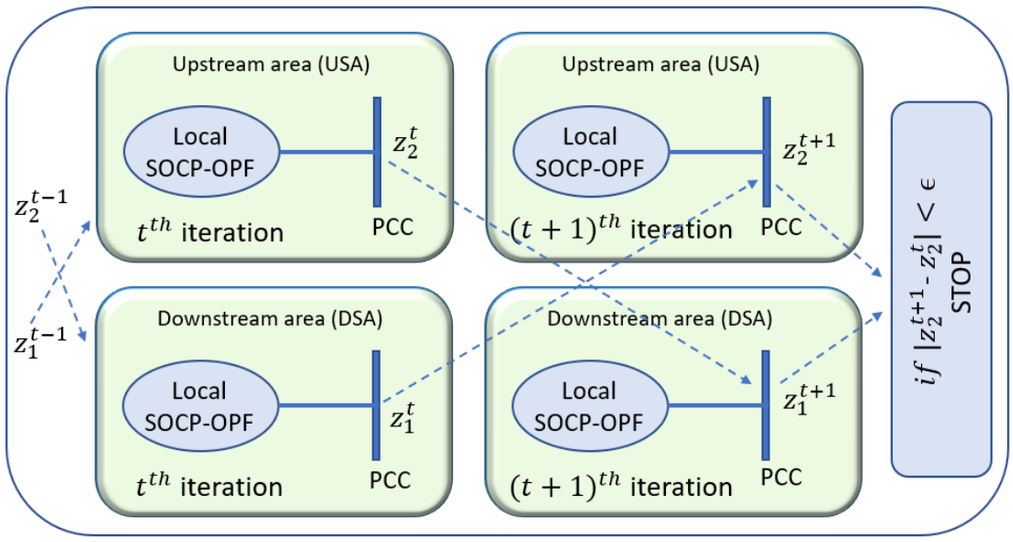

Figure 7.2: Data exchange between a USA and a DSA for the SOCP D-OPF.

subject to (*s.t.*): (7.15a)-(7.15d) and,

$$s.t. \begin{cases} \underline{u}_i \leq u_i \leq \overline{u}_i \\ \underline{p}_i^g \leq p_i^g \leq \overline{p}_i^g \\ \underline{q}_i^g \leq q_i^g \leq \overline{q}_i^g \\ l_{ij} \leq \bar{l}_{ij} \end{cases} \tag{7.5}$$

where $\underline{p}_i^g$ and $\overline{p}_i^g$ are the minimum and maximum limit of real power injection and $\underline{q}_i^g$ and $\overline{q}_i^g$ are the minimum and maximum limit of reactive power injection from the DERs at the bus $i \in \mathcal{N}_g$. For voltage, the operational minimum and maximum limits are defined as $\underline{u}_i = |\underline{V}_i|^2$ and $\overline{u}_i = |\overline{V}_i|^2$; $i \in \mathcal{N}$. Network thermal limit is considered as, $\bar{l}_{ij} = |\overline{I}_{ij}|^2$. $\overline{I}_{ij}$ represents the rated current for $L_{ij} \in \mathcal{L}$.

7.2.2 Proposed SOCP D-OPF Model

The SOCP-based distributed OPF (D-OPF) model divides the power network into several sections, which provides the benefits of local area control and minimizes the cyber-physical attack's effect on the whole power system network. The divided area sections are considered as up-stream area (USA) and down-stream area (DSA) as shown in Fig. 7.1. If a section is in the middle of two sections, then it will operate as USA for the section towards the radial

end and as DSA for the section towards the sub-station. The SOCP-OPF analysis shown in the previous section is executed for each area for a local optimal operation point. Then the information is exchanged between the USA and DSA for the next macro iteration, illustrated in Fig. 7.2.

The data z_1 (i.e., p_g, q_g) from the DSA is passed to the USA, and z_2 (i.e., V) from the USA is passed to the DSA for the next macro iteration at the point of common connection (PCC). The iteration continues until the value of z_2 is under a particular mismatch tolerance value 'ϵ'. For a USA network section, if the PCC bus is labeled as bus $j \in \mathcal{N}$, then at the PCC for the up-stream area at the t^{th} macro-iteration follows the power balance and voltage relationship as follows:

$$p_j^t + P_{ij}^t - r_{ij} l_{ij}^t - g_j u_j^t = 0 \tag{7.6a}$$

$$q_j^t + Q_{i,j}^t - x_{ij} l_{ij}^t - b_j u_j^t = 0 \tag{7.6b}$$

where $p_j^t = p_j^{gt} - p_j^d - [p_{DSA}^g]^{t-1}$ and $q_j^t = q_j^{gt} - q_j^d - [q_{DSA}^g]^{t-1}$. Here, $[p_{DSA}^g]^{t-1}$ and $[q_{DSA}^g]^{t-1}$ is the total amount of real and reactive power injection from the PCC to the DSA section at the $(t-1)^{th}$ macro-iteration. The voltage at the bus $j \in \mathcal{N}$ is determined as follows within the conic space.

$$u_i^t - u_j^t - 2(r_{ij} P_{i,j}^t + x_{ij} Q_{ij}^t) + (r_{ij}^2 + x_{ij}^2) l_{ij}^t = 0 \tag{7.6c}$$

$$u_i^t + l_{ij}^t \geq \left\| \begin{array}{c} 2P_{ij}^t \\ 2Q_{ij}^t \\ u_i^t - l_{ij}^t \end{array} \right\| \tag{7.6d}$$

For a DSA network section, if the PCC bus is labeled as bus $j \in \mathcal{N}$. The PCC voltage in the USA from the t^{th} macro-iteration is labeled as $u_j^{ref} = u_{j,USA}^t$. Then for the down-stream area for the $(t+1)^{th}$ iteration at the PCC:

$$[p_{DSA}^g]^{t+1} = \sum_{k:j \to k} P_{jk}^{t+1} + g_j u_j^{t+1} \tag{7.7a}$$

$$[q_{gDSA}]^{t+1} = \sum_{k:j \to k} Q_{jk}^{t+1} + b_j u_j^{t+1} \tag{7.7b}$$

$$u_j^{t+1} = u_j^{ref} \tag{7.7c}$$

Based on this formulation, the SOCP D-OPF model implementation is discussed in the following section.

7.2.2.1 Model Implementation

If a network is split into a 'N_A' number of areas, then for the proposed D-OPF model, there will be $(N_A - 1)$ numbers of PCCs. At each PCC, the variable z_2 (u_{pcc} for this article) is compared for consecutive iterations until the change of z_2 is lower than a certain value (ϵ) as $|z_{2,PCC}^{t+1} - z_{2,PCC}^{t}| \leq \epsilon$. In this article, $\epsilon = 1 \times 10^{-6}$. When the voltage at all the PCCs satisfies this condition, the D-OPF analysis converges. The area with the sub-station is always the USA, and an area with a radial end is always a DSA. The intermediate areas are considered as both USA and DSA with two PCCs. The variable $z_{1,PCC}$ is the $(p_{PCC}^{d}, q_{PCC}^{d})$ for the USA and $(p_{PCC}^{g}, q_{PCC}^{g})$ for the DSA. The exchange of the variables of z_1 and z_2 of the proposed SOCP D-OPF model is illustrated in the Algorithm 4. Apart from the PCC buses, other parts of the area networks follow (7.15a)-(7.15d) for the power balance and voltage determination for (7.16) and (7.17).

Algorithm 4 Data exchange of SOCP D-OPF

$\epsilon = 1 \times 10^{-6}$, $\Delta z = 1$ and $n = 1$ (macro-iteration)
while $\Delta z \geq \epsilon$ **do**
  if *An area A_i is only a USA or a DSA* **then**
    if $n = 1$ **then**
      z_1 & $z_2 \leftarrow$ initial value.
    end
    if $n > 1$ **then**
      $z_{1,USA(A_i)}^{t+1} \leftarrow z_{1,DSA(A_{i+1})}^{t}$ *(For USA)
      $z_{2,DSA(A_{i+1})}^{t+1} \leftarrow z_{2,USA(A_i)}^{t}$ *(For DSA)
    end
    $\Delta z_i = |z_2^{t+1} - z_2^{t}|$
  end
  if *An area A_i is both USA & DSA* **then**
    if $n = 1$ **then**
      x_1 & $x_2 \leftarrow$ initial value.
    end
    if $n > 1$ **then**
      $z_{1,USA(A_i)}^{t+1} \leftarrow z_{1,DSA(A_{i+1})}^{t}$
      $z_{2,DSA(A_i)}^{t+1} \leftarrow z_{2,USA(A_{i-1})}^{t}$
    end
    $\Delta z_i = |z_2^{t+1} - z_2^{t}|$
    ▷ *Two Δz_{A_i} values from two PCCs
  end
  $\Delta z = \max\{\Delta z_1, \Delta z_2 ..... \Delta z_{N_A - 1}\}$
  $n \leftarrow n + 1$
end

In D-OPF models, the local OPF analysis is performed in the micro-iteration time period for each area. While the exchange of variables and operational information among the

decision-making agents is performed at the macro-iterations. The macro-iterations are dictated to the communication systems. For power system analysis with the D-OPF algorithm, the time of convergence (ToC) is decided from both micro and macro iterations together. As SOCP-base OPF models are computationally very efficient, the proposed ENApp-based D-OPF model requires very few micro and macro iterations. While the existing OPF models based on alternating direction method of multipliers (ADMM) algorithms require a large number of macro-iterations (i.e., ≥ 100 iterations) for relatively small systems [159, 160]. In this article, we have compared the benefits and the efficiency of the proposed SOCP D-OPF model with ADMM based D-OPF model.

7.2.3 ADMM Based D-OPF Model

The OPF problem defined in this article can be expressed as follows [161] and adopted from [162]:

$$min \;\; f(x) + g(z) \tag{7.8a}$$

$$subject \;\; to \;\; Ax + Bz = c \tag{7.8b}$$

where $x \in \mathbf{R}^n$, $z \in \mathbf{R}^m$, $A \in \mathbf{R}^{p \times n}, B \in \mathbf{R}^{p \times m}$ and $c \in \mathbf{R}^p$. n, m and p are the number of variables in x, z and the number of rows in (7.8b), respectively. The variables of the objective function (7.16) are separated into two parts, x and z, where f and g are convex functions. Based on (7.8), the augmented Lagrangian matrix is formed as follows:

$$L(x, z, \lambda) = f(x) + g(z) + \lambda^T(Ax + Bz - c) + (\rho/2)||Ax + Bz - C||_2^2 \tag{7.9}$$

where $\rho > 0$ is the augmented Lagrangian parameter, and λ is the Lagrangian multiplier. The variables are updated as follows:

$$x^{t+1} := \arg\min_x L(x, z^t, \lambda^t) \tag{7.10a}$$

$$z^{t+1} := \arg\min_z L(x^{t+1}, z, y^t) \tag{7.10b}$$

$$\lambda^{t+1} := \lambda^t + \rho(Ax^{t+1} + Bz^{t+1} - c) \tag{7.10c}$$

The dual and primal residual at $(t+1)^{th}$ iteration are:

$$s^{t+1} = \rho A^T B(z^{t+1} - z^t) \tag{7.11}$$

$$r^{t+1} = Ax^{t+1} + Bz^{t+1} - c \tag{7.12}$$

The ADMM-based D-OPF iterations will converge when the residual and primal are less than the tolerance 10^{-6}.

7.3 Simulation and Evaluation (D-OPF)

The distributed SOCP D-OPF model is analyzed in the Matlab platform using the MOSEK solver. For test cases, we have considered multiple IEEE standard test cases (i.e., IEEE 123-bus and 8500-bus network systems) for experimental analysis. The optimal solution from the SOCP D-OPF is compared and analyzed with the centralized SOCP C-OPF. Further, the ToC from the SOCP D-OPF proposed in this article is also compared with ADMM based OPF model and the observations are discussed below.

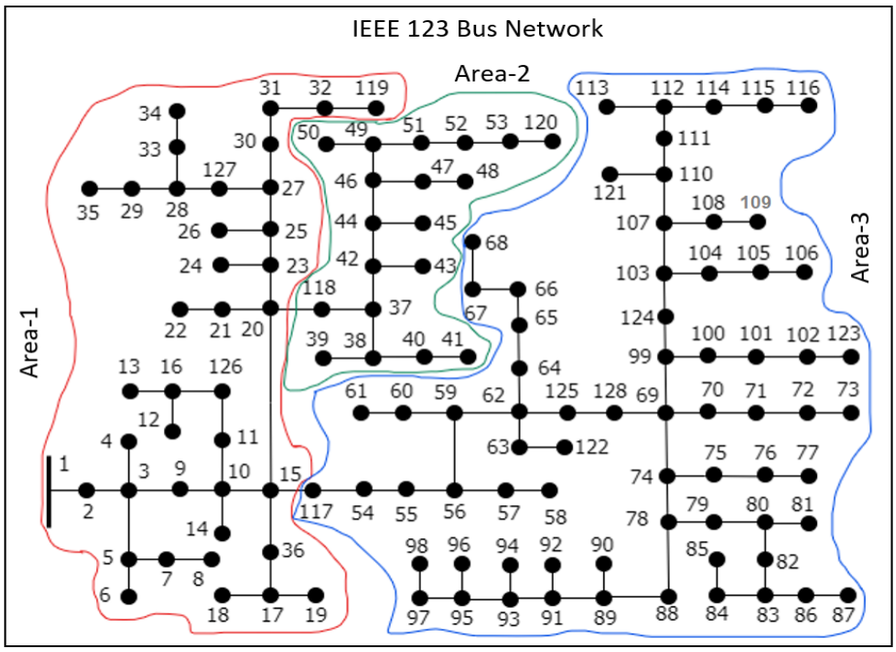

Figure 7.3: IEEE 123-bus network (re-numbered) with area divisions.

7.3.1 Case 1 (IEEE 123-bus Network)

For robustness, the OPF model is simulated in the base case and with penetration of DERs on the IEEE standard 123-bus network. The area division and the renumbering of the network are shown in Fig. 7.3. The areas are divided at the switching buses of the network. The Area-1 is the USA, while Area-2 and Area-3 are DSAs for the Area-1. For these three areas of the 123-bus network, there are two PCCs. PCC-1 is the connection point between Area-1 and Area-2, while PCC-2 is for Area-1 and Area-3. The voltages (z_2) at the PCCs are illustrated in Fig. 7.4 with D-OPF macro-iterations with DERs which shows that the D-OPF converges after the fifth iteration. The voltage profiles are compared with the centralized SOCP-OPF (C-OPF) and illustrated in Fig. 7.5 considering both the base case and with DERs. The mismatch between voltages from the D-OPF and C-OPF for both cases is less than 0.01%. The power injection from the DERs is shown in Table 7.1, and the percent of network loss is illustrated in Fig. 7.6. For calculating the percent of loss for the D-OPF, the loss of the PCC branches is not considered, which is very negligible. The results show that the simulation results from the proposed D-OPF match the C-OPF model. The 123-bus

network is divided into areas as only USA and DSA. However, for the proposed D-OPF, a power network may have an area that operates as both USA and DSA. The model is further simulated and analyzed for large networks to evaluate the performance of the SOCP D-OPF for those areas.

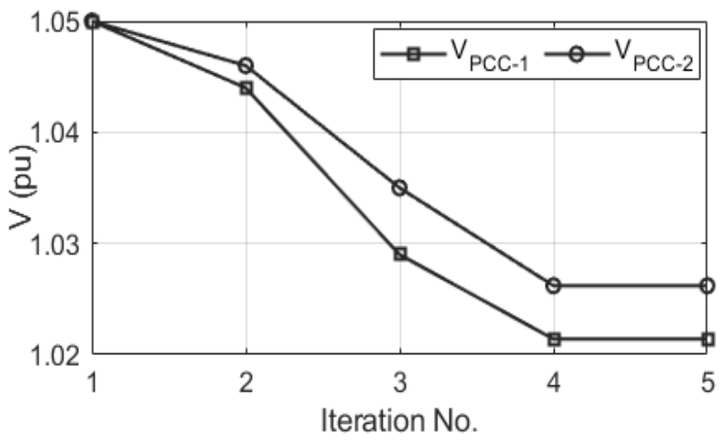

Figure 7.4: Voltage at the PCCs with macro-iterations in IEEE 123-bus network (with DERs).

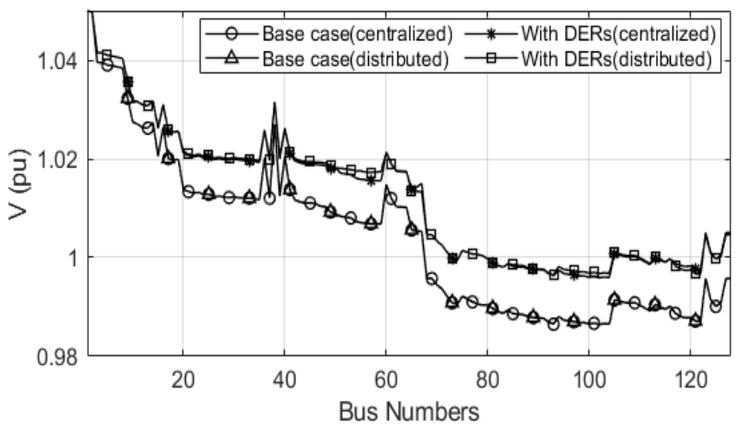

Figure 7.5: Voltage profile comparison between SOCP-based distributed OPF (D-OPF) and centralized OPF (C-OPF) for IEEE 123-bus network. 'Base' and 'DERs' are for the base case and with DERs in the network.

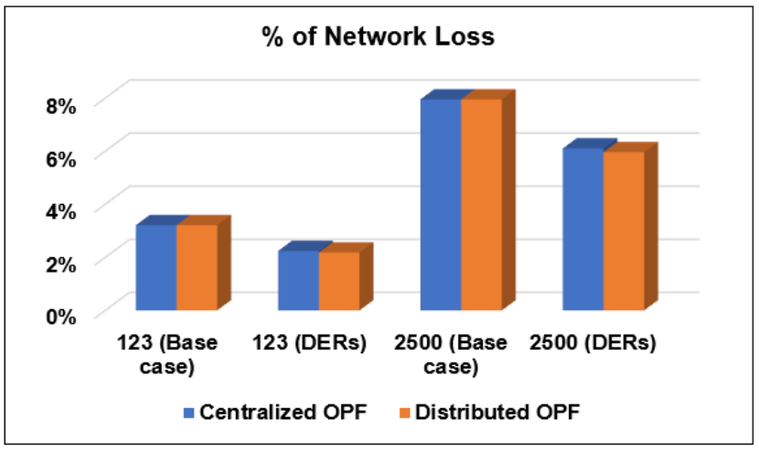

Figure 7.6: Network loss comparison between centralized OPF (C-OPF) and distributed OPF (D-OPF).

7.3.2 Case 2 (IEEE 8500-bus Network)

For analyzing the scalability, we have considered the IEEE 8500-bus distribution system network. The network is converted to a single-phase equivalent 2522-node system network

Table 7.1: Power injection from the DERs
(IEEE 123-bus network)

DERs (Bus No.)	Centralized OPF		Distributed OPF	
	$p_g(KW)$	$q_g(KVAR)$	$p_g(KW)$	$q_g(KVAR)$
1(Sub-station)	998.0	563.3	997.6	562.0
11	13.30	8.82	13.30	8.85
30	13.30	8.80	13.35	8.80
60	6.75	4.45	6.75	4.44
67	46.75	30.9	46.75	30.85
78	13.30	8.80	13.30	8.83
89	13.30	8.80	13.30	8.83
50	70.00	46.42	70.00	46.45
120	13.30	8.80	13.30	8.80

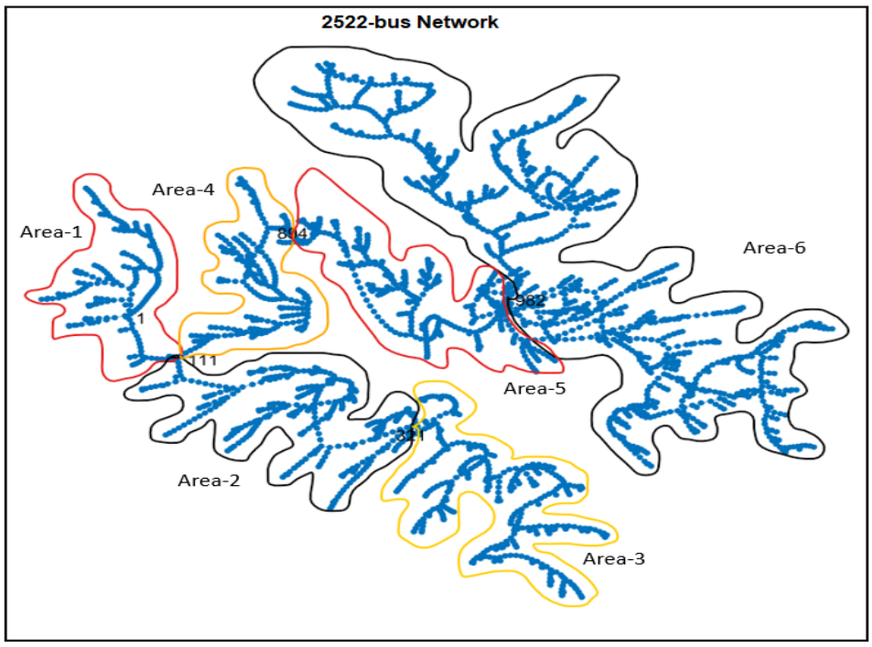

Figure 7.7: IEEE 8500-bus (2522 nodes) network (network is divided into six areas).

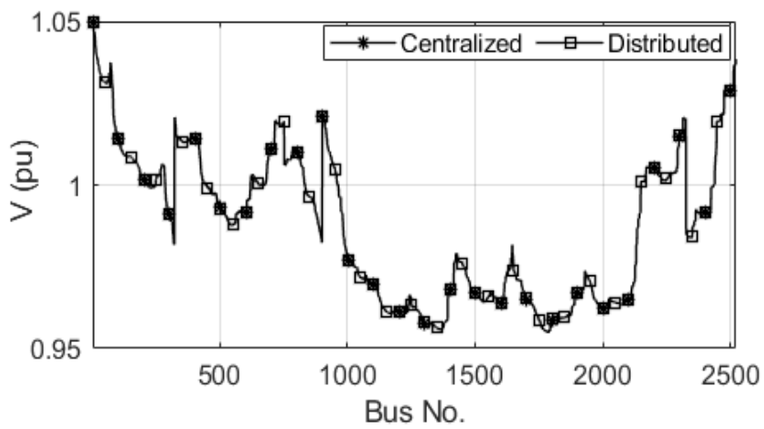

Figure 7.8: Voltage profile comparison between SOCP-based distributed OPF (D-OPF) and centralized OPF (C-OPF) for IEEE 8500-bus network (2522 Nodes) with DERs.

[158]. For analysis, the 2522-bus network is divided into three and six areas as shown in Fig. 7.7. Area-1 is always the USA for the six area divisions, and Area-3 & 6 are always DSAs. However, Area-2, 4 & 5 operate as both USAs and DSAs. The voltage profile for the 2522-node system with DERs penetration is illustrated in Fig. 7.8. The mismatch of the voltage amplitude solution from the D-OPF and C-OPF is less than 0.01% for both three

Table 7.2: Comparison of time of convergence (ToC) between centralized (C-OPF) and distributed (D-OPF) models

Test case	C-OPF	D-OPF		
	Time (sec)	No. of	Time (sec)	
	SOCP	Areas	SOCP	ADMM
123-bus (Base case)	0.25	3	0.88	136
123-bus (DERs)	0.30	3	0.52	93
8500-bus (Base case)	1.06	3	2.68	681
8500-bus (DERs)	1.53	3	3.12	476
8500-bus (Base case)	1.06	6	7.56	N/A
8500-bus (DERs)	1.53	6	8.66	N/A

and six-area divisions. The percent of network loss for the 2522-node network is illustrated in Fig. 7.6. Besides these, We have compared the solution from the SOCP D-OPF model with an ADMM-based OPF model for IEEE 123-bus and 2522-bus networks for three area divisions. The time of convergence (ToC) for different OPF models is illustrated in Table 7.2. Due to the macro-iterations, the ToC is higher for the SOCP D-OPF model than the SOCP C-OPF but significantly lower than the ADMM-based D-OPF model. As the SOCP D-OPF model can be applied to any number of divisions, the model can be solved for very large power with the least risk of a cyber-physical attack on the whole power system network.

7.4 Real-time OPF Analysis

The modern power grid incorporates many DERs and controllable loads, introducing randomness and fluctuations, increasing the complexity of modern power distribution system networks [6]. So the OPF analysis for modern power grid networks is crucial for efficient and reliable operation. For this reason, the real-time-based OPF analysis is getting much attention [163], and traditional optimal power flow methods are only appropriate for applications that operate on a slow timescale [163]. The time-dependent OPF model is applied on a Real-time based power grid designed in a real-time platform. For the real-time OPF analysis, a communication channel is needed to interchange the information between the OPF model and the power grid. That information on load change contingency is immediately transferred to the OPF model analysis platform to find the new optimal grid operation reference point. This project has three major parts: the time-dependent convex SOCP-OPF model, the communication platform, and the grid model in the real-time simulator platform, as shown in Fig. 7.9. The real-time-based model computes the optimal reference signal to the DERs, ensuring stable power-sharing among the DERs.

7.4.1 Time Dependent OPF Methodology

Time-varying loads and generations are considered for the branch flow-based real-time OPF analysis. For the model formulation, $\mathcal{L}$ is noted as the set of all the branches, and $\mathcal{N}$ is

Figure 7.9: Proposed real-time OPF analysis platform.

the set of all buses in a power network. The set of time instants is assumed to be a discrete set and is denoted by $\mathcal{T}$. $t \in \mathcal{T}$ is a time instant of the network operation. For each bus $i \in \mathcal{N}$, let $V_i(t)$ is the complex voltage phasor, and $s_i(t)$ be the net apparent power injections at bus i at time t. The complex current phasor through line $L_{ij} \in \mathcal{L}$ is denoted by $I_{ij}(t)$ for a time instant t. For steady states, the power flow equations are as follows:

$$S_{ij}(t) = V_i(t)I_{ij}^*(t) \tag{7.13a}$$

where $S_{ij}(t)$ stands for the apparent power flow through the branch $L_{ij} \in \mathcal{L}$ at the time instant t. Further voltage drop and power balance relations are as follows:

$$V_j(t) = V_i(t) - \frac{z_{ij}S_{ij}^*(t)}{V_i^*(t)} \tag{7.13b}$$

$$s_j^g(t) - s_j^d(t) = \sum_{k:j\to k} S_{jk}(t) - \sum_{i:i\to j}(S_{ij}(t) - z_{ij}|I_{ij}(t)|^2) + y_j^*|V_j(t)|^2 \tag{7.13c}$$

where $z_{ij} = r_{ij} + jx_{ij}$ is the impedance of a branch $L_{ij} \in \mathcal{L}$. $s_j^g(t)$ is the apparent power injection, and $s_j^d(t)$ is the apparent power of load associated with the bus $j \in \mathcal{N}$ at a time instant $t \in \mathcal{T}$.

7.4.1.1 Angle Relaxation

This article analyzes the real-time OPF analysis for radial power distribution networks. The non-convex power flow equations in (7.13a) - (7.13c) are convexified with angle and conic relaxations in this section. With angle relaxation, new variables have been introduced as $|I_{ij}(t)|^2 = l_{ij}(t)$; $|V_j(t)|^2 = u_j(t)$ and $|V_i(t)|^2 = u_i(t)$. So the power flow equation (7.13a)-(7.13c) are converted as follows:

$$S_{ij}^2(t) = u_i(t)l_{ij}(t) \tag{7.14a}$$

Taking the voltage magnitude square in (7.13b):

$$u_j(t) = u_i(t) + |z_{ij}|^2 l_{ij}(t) - (z_{ij}S_{ij}^*(t) + z_{ij}^* S_{ij}(t)) \tag{7.14b}$$

Further considering the new-defined variables and with angle relaxation (7.13b) at the bus $j \in \mathcal{N}$ for the time instant $t \in \mathcal{T}$ is represented as follows:

$$s_j^g(t) - s_j^d(t) = \sum_{k:j\to k} S_{jk}(t) - \sum_{i:i\to j} (S_{ij}(t) - z_{ij} l_{ij}(t)) + y_j u_j(t) \tag{7.14c}$$

Further considering $S_{ij}(t) = P_{ij}(t) + jQ_{ij}(t)$, $y_j = g_j + jb_j$, $s_j^g(t) = p_j^g(t) + jq_j^g(t)$, and $s_j^d(t) = p_j^d(t) + jq_j^d(t)$; (7.14c) is split in terms of real and reactive power as follows:

$$p_j^g(t) - p_j^d(t) = \sum_{k:j\to k} P_{jk}(t) - \sum_{i:i\to j} (P_{ij}(t) - r_{ij} l_{ij}(t)) + g_j u_j(t) \tag{7.15a}$$

$$q_j^g(t) - q_j^d(t) = \sum_{k:j\to k} Q_{jk}(t) - \sum_{i:i\to j} (Q_{ij}(t) - x_{ij} l_{ij}(t)) + b_j u_j(t) \tag{7.15b}$$

where $y_j = g_j + jb_j$ is the half lump shunt admittance equivalent of the line at bus $j \in \mathcal{N}$. With further simplification in (7.14b) the voltage relationship is obtained as:

$$u_j(t) = u_i(t) - 2(r_{ij} P_{ij}(t) + x_{ij} Q_{ij}(t)) + (r_{ij}^2 + x_{ij}^2) l_{ij}(t) \tag{7.15c}$$

7.4.1.2 Conic Relaxation

As (7.14a) is still a non-convex relation. For a time instance $t \in \mathcal{T}$, (7.14a) is relaxed With further conic relaxation. The solution space is relaxed with a convex solution space. The second-order cone relaxation is as follows:

$$u_i(t) + l_{ij}(t) \geq \left\| \begin{array}{c} 2P_{ij}(t) \\ 2Q_{ij}(t) \\ u_i(t) - l_{ij}(t) \end{array} \right\|_2 \tag{7.15d}$$

7.4.1.3 Time Dependent R-OPF Model

With the capability of fast convergence, SOCP-OPF models are a good candidate for real-time OPF (R-OPF) analysis. The R-OPF analysis depends on the feedback for the time-varying loads and renewable generations on a faster timescale. The proposed model aims to optimize an operational objective under the network's physical and operational constraints for any time period $t \in \mathcal{T}$ with controllable devices in the network. The proposed OPF model considers convex objective functions $f(x(t))$ (i.e., network loss minimization as, $min \sum r_{ij} l_{ij}(t)$ and generation cost minimization as, $min \sum [c_2^i (P_i^g(t))^2 + c_1^i P_i^g(t) + c_0^i]$). Here, $c_2^i (\$/MWh^2)$, $c_1^i (\$/MWh)$ and $c_0^i (\$/h)$ represent the quadratic cost coefficients of the generators. The SOCP-OPF model is as follows:

$$min \ f(x(t)) \tag{7.16}$$

subject to: (7.15a)-(7.15d) and,

$$\begin{cases} \underline{p}_i^g \leq p_i^g \leq \overline{p}_i^g \\ \underline{q}_i^g \leq q_i^g \leq \overline{q}_i^g \\ l_{ij} \leq \bar{l}_{ij} \\ \underline{u}_i \leq u_i \leq \overline{u}_i \end{cases} \tag{7.17}$$

where $\mathcal{N}_g$ is the set of all buses with DERs, $\underline{(.)}$ and $\overline{(.)}$ represents the minimum and maximum limits of the variables and parameters. Current flow limit is defined as $\bar{l}_{ij} = |\overline{I}_{ij}|^2$. $\overline{I}_{ij}$ is the rated current for the branch $L_{ij} \in \mathcal{L}$.

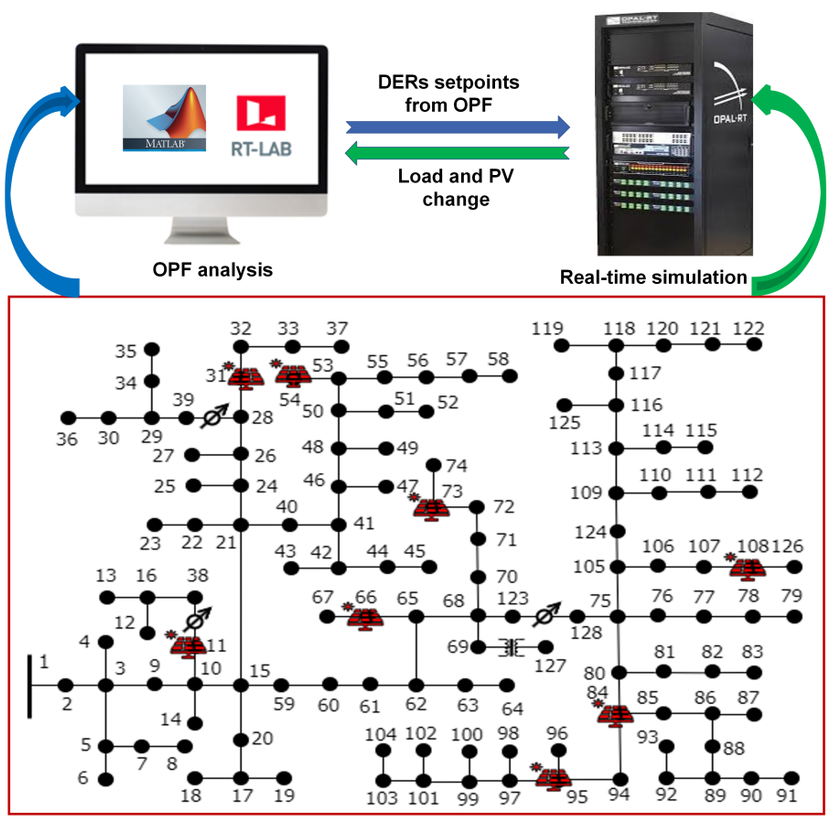

Figure 7.10: Real-time OPF analysis setup.

7.4.2 Simulation and Evaluation (R-OPF)

Matlab platform is used to simulate and analyze the proposed time-dependent OPF model. For real-time analysis, Opal-Rt is used with the Rt-lab platform. A real-time compatible IEEE 123-bus network is modeled using Rt-lab and Simulink for the Opal-Rt platform. DERs are modeled and connected at the buses shown in Fig. 7.10. The SOCP-OPF analysis is performed with Matlab for a load profile at the time instance $t \in \mathcal{T}$ for the objective of minimum network loss $f(x(t)) = min \sum r_{ij} l_{ij}$. The set-points of the DERs are transferred

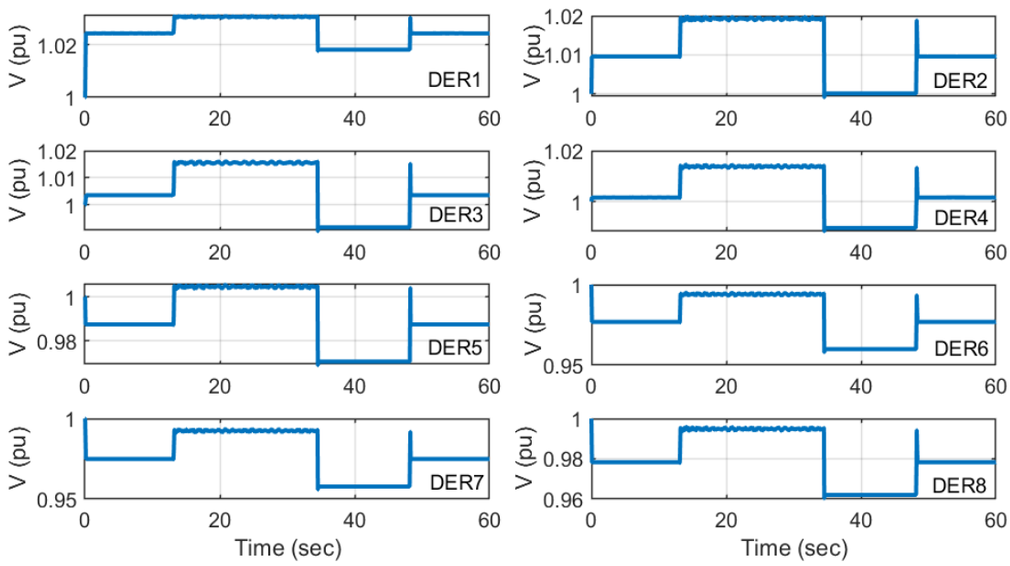

Figure 7.11: Voltage change at the buses with DERs in real-time analysis.

from the OPF platform to the DERs in Opal-Rt. Any load change or any contingency to the network information is transferred to the OPF platform for new set-points of the DERs. Operational performance is illustrated in Fig 7.11 with the voltage profiles of the buses connected with the DERs. With high computational efficiency, the SOCP-OPF model converges very fast. So a snapshot of one minute of the grid operation is illustrated with the voltage profile. within this 60 seconds time frame, at 15 seconds, the DERs start to dispatch power with the set-points from the OPF analysis, and load changes at 35 and 48 seconds. This information of load change is transferred to the OPF platform, and the new set-points of DERs are again determined for the next minutes.

7.5 Summary

This chapter proposes and analyzes a SOCP D-OPF model for radial-type power system networks and a real-time-based R-OPF model. The D-OPF model is analyzed with the simulation and evaluation for different standard IEEE distribution test feeders and compared with the centralized SOCP-based C-OPF and ADMM-based D-OPF models. From the result analysis, the angle and conic relaxations are tight for the D-OPF model, and the model produces optimal global solutions for convex objective functions like C-OPF. Besides that, for the capability of dividing a network into several areas, the proposed OPF model offers convenient local area control and minimum risk of cyber-physical attack on the whole power system network. Due to the computational efficiency, SOCP base OPF models are good candidates for real-time OPF analysis of the power grids. For future research, the D-OPF and the R-OPF model are extendable for OPF analysis in transmission-distribution (T&D) networks. Though the conic relaxation is always exact for the meshed transmission networks, the angle relaxation may not always be. So the bus voltage cyclic angle constraints must be satisfied for the OPF models for T&D OPF analysis.

CHAPTER 8: CONCLUSION AND FUTURE WORK

8.1 Conclusion

This dissertation has proposed novel and efficient OPF models for power distribution and transmission networks using second-order cone programming (SOCP) for reliable and optimal power system planning and operation of the complex modern power grid. This research analyses the global optimality and exactness of the proposed OPF models with the necessary conditions for the tightness of the angle and conic relaxations. In conclusion,

- This dissertation proposes a novel SOCP-OPF model with bus voltage angle recovery for voltage regulation with reactive power flow control in radial power distribution networks. The voltage control algorithm provides a better control scheme.
- This research also proposes a novel SOCP-based AC-OPF model for unbalanced three-phase radial power distribution networks considering the mutual coupling effects on the three-phase unbalanced lines with a coupling coefficient approach.
- Besides the distribution networks, this work also presents a novel SOCP-based OPF formulation for transmission system power networks with exact angle relaxation satisfying the cyclic angle constraints. This dissertation derives a convex envelope for the proposed OPF model for meshed transmission networks.
- With the high penetration of DERs and efficient converters, power grids are proposing an AC-DC-based hybrid network structure. This dissertation also presents an OPF formulation for AC-DC hybrid power distribution networks with SOCP and McCormick relaxation for the optimal modulation index for the converters.
- This research proposes a distributed OPF (D-OPF) model for distribution networks extendable to transmission-distribution (T&D) coupled networks. Finally, the dissertation is concluded with a time-dependent OPF model with a real-time platform.

All the proposed OPF models in this dissertation are analyzed in multiple and extensive networks, and the results show that the models are exact and produce globally optimal solutions to heavily DER-connected power grids. With the convexness and computational efficiency, the solution time of convergence of the SOCP-OPF models is superior to the NLP-OPF and SDP-OPF models with less computational burden. Due to the optimal solution feasibility, the proposed SOCP-OPF models in this dissertation are promising solutions for the OPF analysis for complex modern power grids.

8.2 Future Works

Some of the future research in this direction includes

- We have proposed convex OPF models for power distribution and transmission networks. The SOCP-OPF models are extendable for mixed integer type OPF analysis and for receding horizon control (RHC) optimization for power systems.

- This thesis work has proposed a distributed convex D-OPF model for distribution networks which is extendable to co-OPF analysis for transmission-distribution (T&D) coupled power system networks. The real-time R-OPF model is also extendable to the real-time-based operation and control for T&D networks in future work.

CHAPTER 9: LIST OF PUBLICATIONS

1. **M. M. -U. -T. Chowdhury**, B. D. Biswas and S. Kamalasadan, "Second-Order Cone Programming (SOCP) Model for Three Phase Optimal Power Flow (OPF) in Active Distribution Networks," in **IEEE Transactions on Smart Grid**, doi: 10.1109/TSG.2023.3241216.

2. **M. M. -U -T. Chowdhury**, S. Kamalasadan and S. Paudyal, "A Second-Order Cone Programming (SOCP) Based Optimal Power Flow (OPF) Model with Cyclic Constraints for Power Transmission Systems," in **IEEE Transactions on Power Systems**, doi: 10.1109/TPWRS.2023.3247891.

3. **T. Chowdhury** and S. Kamalasadan, "A New Second-Order Cone Programming Model for Voltage Control of Power Distribution System with Inverter Based Distributed Generation," in **IEEE Transactions on Industry Applications**, doi: 10.1109/TIA.2021.3107825.

4. **M. M. -U. -T. Chowdhury**, Krishna Murari, Md Shamim Hasan and S. Kamalasadan, "Second Order Cone Programming based Optimal Power Flow Model for AC-DC Distribution Network with Distributed Energy Resources," in **IEEE Transactions on Industrial Informatics** (under review).

5. **M. M. Chowdhury** and S. Kamalasadan, "An Angle Included Optimal Power Flow (OPF) Model for Power Distribution Network Using Second Order Cone Programming (SOCP)," 2020 IEEE Industry Applications Society Annual Meeting, 2020, pp. 1-7, doi: 10.1109/IAS44978.2020.9334785.

6. **M. M. -U. -T. Chowdhury**, Md Shamim Hasan and S. Kamalasadan, "A Distributed Optimal Power Flow (D-OPF) Model for Radial Distribution Networks with Second-Order Cone Programming (SOCP)," in IAS Annual Meeting (accepted).

7. **M. M. -U. -T. Chowdhury**, Md Shamim Hasan and S. Kamalasadan, "Real-time Optimal Power Flow (OPF) Model with Second Order Cone Programming (SOCP) for Radial Power Distribution Networks," in 2023 IEEE International Conference on Energy Technologies for Future Grids (ETFG) (accepted).

Bibliography

[1] O. Alsac and B. Stott, "Optimal load flow with steady-state security," *IEEE Transactions on Power Apparatus and Systems*, vol. PAS-93, no. 3, pp. 745–751, 1974.

[2] H. Happ, J. Aldrich, P. Chan, M. El-Hawary, C. Gagnon, T. Kennedy, E. Koncel, J. Lamont, H. Limmer, S. Riddington, K. Slater, W. Stadlin, and B. Wollenberg, "Description and bibliography of major economy-security functions part ii-bibliography (1959 - 1972)," *IEEE Transactions on Power Apparatus and Systems*, vol. PAS-100, no. 1, pp. 215–223, 1981.

[3] R. Madani, S. Sojoudi, and J. Lavaei, "Convex relaxation for optimal power flow problem: Mesh networks," *IEEE Transactions on Power Systems*, vol. 30, no. 1, pp. 199–211, 2015.

[4] Z. Tian and W. Wu, "Recover feasible solutions for socp relaxation of optimal power flow problems in mesh networks," *IET Generation, Transmission & Distribution*, vol. 13, no. 7, pp. 1078–1087, 2019.

[5] X. Bai, H. Weihua, K. Fujisawa, and Y. Wang, "Semidefinite programming for optimal power flow problems," *International Journal of Electrical Power Energy Systems*, vol. 30, pp. 383–392, 07 2008.

[6] C. Li, X. Liu, W. Zhang, Y. Cao, X. Dong, F. Wang, and L. Li, "Assessment method and indexes of operating states classification for distribution system with distributed generations," *IEEE Transactions on Smart Grid*, vol. 7, no. 1, pp. 481–490, 2016.

[7] M. Z. Liu, L. F. Ochoa, and S. H. Low, "On the implementation of opf-based setpoints for active distribution networks," *IEEE Transactions on Smart Grid*, pp. 1–1, 2021.

[8] R. Currie, D. MacLeman, G. McLorn, and R. Sims, "Operating the orkney smart grid: Practical experience," in *Proc. 21th Int. Conf. Elect. Dis., CIRED*, pp. 1–4, 2011.

[9] P. Mahat, Z. Chen, B. Bak-Jensen, and C. L. Bak, "A simple adaptive overcurrent protection of distribution systems with distributed generation," *IEEE Transactions on Smart Grid*, vol. 2, no. 3, pp. 428–437, 2011.

[10] M. A. Pedrasa and T. Spooner, "A survey of techniques used to control microgrid generation and storage during island operation," *AUPEC2006*, vol. 1, p. 15, 2006.

[11] Y. Hayashi and J. Matsuki, "Loss minimum configuration of distribution system considering n-1 security of dispersed generators," *IEEE Transactions on Power Systems*, vol. 19, no. 1, pp. 636–642, 2004.

[12] B. Stott, "Optimal power flow basic requirements for real-life problems and their solutions," 2012.

[13] K. Lehmann, A. Grastien, and P. Van Hentenryck, "Ac-feasibility on tree networks is np-hard," *IEEE Transactions on Power Systems*, vol. 31, no. 1, pp. 798–801, 2016.

[14] D. Bienstock and A. Verma, "Strong np-hardness of ac power flows feasibility," *Operations Research Letters*, vol. 47, no. 6, pp. 494–501, 2019.

[15] J. Lavaei and S. H. Low, "Zero duality gap in optimal power flow problem," *IEEE Transactions on Power Systems*, vol. 27, no. 1, pp. 92–107, 2012.

[16] Y. Yang, Z. Wu, Y. Zhang, and H. Wei, "Large-scale opf based on voltage grading and network partition," *CSEE Journal of Power and Energy Systems*, vol. 2, no. 2, pp. 56–61, 2016.

[17] Y. Liu, J. Li, L. Wu, and T. Ortmeyer, "Chordal relaxation based acopf for unbalanced distribution systems with ders and voltage regulation devices," *IEEE Transactions on Power Systems*, vol. 33, no. 1, pp. 970–984, 2018.

[18] M. E. Baran and F. F. Wu, "Network reconfiguration in distribution systems for loss reduction and load balancing," *IEEE Transactions on Power Delivery*, vol. 4, no. 2, pp. 1401–1407, 1989.

[19] L. Halilbašić, P. Pinson, and S. Chatzivasileiadis, "Convex relaxations and approximations of chance-constrained ac-opf problems," *IEEE Transactions on Power Systems*, vol. 34, no. 2, pp. 1459–1470, 2019.

[20] A. Castillo and R. P. O'Neill, "Survey of approaches to solving the acopf (opf paper 4)," *US Federal Energy Regulatory Commission, Tech. Rep*, 2013.

[21] B. Stott, J. Jardim, and O. Alsac, "Dc power flow revisited," *IEEE Transactions on Power Systems*, vol. 24, no. 3, pp. 1290–1300, 2009.

[22] R. A. Jabr, "Radial distribution load flow using conic programming," *IEEE Transactions on Power Systems*, vol. 21, no. 3, pp. 1458–1459, 2006.

[23] Y. Weng, Q. Li, R. Negi, and M. Ilić, "Semidefinite programming for power system state estimation," in *2012 IEEE Power and Energy Society General Meeting*, pp. 1–8, 2012.

[24] B. Zhang, A. Lam, A. Dominguez-Garcia, and D. Tse, "Optimal distributed voltage regulation in power distribution networks," 04 2012.

[25] W. H. Kersting, *Distribution system modeling and analysis*. CRC press, 2017.

[26] S. Bruno, S. Lamonaca, G. Rotondo, U. Stecchi, and M. La Scala, "Unbalanced three-phase optimal power flow for smart grids," *IEEE Transactions on Industrial Electronics*, vol. 58, no. 10, pp. 4504–4513, 2011.

[27] G. F. Reed, B. M. Grainger, A. R. Sparacino, and Z. Mao, "Ship to grid: Medium-voltage dc concepts in theory and practice," *IEEE Power and Energy Magazine*, vol. 10, no. 6, pp. 70–79, 2012.

[28] T. Adefarati, "Integration of renewable distributed generators into the distribution system: a review," *IET Renewable Power Generation*, vol. 10, pp. 873–884(11), August 2016.

[29] C. Zhao, S. Dong, C. Gu, F. Li, Y. Song, and N. P. Padhy, "New problem formulation for optimal demand side response in hybrid ac/dc systems," *IEEE Transactions on Smart Grid*, vol. 9, no. 4, pp. 3154–3165, 2018.

[30] N. Kinhekar, N. P. Padhy, F. Li, and H. O. Gupta, "Utility oriented demand side management using smart ac and micro dc grid cooperative," *IEEE Transactions on Power Systems*, vol. 31, no. 2, pp. 1151–1160, 2016.

[31] D. J. Hammerstrom, "Ac versus dc distribution systemsdid we get it right?," in *2007 IEEE Power Engineering Society General Meeting*, pp. 1–5, 2007.

[32] S. K. Chaudhary, J. M. Guerrero, and R. Teodorescu, "Enhancing the capacity of the ac distribution system using dc interlinks—a step toward future dc grid," *IEEE Transactions on Smart Grid*, vol. 6, no. 4, pp. 1722–1729, 2015.

[33] K. Kurohane, T. Senjyu, A. Yona, N. Urasaki, T. Goya, and T. Funabashi, "A hybrid smart ac/dc power system," *IEEE Transactions on Smart Grid*, vol. 1, no. 2, pp. 199–204, 2010.

[34] M. S. ElNozahy and M. M. A. Salama, "Uncertainty-based design of a bilayer distribution system for improved integration of phevs and pv arrays," *IEEE Transactions on Sustainable Energy*, vol. 6, no. 3, pp. 659–674, 2015.

[35] P. J. Werbos, "Computational intelligence for the smart grid-history, challenges, and opportunities," *IEEE Computational Intelligence Magazine*, vol. 6, no. 3, pp. 14–21, 2011.

[36] J. Carpentier, "Contribution to the economic dispatch problem," *Bulletin de la Societe Francoise des Electriciens*, vol. 3, no. 8, pp. 431–447, 1962.

[37] H. Happ, "Optimal power dispatcha comprehensive survey," *IEEE Transactions on Power Apparatus and Systems*, vol. 96, no. 3, pp. 841–854, 1977.

[38] B. Chowdhury and S. Rahman, "A review of recent advances in economic dispatch," *IEEE Transactions on Power Systems*, vol. 5, no. 4, pp. 1248–1259, 1990.

[39] M. Huneault and F. Galiana, "A survey of the optimal power flow literature," *IEEE Transactions on Power Systems*, vol. 6, no. 2, pp. 762–770, 1991.

[40] Z. Qiu, G. Deconinck, and R. Belmans, "A literature survey of optimal power flow problems in the electricity market context," in *2009 IEEE/PES Power Systems Conference and Exposition*, pp. 1–6, 2009.

[41] W. Zhang, F. Li, and L. M. Tolbert, "Review of reactive power planning: Objectives, constraints, and algorithms," *IEEE Transactions on Power Systems*, vol. 22, no. 4, pp. 2177–2186, 2007.

[42] B. Tamimi, C. A. Canizares, and S. Vaez-Zadeh, "Effect of reactive power limit modeling on maximum system loading and active and reactive power markets," *IEEE Transactions on Power Systems*, vol. 25, no. 2, pp. 1106–1116, 2010.

[43] S. Gill, I. Kockar, and G. W. Ault, "Dynamic optimal power flow for active distribution networks," *IEEE Transactions on Power Systems*, vol. 29, no. 1, pp. 121–131, 2014.

[44] D. K. Molzahn, F. Dörfler, H. Sandberg, S. H. Low, S. Chakrabarti, R. Baldick, and J. Lavaei, "A survey of distributed optimization and control algorithms for electric power systems," *IEEE Transactions on Smart Grid*, vol. 8, no. 6, pp. 2941–2962, 2017.

[45] D. K. Molzahn and I. A. Hiskens, *A Survey of Relaxations and Approximations of the Power Flow Equations*. 2019.

[46] H. Khodr, J. Gomez, L. Barnique, J. Vivas, P. Paiva, J. Yusta, and A. Urdaneta, "A linear programming methodology for the optimization of electric power-generation schemes," *IEEE Transactions on Power Systems*, vol. 17, no. 3, pp. 864–869, 2002.

[47] H. Yuan, F. Li, Y. Wei, and J. Zhu, "Novel linearized power flow and linearized opf models for active distribution networks with application in distribution lmp," *IEEE Transactions on Smart Grid*, vol. 9, no. 1, pp. 438–448, 2018.

[48] G. Torres and V. Quintana, "On a nonlinear multiple-centrality-corrections interior-point method for optimal power flow," *IEEE Transactions on Power Systems*, vol. 16, no. 2, pp. 222–228, 2001.

[49] B. Liu, J. Zhao, Q. Huang, Z. Duan, D. Cai, J. Li, and Z. Zhang, "A novel uncertainty quantification framework for pf and opf considering nonlinear correlated power injections with limited information," *IEEE Transactions on Power Systems*, pp. 1–1, 2021.

[50] X.-P. Zhang, E. Handschin, and M. Yao, "Modeling of the generalized unified power flow controller (gupfc) in a nonlinear interior point opf," *IEEE Transactions on Power Systems*, vol. 16, no. 3, pp. 367–373, 2001.

[51] E. Castronuovo, J. Campagnolo, and R. Salgado, "On the application of high performance computation techniques to nonlinear interior point methods," *IEEE Transactions on Power Systems*, vol. 16, no. 3, pp. 325–331, 2001.

[52] A. Pizano-Martinez, C. R. Fuerte-Esquivel, H. Ambriz-PÉrez, and E. Acha, "Modeling of vsc-based hvdc systems for a newton-raphson opf algorithm," *IEEE Transactions on Power Systems*, vol. 22, no. 4, pp. 1794–1803, 2007.

[53] S. Sivasubramani, "Sequential quadratic programming based differential evolution algorithm for optimal power flow problem," *IET Generation, Transmission Distribution*, vol. 5, pp. 1149–1154(5), November 2011.

[54] S. Chakrabarti, E. Kyriakides, and D. G. Eliades, "Placement of synchronized measurements for power system observability," *IEEE Transactions on Power Delivery*, vol. 24, no. 1, pp. 12–19, 2009.

[55] B. Stott, J. Jardim, and O. Alsac, "Dc power flow revisited," *IEEE Transactions on Power Systems*, vol. 24, no. 3, pp. 1290–1300, 2009.

[56] S. H. Low, "Convex relaxation of optimal power flow—part i: Formulations and equivalence," *IEEE Transactions on Control of Network Systems*, vol. 1, no. 1, pp. 15–27, 2014.

[57] S. H. Low, "Convex relaxation of optimal power flow—part ii: Exactness," *IEEE Transactions on Control of Network Systems*, vol. 1, no. 2, pp. 177–189, 2014.

[58] Z. Miao, L. Fan, H. G. Aghamolki, and B. Zeng, "Least squares estimation based sdp cuts for socp relaxation of ac opf," *IEEE Transactions on Automatic Control*, vol. 63, no. 1, pp. 241–248, 2018.

[59] R. A. Jabr, "A conic quadratic format for the load flow equations of meshed networks," *IEEE Transactions on Power Systems*, vol. 22, no. 4, pp. 2285–2286, 2007.

[60] R. A. Jabr,, "Optimal power flow using an extended conic quadratic formulation," *IEEE Transactions on Power Systems*, vol. 23, no. 3, pp. 1000–1008, 2008.

[61] M. Farivar, C. R. Clarke, S. H. Low, and K. M. Chandy, "Inverter var control for distribution systems with renewables," in *2011 IEEE International Conference on Smart Grid Communications (SmartGridComm)*, pp. 457–462, 2011.

[62] M. Farivar, R. Neal, C. Clarke, and S. Low, "Optimal inverter var control in distribution systems with high pv penetration," in *2012 IEEE Power and Energy Society General Meeting*, pp. 1–7, 2012.

[63] B. Subhonmesh, S. H. Low, and K. M. Chandy, "Equivalence of branch flow and bus injection models," in *2012 50th Annual Allerton Conference on Communication, Control, and Computing (Allerton)*, pp. 1893–1899, 2012.

[64] M. E. Baran and F. F. Wu, "Optimal capacitor placement on radial distribution systems," *IEEE Transactions on Power Delivery*, vol. 4, no. 1, pp. 725–734, 1989.

[65] M. Baran and F. Wu, "Optimal sizing of capacitors placed on a radial distribution system," *IEEE Transactions on Power Delivery*, vol. 4, no. 1, pp. 735–743, 1989.

[66] L. Gan and S. H. Low, "Convex relaxations and linear approximation for optimal power flow in multiphase radial networks," in *2014 Power Systems Computation Conference*, pp. 1–9, 2014.

[67] J. A. Taylor and F. S. Hover, "Convex models of distribution system reconfiguration," *IEEE Transactions on Power Systems*, vol. 27, no. 3, pp. 1407–1413, 2012.

[68] M. Farivar and S. H. Low, "Branch flow model: Relaxations and convexification—part i," *IEEE Transactions on Power Systems*, vol. 28, no. 3, pp. 2554–2564, 2013.

[69] Farivar, Masoud and Low, Steven H., "Branch flow model: Relaxations and convexification—part ii," *IEEE Transactions on Power Systems*, vol. 28, no. 3, pp. 2565–2572, 2013.

[70] N. Li, L. Chen, and S. H. Low, "Exact convex relaxation of opf for radial networks using branch flow model," in *2012 IEEE Third International Conference on Smart Grid Communications (SmartGridComm)*, pp. 7–12, 2012.

[71] A. Gopalakrishnan, A. U. Raghunathan, D. Nikovski, and L. T. Biegler, "Global optimization of optimal power flow using a branch amp; bound algorithm," in *2012 50th Annual Allerton Conference on Communication, Control, and Computing (Allerton)*, pp. 609–616, 2012.

[72] R. A. Jabr, "Exploiting sparsity in sdp relaxations of the opf problem," *IEEE Transactions on Power Systems*, vol. 27, no. 2, pp. 1138–1139, 2012.

[73] X. Bai and H. Wei, "A semidefinite programming method with graph partitioning technique for optimal power flow problems," *International Journal of Electrical Power Energy Systems*, vol. 33, no. 7, pp. 1309–1314, 2011.

[74] B. Kocuk, S. S. Dey, and X. A. Sun, "Strong socp relaxations for the optimal power flow problem," *Operations Research*, vol. 64, no. 6, pp. 1177–1196, 2016.

[75] M. Khanabadi and S. Kamalasadan, "Day ahead scheduling of distribution system with distributed energy resources considering demand response and energy storage," in *2013 North American Power Symposium (NAPS)*, pp. 1–6, IEEE, 2013.

[76] S. Moghadasi and S. Kamalasadan, "Real-time optimal scheduling of smart power distribution systems using integrated receding horizon control and convex conic programming," in *2014 IEEE Industry Application Society Annual Meeting*, pp. 1–7, IEEE, 2014.

[77] S. Moghadasi and S. Kamalasadan, "An architecture for voltage stability constrained optimal power flow using convex semi-definite programming," in *2015 North American Power Symposium (NAPS)*, pp. 1–6, IEEE, 2015.

[78] S. Moghadasi and S. Kamalasadan, "Voltage security cost assessment of integrated ac-dc systems using semidefinite programming," in *2016 IEEE Power & Energy Society Innovative Smart Grid Technologies Conference (ISGT)*, pp. 1–5, IEEE, 2016.

[79] Z. Yang, H. Zhong, A. Bose, T. Zheng, Q. Xia, and C. Kang, "A linearized opf model with reactive power and voltage magnitude: A pathway to improve the mw-only dc opf," *IEEE Transactions on Power Systems*, vol. 33, no. 2, pp. 1734–1745, 2018.

[80] A. J. Wood and F. Bruce, "Wollenberg."power generation, operation and control"," *John Wily & Sons, Inc, USA*, 1996.

[81] Z. Yang, H. Zhong, A. Bose, T. Zheng, Q. Xia, and C. Kang, "A linearized opf model with reactive power and voltage magnitude: A pathway to improve the mw-only dc opf," *IEEE Transactions on Power Systems*, vol. 33, no. 2, pp. 1734–1745, 2018.

[82] M. Huneault and F. D. Galiana, "A survey of the optimal power flow literature," *IEEE Transactions on Power Systems*, vol. 6, no. 2, pp. 762–770, 1991.

[83] J. A. Momoh, R. Adapa, and M. E. El-Hawary, "A review of selected optimal power flow literature to 1993. i. nonlinear and quadratic programming approaches," *IEEE Transactions on Power Systems*, vol. 14, no. 1, pp. 96–104, 1999.

[84] H. H. Happ, "Optimal power dispatcha comprehensive survey," *IEEE Transactions on Power Apparatus and Systems*, vol. 96, no. 3, pp. 841–854, 1977.

[85] A. Gómez Expósito and E. Romero Ramos, "Reliable load flow technique for radial distribution networks," *IEEE Transactions on Power Systems*, vol. 14, no. 3, pp. 1063–1069, 1999.

[86] D. Das, D. Kothari, and A. Kalam, "Simple and efficient method for load flow solution of radial distribution networks," *International Journal of Electrical Power Energy Systems*, vol. 17, no. 5, pp. 335 – 346, 1995.

[87] R. Ranjan, "Simple and efficient computer algorithm to solve radial distribution networks," *Electric Power Components and Systems - ELECTR POWER COMPON SYST*, vol. 31, pp. 95–107, 01 2003.

[88] D. K. Molzahn and I. A. Hiskens, *A Survey of Relaxations and Approximations of the Power Flow Equations*. 2019.

[89] H. Saadat *et al.*, *Power system analysis*, vol. 2. McGraw-hill, 1999.

[90] L. Gan, N. Li, U. Topcu, and S. H. Low, "Exact convex relaxation of optimal power flow in radial networks," *IEEE Transactions on Automatic Control*, vol. 60, no. 1, pp. 72–87, 2015.

[91] Y. Weng, Q. Li, R. Negi, and M. Ilić, "Semidefinite programming for power system state estimation," in *2012 IEEE Power and Energy Society General Meeting*, pp. 1–8, 2012.

[92] T. G. Paul, S. J. Hossain, S. Ghosh, P. Mandal, and S. Kamalasadan, "A quadratic programming based optimal power and battery dispatch for grid-connected microgrid," *IEEE Transactions on Industry Applications*, vol. 54, no. 2, pp. 1793–1805, 2018.

[93] S. Moghadasi and S. Kamalasadan, "Optimal fast control and scheduling of power distribution system using integrated receding horizon control and convex conic programming," *IEEE Transactions on Industry Applications*, vol. 52, no. 3, pp. 2596–2606, 2016.

[94] H. Ying-Yi and W. Fu-Ming, "Development of three-phase newton optimal power flow for studying imbalance/security in transmission systems," *Electric Power Systems Research*, vol. 55, no. 1, pp. 39–48, 2000.

[95] A. R. Baran and T. S. Fernandes, "A three-phase optimal power flow applied to the planning of unbalanced distribution networks," *International Journal of Electrical Power Energy Systems*, vol. 74, pp. 301–309, 2016.

[96] H. Li, X. Yan, J. Yan, A. Zhang, and F. Zhang, "A three-phase unbalanced linear power flow solution with pv bus and zip load," *IEEE Access*, vol. 7, pp. 138879–138889, 2019.

[97] W. Wang and N. Yu, "Chordal conversion based convex iteration algorithm for three-phase optimal power flow problems," *IEEE Transactions on Power Systems*, vol. 33, no. 2, pp. 1603–1613, 2018.

[98] C. Zhao, E. Dall'Anese, and S. H. Low, "Convex relaxation of opf in multiphase radial networks with delta connection," in *Proceedings of the 10th bulk power systems dynamics and control symposium*, pp. 0885–8950, 2017.

[99] F. Zhou, A. S. Zamzam, S. H. Low, and N. D. Sidiropoulos, "Exactness of opf relaxation on three-phase radial networks with delta connections," *IEEE Transactions on Smart Grid*, vol. 12, no. 4, pp. 3232–3241, 2021.

[100] E. Dall'Anese, H. Zhu, and G. B. Giannakis, "Distributed optimal power flow for smart microgrids," *IEEE Transactions on Smart Grid*, vol. 4, no. 3, pp. 1464–1475, 2013.

[101] B. C. Lesieutre, D. K. Molzahn, A. R. Borden, and C. L. DeMarco, "Examining the limits of the application of semidefinite programming to power flow problems," in *2011 49th Annual Allerton Conference on Communication, Control, and Computing (Allerton)*, pp. 1492–1499, 2011.

[102] W. A. Bukhsh, A. Grothey, K. I. McKinnon, and P. A. Trodden, "Local solutions of the optimal power flow problem," *IEEE Transactions on Power Systems*, vol. 28, no. 4, pp. 4780–4788, 2013.

[103] Z. Miao, L. Fan, H. G. Aghamolki, and B. Zeng, "Least squares estimation based sdp cuts for socp relaxation of ac opf," *IEEE Transactions on Automatic Control*, vol. 63, no. 1, pp. 241–248, 2018.

[104] D. K. Molzahn, J. T. Holzer, B. C. Lesieutre, and C. L. DeMarco, "Implementation of a large-scale optimal power flow solver based on semidefinite programming," *IEEE Transactions on Power Systems*, vol. 28, no. 4, pp. 3987–3998, 2013.

[105] C. Coffrin, H. L. Hijazi, and P. Van Hentenryck, "The qc relaxation: A theoretical and computational study on optimal power flow," *IEEE Transactions on Power Systems*, vol. 31, no. 4, pp. 3008–3018, 2016.

[106] T. Chowdhury and S. Kamalasadan, "A new second-order cone programming model for voltage control of power distribution system with inverter based distributed generation," *IEEE Transactions on Industry Applications*, pp. 1–1, 2021.

[107] D. K. Molzahn and I. A. Hiskens, *A Survey of Relaxations and Approximations of the Power Flow Equations*. 2019.

[108] W. M. Siti, A. Jimoh, and D. Nicolae, "Distribution network phase load balancing as a combinatorial optimization problem using fuzzy logic and newton–raphson," *Electric Power Systems Research*, vol. 81, no. 5, pp. 1079–1087, 2011.

[109] S. Civanlar, J. Grainger, H. Yin, and S. Lee, "Distribution feeder reconfiguration for loss reduction," *IEEE Transactions on Power Delivery*, vol. 3, no. 3, pp. 1217–1223, 1988.

[110] D. K. Molzahn, B. C. Lesieutre, and C. L. DeMarco, "Approximate representation of zip loads in a semidefinite relaxation of the opf problem," *IEEE Transactions on Power Systems*, vol. 29, no. 4, pp. 1864–1865, 2014.

[111] H. Xu, A. D. Domínguez-García, and P. W. Sauer, "Optimal tap setting of voltage regulation transformers using batch reinforcement learning," *IEEE Transactions on Power Systems*, vol. 35, no. 3, pp. 1990–2001, 2020.

[112] J. Momoh, R. Adapa, and M. El-Hawary, "A review of selected optimal power flow literature to 1993. i. nonlinear and quadratic programming approaches," *IEEE Transactions on Power Systems*, vol. 14, no. 1, pp. 96–104, 1999.

[113] K. Pandya and S. Joshi, "A survey of optimal power flow methods," *Journal of Theoretical and Applied Information Technology*, vol. 4, p. 450–458, 01 2008.

[114] S. Frank, I. Steponavice, and S. Rebennack, "Optimal power flow: a bibliographic survey i," *Energy systems*, vol. 3, no. 3, pp. 221–258, 2012.

[115] M. Khanabadi, S. Moghadasi, and S. Kamalasadan, "Real-time optimization of distribution system considering interaction between markets," in *2013 IEEE Industry Applications Society Annual Meeting*, pp. 1–8, IEEE, 2013.

[116] S. Moghadasi,and S. Kamalasadan, "Optimal fast control and scheduling of power distribution system using integrated receding horizon control and convex conic programming," *IEEE Transactions on Industry Applications*, vol. 52, no. 3, pp. 2596–2606, 2016.

[117] C. Coffrin, H. L. Hijazi, and P. Van Hentenryck, "The qc relaxation: A theoretical and computational study on optimal power flow," *IEEE Transactions on Power Systems*, vol. 31, no. 4, pp. 3008–3018, 2016.

[118] M. R. Narimani, D. K. Molzahn, and M. L. Crow, "Tightening qc relaxations of ac optimal power flow problems via complex per unit normalization," *IEEE Transactions on Power Systems*, vol. 36, no. 1, pp. 281–291, 2021.

[119] D. Lee, K. Turitsyn, D. K. Molzahn, and L. A. Roald, "Robust ac optimal power flow with robust convex restriction," *IEEE Transactions on Power Systems*, vol. 36, no. 6, pp. 4953–4966, 2021.

[120] R. A. Jabr, "A conic quadratic format for the load flow equations of meshed networks," *IEEE Transactions on Power Systems*, vol. 22, no. 4, pp. 2285–2286, 2007.

[121] Z. Tian and W. Wu, "Recover feasible solutions for SOCP relaxation of optimal power flow problems in mesh networks," *IET Generation, Transmission Distribution*, vol. 13, no. 7, pp. 1078–1087, 2019.

[122] Z. Miao, L. Fan, H. G. Aghamolki, and B. Zeng, "Least squares estimation based sdp cuts for socp relaxation of ac opf," *IEEE Transactions on Automatic Control*, vol. 63, no. 1, pp. 241–248, 2018.

[123] A. F. Soofi, S. D. Manshadi, G. Liu, and R. Dai, "A socp relaxation for cycle constraints in the optimal power flow problem," *IEEE Transactions on Smart Grid*, vol. 12, no. 2, pp. 1663–1673, 2021.

[124] D. K. Molzahn, B. C. Lesieutre, and C. L. DeMarco, "A sufficient condition for global optimality of solutions to the optimal power flow problem," *IEEE Transactions on Power Systems*, vol. 29, no. 2, pp. 978–979, 2014.

[125] B. C. Lesieutre, D. K. Molzahn, A. R. Borden, and C. L. DeMarco, "Examining the limits of the application of semidefinite programming to power flow problems," in *Proc. 49th Annual Allerton Conference on Communication, Control, and Computing (Allerton)*, pp. 1492–1499, 2011.

[126] M. M.-U.-T. Chowdhury and S. Kamalasadan, "An angle included optimal power flow (opf) model for power distribution network using second order cone programming (socp)," in *2020 IEEE Industry Applications Society Annual Meeting*, pp. 1–7, 2020.

[127] R. D. Zimmerman, C. E. Murillo-Sánchez, and R. J. Thomas, "Matpower: Steady-state operations, planning, and analysis tools for power systems research and education," *IEEE Transactions on Power Systems*, vol. 26, no. 1, pp. 12–19, 2011.

[128] S. Huang, Q. Wu, J. Wang, and H. Zhao, "A sufficient condition on convex relaxation of ac optimal power flow in distribution networks," *IEEE Transactions on Power Systems*, vol. 32, no. 2, pp. 1359–1368, 2017.

[129] A. B. Birchfield, T. Xu, K. M. Gegner, K. S. Shetye, and T. J. Overbye, "Grid structural characteristics as validation criteria for synthetic networks," *IEEE Transactions on Power Systems*, vol. 32, no. 4, pp. 3258–3265, 2017.

[130] P. Wang, L. Goel, X. Liu, and F. H. Choo, "Harmonizing ac and dc: A hybrid ac/dc future grid solution," *IEEE Power and Energy Magazine*, vol. 11, no. 3, pp. 76–83, 2013.

[131] A. A. Eajal, M. F. Shaaban, K. Ponnambalam, and E. F. El-Saadany, "Stochastic centralized dispatch scheme for ac/dc hybrid smart distribution systems," *IEEE Transactions on Sustainable Energy*, vol. 7, no. 3, pp. 1046–1059, 2016.

[132] S. Li, P. Shen, K.-s. Wong, Z. Huang, Y. Zhang, and H. Li, "Simulation study of ac and dc distribution efficiency in an office room in shenzhen," in *2021 IEEE 3rd International Conference on Circuits and Systems (ICCS)*, pp. 218–224, 2021.

[133] M. Starke, F. Li, L. M. Tolbert, and B. Ozpineci, "Ac vs. dc distribution: Maximum transfer capability," in *2008 IEEE Power and Energy Society General Meeting - Conversion and Delivery of Electrical Energy in the 21st Century*, pp. 1–6, 2008.

[134] K. Murari and N. P. Padhy, "A network-topology-based approach for the load-flow solution of ac–dc distribution system with distributed generations," *IEEE Transactions on Industrial Informatics*, vol. 15, no. 3, pp. 1508–1520, 2019.

[135] P. Teimourzadeh Baboli, M. Shahparasti, M. Parsa Moghaddam, M. R. Haghifam, and M. Mohamadian, "Energy management and operation modelling of hybrid ac–dc microgrid," *IET Generation, Transmission & Distribution*, vol. 8, no. 10, pp. 1700–1711, 2014.

[136] S. Paul, A. Sharma, and N. P. Padhy, "Risk constrained energy efficient optimal operation of a converter governed ac/dc hybrid distribution network with distributed energy resources and volt-var controlling devices," *IEEE Transactions on Industry Applications*, vol. 57, no. 4, pp. 4263–4277, 2021.

[137] A. Castillo and R. P. O'Neill, "Computational performance of solution techniques applied to the acopf," 2013.

[138] A. Pizano-Martinez, C. R. Fuerte-Esquivel, H. Ambriz-PÉrez, and E. Acha, "Modeling of vsc-based hvdc systems for a newton-raphson opf algorithm," *IEEE Transactions on Power Systems*, vol. 22, no. 4, pp. 1794–1803, 2007.

[139] H. M. A. Ahmed, A. B. Eltantawy, and M. M. A. Salama, "A generalized approach to the load flow analysis of ac–dc hybrid distribution systems," *IEEE Transactions on Power Systems*, vol. 33, no. 2, pp. 2117–2127, 2018.

[140] A. Mešanović, U. Münz, and C. Ebenbauer, "Robust optimal power flow for mixed ac/dc transmission systems with volatile renewables," *IEEE Transactions on Power Systems*, vol. 33, no. 5, pp. 5171–5182, 2018.

[141] S. Frank, I. Steponavičė, and S. Rebennack, "Optimal power flow: a bibliographic survey i," *Energy Systems*, vol. 3, 09 2012.

[142] Frank, Stephen and Steponavičė, Ingrida and Rebennack, Steffen, "Optimal power flow: a bibliographic survey ii," *Energy Systems*, vol. 3, 09 2012.

[143] L. Gan, N. Li, U. Topcu, and S. Low, "On the exactness of convex relaxation for optimal power flow in tree networks," in *Proc. 51st IEEE Conference on Decision and Control (CDC)*, pp. 465–471, 2012.

[144] M. Baradar, M. R. Hesamzadeh, and M. Ghandhari, "Second-order cone programming for optimal power flow in vsc-type ac-dc grids," *IEEE Transactions on Power Systems*, vol. 28, no. 4, pp. 4282–4291, 2013.

[145] K. Murari and N. P. Padhy, "Graph-theoretic-based approach for solving load flow problem of ac–dc radial distribution network with distributed generations," *IET Generation, Transmission & Distribution*, vol. 14, no. 22, pp. 5327–5346, 2020.

[146] K. Murari, N. Prasad Padhy, and S. Kamalasadan, "Backward-forward sweep based power flow algorithm for radial and meshed ac-dc distribution system," in *2021 IEEE Industry Applications Society Annual Meeting (IAS)*, pp. 1–8, 2021.

[147] C. Dai, W. Chen, Y. Zhu, and X. Zhang, "Reactive power dispatch considering voltage stability with seeker optimization algorithm," *Electric Power Systems Research*, vol. 79, no. 10, pp. 1462–1471, 2009.

[148] W. Zhang and Y. Liu, "Multi-objective reactive power and voltage control based on fuzzy optimization strategy and fuzzy adaptive particle swarm," *International Journal of Electrical Power & Energy Systems*, vol. 30, pp. 525–532, 2008.

[149] M. Baran and F. Wu, "Network reconfiguration in distribution systems for loss reduction and load balancing," *IEEE Transactions on Power Delivery*, vol. 4, no. 2, pp. 1401–1407, 1989.

[150] B. Stott, J. Jardim, and O. Alsac, "Dc power flow revisited," *IEEE Transactions on Power Systems*, vol. 24, no. 3, pp. 1290–1300, 2009.

[151] J. A. Taylor, *Convex optimization of power systems*. Cambridge University Press, 2015.

[152] M. M.-U.-T. Chowdhury and S. Kamalasadan, "A new second-order cone programming model for voltage control of power distribution system with inverter-based distributed generation," *IEEE Transactions on Industry Applications*, vol. 57, no. 6, pp. 6559–6567, 2021.

[153] M. M.-U.-T. Chowdhury, S. Kamalasadan, and S. Paudyal, "A second-order cone programming (socp) based optimal power flow (opf) model with cyclic constraints for power transmission systems," *IEEE Transactions on Power Systems*, pp. 1–12, 2023.

[154] H. Li, X. Yan, J. Yan, A. Zhang, and F. Zhang, "A three-phase unbalanced linear power flow solution with pv bus and zip load," *IEEE Access*, vol. 7, pp. 138879–138889, 2019.

[155] A. S. Zamzam, N. D. Sidiropoulos, and E. Dall'Anese, "Beyond relaxation and newton–raphson: Solving ac opf for multi-phase systems with renewables," *IEEE Transactions on Smart Grid*, vol. 9, no. 5, pp. 3966–3975, 2018.

[156] T. T. Hashim, A. Mohamed, and H. Shareef, "A review on voltage control methods for active distribution networks," *Prz. Elektrotech*, vol. 88, no. 6, pp. 304–312, 2012.

[157] S. M. Amin, "Smart grid security, privacy, and resilient architectures: Opportunities and challenges," in *2012 IEEE Power and Energy Society General Meeting*, pp. 1–2, IEEE, 2012.

[158] R. Sadnan and A. Dubey, "Distributed optimization using reduced network equivalents for radial power distribution systems," *IEEE Transactions on Power Systems*, vol. 36, no. 4, pp. 3645–3656, 2021.

[159] E. Dall'Anese, H. Zhu, and G. B. Giannakis, "Distributed optimal power flow for smart microgrids," *IEEE Transactions on Smart Grid*, vol. 4, no. 3, pp. 1464–1475, 2013.

[160] T. Erseghe, "Distributed optimal power flow using admm," *IEEE Transactions on Power Systems*, vol. 29, no. 5, pp. 2370–2380, 2014.

[161] S. Boyd, N. Parikh, E. Chu, B. Peleato, J. Eckstein, *et al.*, "Distributed optimization and statistical learning via the alternating direction method of multipliers," *Foundations and Trends® in Machine learning*, vol. 3, no. 1, pp. 1–122, 2011.

[162] W. Zheng, W. Wu, B. Zhang, H. Sun, and Y. Liu, "A fully distributed reactive power optimization and control method for active distribution networks," *IEEE Transactions on Smart Grid*, vol. 7, no. 2, pp. 1021–1033, 2016.

[163] Y. Tang, K. Dvijotham, and S. Low, "Real-time optimal power flow," *IEEE Transactions on Smart Grid*, vol. 8, no. 6, pp. 2963–2973, 2017.